PERIODICAL
10(1)
Oceanographical Magazine
10(1)
N.D.

気象庁欧文海洋報告

第10巻 第1号

THE OCEANOGRAPHICAL MAGAZINE

Vol. 10 No. 1

CONTENTS

J. Masuzawa: A short-period fluctuation of the Kuroshio east of Cape Kinkazan 1
T. Kawamoto: The construction of parachute drogue 9
Y. Takenouti: Measurements of subsurface current in the cold-belt along the northern boundary of Kuroshio 13
T. Ichiye: The response of a stratified, bounded ocean to variable wind stresses 19
M. Miyazaki: A method for the harmonic analysis of tides 65
S. Moriyasu: On the fluctuation of the Kuroshio south of Honshū 81
M. Hanzawa: Studies on the inter-relationship between the sea and the atmosphere (part 3) 91
T. Ichiye: On convective circulation and density distribution in a zonally uniform ocean 97
A. Okubo: The distribution of dissolved oxygen in the north-western part of the North Pacific Ocean in the aspect of physical oceanography. Part 1. General features of the oxygen distribution (1) 137

Published by the Japan Meteorological Agency

June 1958

The Oceanographical Magazine
Vol. 10. No. 1 June 1958

A Short-period Fluctuation of the Kuroshio East of Cape Kinkazan*

By

Jotaro MASUZAWA

Japan Meteorological Agency

1. *Introduction*

The multiple ship current measurement east of Japan was carried out in June~July 1957 as the first oceanographic project in the IGY 1957~1958. Participating ships were four ships, the *Ryofu-maru* of Japan Meteorological Agency, *Shumpu-maru* of Kōbe Marine Observatory, the *Yushio-maru* of the Hakodate Marine Observatory and the *Kaiyō* of Marine Safety Agency. The principal purpose of this project is to obtain a fundamental knowledge on the mechanism of the northward transport of warmer water. The sea region east of Japan is an original region for mixing in the oceanic polar frontal zone between the subtropical warm water (the Kuroshio) and the sub-arctic cold water (the Oyashio). This project placed great emphasis on the observation of actual short-period oceanic fluctuations in the northern side of the Kuroshio.

2. *General current pattern*

The general current pattern east of Honshū was at first obtained in the shorter period (June 9~11) from simultaneous observations on board of four ships (Operation *CM*). These observations were carried out particularly with the Bathythermograph (BT) and Geomagnetic Electro-Kinetograph (GEK) as quickly as possible. It has formerly taken two or three weeks to obtain the general distribution of currents and water masses in this sea area. But, this semi-simultaneous observation does not any essentially different knowledges on the current pattern from our former ones. The distribution of surface currents observed with GEK is generally correspondent to the distribution of mean temperature in the upper

* Currents and Water Masses of the Kuroshio System X.

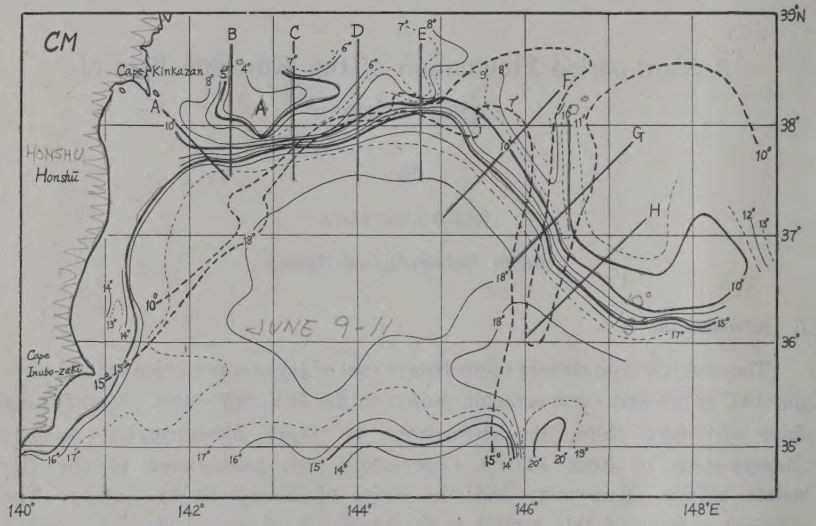

Fig. 1. The mean temperature of the upper 200 m layer in June 9～11. Broken lines show isotherms in May. A～H are standard observational lines in Operation GS.

200 m layer and the stream-axis of the Kuroshio can be followed by the isotherm of 15°C in the mean temperature distribution (Fig. 1). Comparing this current pattern with one obtained by the routine observation on board the *Ryōfu-maru* in May, we can find out some remarkable differences between two patterns. In May, the Kuroshio flowed northeastwards from Cape Inubō-zaki and its stream-axis on the parallel of 37°N latitude was as far as about 100 nautical miles from the coast with the surface maximum velocity of 4.3 knots. In June 9～11, the Kuroshio flows northwards near the coast and its velocity is generally smaller, the observed surface maximum velocity being only 2.6 knots on the above-mentioned parallel. Furthermore, in May the Kuroshio turned to the south at the vicinity of 38°N, 146°E and flowed down to the south of 35°N along the meridian of 146°E longitude and at the same time the narrow cold water stretched to the south along the eastern side of the southward stream-axis. In June, however we can not see a remarkable meandering path like this but find a cold water to the south of 35°N. It may have been cut off from the above-mentioned narrow cold trough.

The coldest water is found along the northern edge of the semi-isolated warm watermass which occupied the large area (35°～38°N, 141°～146°E), but at its northeast corner a warm water extending to the northeast since May becomes gradually less remarkable.

3. *States of the cold water along the northern boundary of the Kuroshio*

In the next GS operation, in order to see some fluctuating states of the cold water along the northern boundary of the Kuroshio in the shorter period, we observed four times those standard lines as shown in Fig. 1 once in five days (Fig. 2). In Operation GS_1 and GS_2, the narrow continuous coldest belt apparently stretches from the coast to the offing as far as 250 nautical miles along the northern edge of the Kuroshio.. The minimum width of the cold belt is only 10～20 nautical miles in Operation GS_2. In Operation GS_3 and GS_4, however it seems to be a train of cold water patches. It is sure that this difference is not caused only by the vertical displacement of the subsurface water. When we mark coldest parts in the cold belt in Operation CM, GS_1, and GS_3, we are possible to suppose the existence of advection along the northern edge of the Kuroshio. That is, if the coldest water (A) near Cape Kinkazan in Operation CM is correspondent to the coldest water (A′) in the vicinity of 37.5°N, 146°E in Operation GS_1 and also the water (B) in Operation GS_1 to the water (B′) in Operation GS_3, it is estimated that those coldest waters are flowing at the rate of 20～30 nautical miles a day or about one knot. According to direct current measurements with parachute drague system carried out in the period between Operation GS_1 and GS_2 and between Operation GS_2 and GS_3, the current-velocity in the subsurface layer (100～200 m) of the cold belt is of the same order. In the later half of June, the cold water was flowing considerably strongly from the coast to the offing as far as at least 300 nautical miles along the northern edge of the Kuroshio, and so it might cut off the warmer water extending to the northeast in the vicinity of 38°N, 145.5°E in the period from May to the beginning of June. A remarkable warmer watermass (W) which is a stronger anticyclonic eddy with the speed of 2 knots existed to the north of the cold belt in the vicinity of 39°N. 143°E in Operation GS_3 and GS_4. Before May or June, therefore, the warm water would extend remarkably to the north without prevention of the cold water's advection along the northern edge of the warm water.

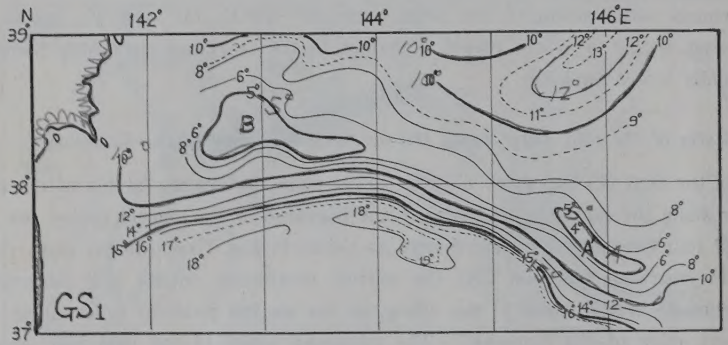

a

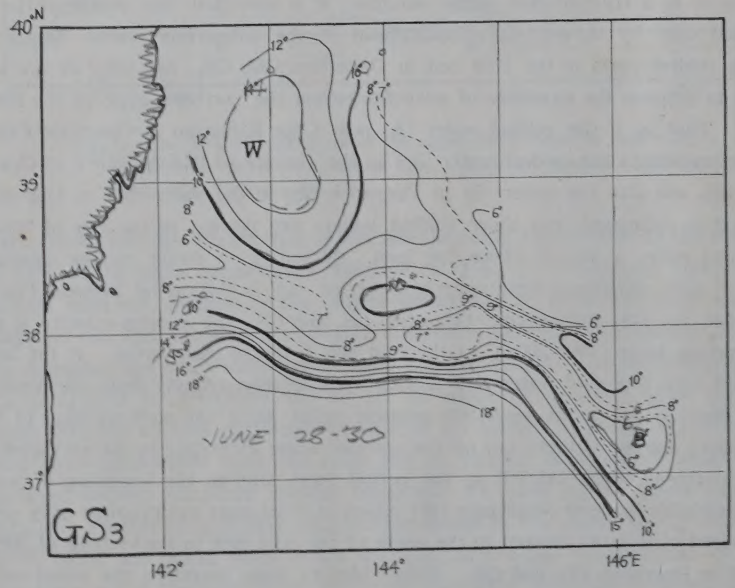

c

Fig. 2. The mean temperature of the upper 200 m layer and GS_4 (July 1–3).

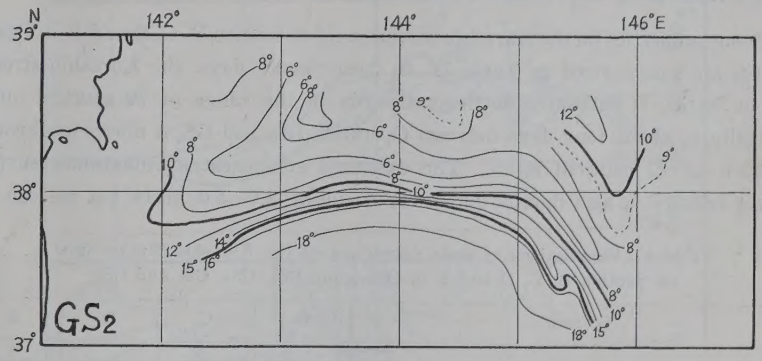

b

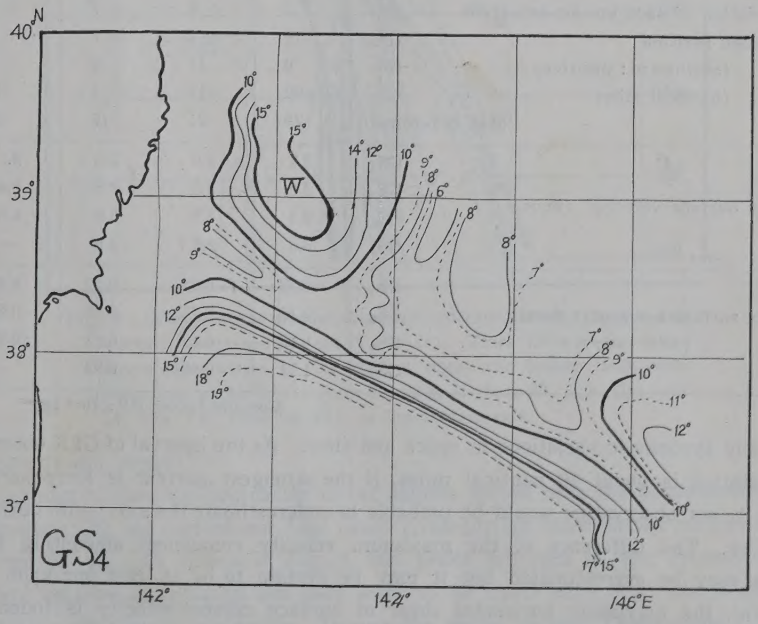

d

in GS_1 (June 17-19), GS_2 (June 22-24), GS_3 (June 28-30)

4. Fluctuations of the Kuroshio stream-axis

Some properties on the Kuroshio stream-axis on Section B, C, D and E in Operation GS are summarized as Table 1. In these twenty days, the Kuroshio stream-axis in Section B fluctuates north-southwards in the range of 39 nautical miles, especially in about four days between Operation GS_3 and GS_4 it moves northwards as much as 22 nautical miles. The eastward component of maximum surface current-velocity is also fluctuating in the range of 2.0~4.0 knots but we can not

Table 1. Fluctuations of some properties on the Kuroshio Stream-axis on Section B, C, D and E in Operation GS_1, GS_2, GS_3 and GS_4.

Section		B	C	D	E
Mean Position of stream-axis (N latitude)		37°53′	37°52′	37°49′	37°42′
Deviation of each stream-axis from mean position (northward: positive) (nautical mile)	GS_1	− 7	+ 2	+ 7	+ 7
	GS_2	−16	+ 1	+ 7	+ 8
	GS_3	0	−11	− 9	− 2
	GS_4	+22	+10	− 4	−14
	Max difference	39	21	16	22
Max Surface velocity (knot)	GS_1	2.7	2.0	>2.5	2.1
	GS_2	3.2	3.5	2.8	2.4
	GS_3	3.1	2.8	3.6	4.0
	GS_4	3.6	2.6 ?	>3.0	—
Max surface horizontal shear ($\times 10^{-4}$ sec^{-1})	GS_1	0.73	0.22	0.52	0.45
	GS_2	1.15	0.70	0.58	0.65
	GS_3	0.88	0.49	0.62	0.94
	GS_4	1.11	0.42	0.93	—

Coriolis factor 0.9×10^{-4} sec^{-1}

find any systematic variations in space and time. As the interval of GEK observation station is about 10 nautical miles, if the strongest current is more narrow than it, our observation would be probable to underestimate the maximum current-velocity. The difference of the maximum velocity component amounting to 2 knots may be overestimated but it may be certain to be at least one knot. In general, the maximum horizontal shear of surface current-velocity is found at the left side of stream-axis. This maximum cyclonic shear fluctuates in the range of $0.22 \sim 1.15 \times 10^{-4}$ per second and four cases of fifteen examples are over the Coriolis factor 0.9×10^{-4} per second. And also it is inclined to be the larger, the maximum

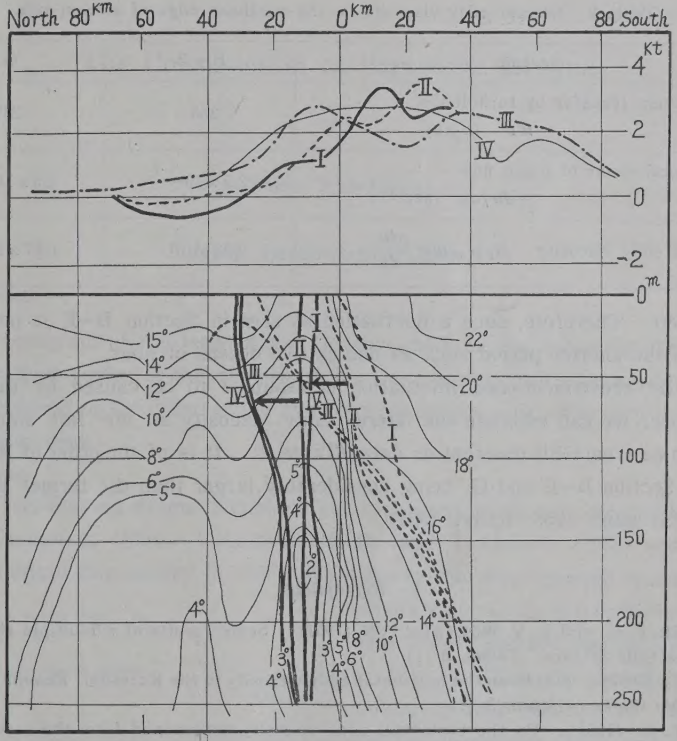

Fig. 3. Cross-current profiles of surface current-velocity (upper) and water temperature in Case II (lower). Thick lines in the lower figure show axises of the coldest water and broken lines show isotherms of 15°C. I: June 23, 02 h, II: June 23, 12 h, III: June 24, 01 h, IV: June 24, 20 h at the stream-axis.

velocity is the larger.

In order to know the fluctuation in the shorter period than the above-mentioned observation GS, we carried out four times cross-current observations on Section G in June 23~24. As shown in Fig. 3, two peaks are seen in the cross-current surface velocity distribution and they seem to be apart each other and decrease the maximum velocity gradually. During the period between Observation II and III, the left peak of surface current velocity moves to the left as much as 20 km and at the same time the surface water from surface to at least 100 m depth moves

Table 2. Lateral eddy viscosity on the northern edge of stream-axis.

Section	B~E	G
Momentum transfer by turbulence $\overline{u'v'}$ (c g s)	200	217
Horizontal shear of mean flow $-du/dy$ (sec^{-1})	2.2×10^{-5}	2.5×10^{-5}
Lateral eddy viscosity $K_y=-\overline{u'v'}/\frac{du}{dy}$	0.92×10^{7}	0.87×10^{7}

to the left. Therefore, such a fluctuation as seen in Section B~E is possible to occur in the shorter period such as one or two dozens of hour.

If the above-mentioned fluctuation is assumed to be caused by the lateral turburence, we can estimate the lateral eddy viscosity at the left side of the stream-axis from GEK observation data (Table 2). It is of the order of 10^7 (c g s) in both Section B~E and G, being considerably larger than the former estimated values (STOMMEL 1955, ICHIYE 1957).

References

FUGLISTER, F. C. and L. V. WORTHINGTON (1951): Some results of a multiple ship survey of the Gulf Stream. *Tellus*, **3** (1)

ICHIYE, T. (1957): A note on the horizontal eddy viscosity in the Kuroshio. *Records of Oceanographic Works in Japan*, **3** (1)

STOMMEL, H. (1955): On the horizontal eddy viscosity determined from the serial current observation. *Deep Sea Research*, **2** (3)

The Oceanographical Magazine
Vol. 10. No. 1 June 1958

The Construction of Parachute Drogue

By

Takeo KAWAMOTO

Japan Meteorological Agency

Introduction

As a program of the International Geophysical Year, the subsurface current in the polar front region of the western Pacific was measured with parachute drogue. Here, we report on the construction of parachute drogue which was used in the present measurement.

1. Drogue

The free-floating drogue technique has been used in recent years by STOMMEL (1954), CROMWELL (1954), VOLKMANN (1956), and TAKENOUTI (1956) and others. In the multiple ship survey in 1957, the drogue system was consisted of a standard aviator's parachute suspended by a piano wire from a surface float as illustrated in Fig. 1. This drogue system was similar to that reported by Takenouti and his co-operator (1956) and designed in two points in mind in addition to their system: (1) The blinking signal should be lighted at night from the surface drag. (2) The surface drag should be tracked by the marine radar up to ranges of 8 miles.

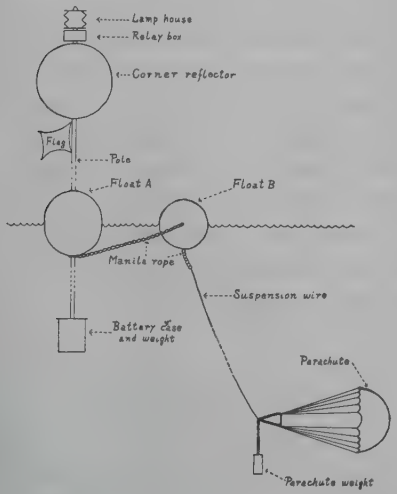

Fig. 1. Schematic illustration of the parachute drogue system

2. Floats and wire

The float A and B were used the polystyrol fishing float of diameter 34 and 30 cm, and their surplus bouyancy was approximately 25 and 20 Kg. re-

spectively. The float A was connected to a pole which was made of rigid vinyl-chloride pipe, about 3.0 cm in outside diameter. At the top of this pole there were attached a lamp house, a relay box, a corner reflector and a flag, at the other end, a battery case and a balancing weight. The length of pole was about 1.0 m from float A to corner reflector and about 2 m to battery case. In the lamp house an electric lamp and a photo-transistor were set up. This photo-transistor operated the relay circuit and switched on or off the lamp at night, and the blinking signal was light about 1 sec. and dark about 10 sec. The corner reflector was bedded mechanically into the polystyrol foam sphere, about 65 cm in diameter.

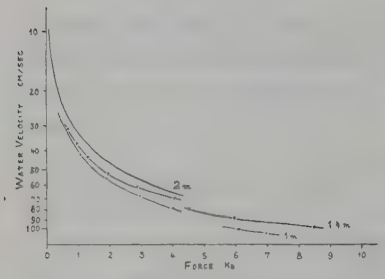

Fig. 2. Drag forces of the drogue system.
—·— observed, 1 m of pole
—×— observed, 1.4 m of pole
—— computed, 2 m of pole

Fig. 2 shows a plot of drag force as a function of speed through the water. These drag forces at different speeds measured by the submerged-body dynamometer for a surface float consisting of float A (submerged the hemispher), 1 or 1.4 m length of pole and battery case at an experimental state. And then the drag force at the working state was computed by the extrapolation for 2 m length of pole, and corrections to reduce the drag velocities to current velocities were obtained.

The float A was connected to the float B with manila rope, and the suspension wire, piano wire of diameter 0.8 mm, was joined to the bottom of the float B. The length of wire was previously adjusted according to the depth of measurement and winded on a wooden drum. The both ends of wire were crimped with thimbles and leader sleaves. These crimps served to connect the wire to the parachute and the float with shackle.

3. *Parachute and release*

The parachute used has an effective cross section of about 18.5 sq. m when completly open, and they are almost weightless in water. At the apex of parachute, a weight of 9 Kg. was connected with neylon cords as a sinking weight besides the parachute weight of 9 Kg. Between the parachute and the sinking weight, a simple release apparatus was inserted. This sinking weight serve to sink the

parachute in closed state to the planned depth. Here, the additional float B served as a signalling device. When the parachute was at depth, this float B submerged under the additional sinking weight, but reappeared when this weight was released.

A small bullet made of wheat gluten, "budodama", was used as a release apparatus reported by Takenouti and co-operator (1956). Preliminary experiments showed that it was strong enough to sustain a sinking weight and dissolved in sea water with almost constant speed irrespective of water temperature. The budodama was wrapped with bolting silk, the hems were passed through a metal ring and tied with the sinking weight. This ring was connected to the apex of parachute with nylon cord. When the budodama of 2.5 cm in diameter was wrapped with bolting silk of No. 000 and the diameter of ring was 1.5 cm, the sinking weight was to be released in sea water in 40 to 60 minutes, judging from the results of preliminary experiments. This release apparatus is very suitable for the measurement in some hundreds meter layer.

4. Setting of drogue

The float A and B were at first set adrift from the stern of the ship, then the ship went ahead very slowly (about 0.5 knot) paying out the suspension wire, an end of it was connected to the float B previously. When all of the suspension wire was payed out, the other end of the wire was hold with thimble and the parachute weight was connected quickly, then the parachute was poured, the sinking weight was thrown into the sea and soon the parachute weight too. When the whole drogue system was set adrift, it was necessary to watch the float B carefully. The additional float B was at first floating more than half of it above the surface, after a while it sunk beneath the sea surface, and this fact showed that the parachute reached to the depth. Then the float B reappeared to the sea surface, and this fact showed that the sinking weight was released and the parachute was opened. Thus, the current was measured by tracing the movement of the float A. The ship position was fixed with the Loran, and the position of float relative to the ship and the distance to the float from the ship were measured with the marine radar.

The complete account of data and results of measurement are discussed by Takenouti's paper of this volume.

5 Summary

1) The parachute drogue system was constructed for the measurement of

subsurface ocean currents.

2) It was found that this drogue is very useful equipment for the study of the subsurface current in the cold-belt along the northern boundary of Kuroshio.

Acknowledgment

We wish to express our thanks to Dr. Inui of the Tokyo University for the measurement of the drag force by the submerged-body dynamometer.

References

CROMWELL, T., R.B. MONTOGOMERY, and E. D. STROUP (1954): Equatorial undercurrent in the Pacific Ocean revealed by new methods, *Science*, **119**, 648-649.

STOMMEL, H. (1954): Serial observations of drift currents in the central North Atlantic Ocean, *Tellus*, **6** 203-214.

TAKENOUTI, Y., J. MASUZAWA, T. YASUI, A. OHKUBO, and S. NAKAI (1956): Current measurements in the Kuroshio with the parachute current drogue (in Japanese), *Oceanogr. Rep.* J.M.A., **5**, 157-169.

VOLKMANN, G., J. KNAUSS and A. VINE (1956): The use of parachute drogues in the measurement of subsurface ocean current, *Trans., American Geoph Union*, **37**. 573-577.

The Oceanographical Magazine
Vol. 10, No. 1 June 1958

Measurements of Subsurface Current in the Cold-belt along the Northern Boundary of Kuroshio

By

Yoshitada TAKENOUTI

1. *Introduction*

Multiple Ship Survey[1] in the polar front region had operated in June to July 1957 as a program of the International Geophysical Year. The survey was composed of several operations; these operations were named CM, GS–1, PD–1, GS–2, PD–2, GS–3, IW and GS–4. In the operation PD–1 and PD–2, which were operated during from 19th to 22nd, June and from 25th to 26th, June respectively, the subsurface current was measured with parachute drogue. The author wishes to discuss the results[2] of subsurface current measurements, and to explain how the cold belt along the northern boundary of Kuroshio is formed. As is discussed by J. Masuzawa[3] the oceanographic conditions along the Kuroshio, it showed remarkable waving during the period of survey and accompanied with the waving the cold belt to the north of Kuroshio varied its shape and localities, although it was always observed during the survey.

2. *Method of Measurement*

For the construction of parachute-drogue which was used in the present measurement, readers may refer to Kawamoto's[4] papers. The lengths of music wire suspending a parachutes were 75, 125, 250 and 750 m, they are called 50 m, 100 m, 200 m and 600 m-drogue respectively although the depth of parachute was not exactly at these depth.

The position of drogue was fixed against the ship with RADER, while the ship position was fixed with LORAN. The surface current and the surface wind were also measured, and using these data corrections for drift due to wind and surface current were computed. The largest drift due to wind and surface current was met at, but the correction was only 0.2 knots (about 1/10 of the subsurface current). Therefore, although Fig. 1 is illustrating the position of

parachute-drogue, it may consider that the figures are illustrating the movement of water-parcel at the depth of parachute.

The water-temperature down to the 250 m were also measured with bathythermograph. In the figures, temperature distribution at 100 m layer before, during and after the current measurements are also illustrated. As noticeable from the figure, the drogues were liberated in a cold belt at the northern boundary of the stream axis of Kuroshio.

In PD-1, 50 m, 200 m and 600 m-drogues were purchased for about 48 hours, in the figure, however, the positions for several hours at the beginning were omitted in order to avoid the doubt whether the parachute had already opened or not. In PD-2 the operation was only conducted for 24 hours owing to the damage of parachute due to rough weather, and 50 m, 100 m and 200 m-drogues were employed.

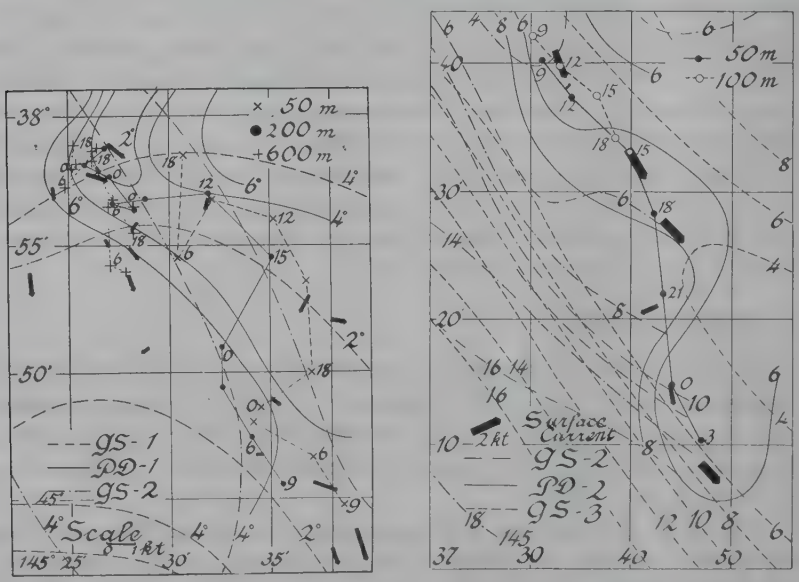

Fig. 1. Showing the drift of parachute drogues from June 20 to 22 (a) and from June 25 to 26 (b) and the isotherms of 100 m layer before, during and after the measurement of subsurface current. Numerals in the figure denote the time when the drogue is at the position indicated.

3. *Discussions for the results*

In PD-1 the 600 m drogue moved 5 miles southwards during 42 hours, the velocity is about 0.1 knots. Oceanographic observations had been made frequently in this region, the results of these observations showed that at the depth of 600 m the water-type belongs to the deep-water of North-Pacific originated from sub-arctic area.[5] The deep water is generally flowing southwards below the strong eastwards current, Kuroshio, and its velocity about 2 to 3 miles per day.

The movement of 200 m drogue was very interesting, i.e. it moved almost similar with 600 m drogue till 2100 JST on 21st June, then its suddenly moved swifter than before.* The isotherms at 100 m layer during the current measurement, which were illustrated in the figure, showed that the 200 m drogue moved slowly in the very cold water-mass (characterized with the temperature at 100 m below 2°C) and became fast in the mixed water-mass (characterized with the temperature at 100 m above 2°C). As noticeable from the isotherms in 100 m layer[6] the Oyashio water had temperature below 2°C at 100 m layer. The movement of drogue shows that in the Oyashio water-masses water column below the layer of minimum temperature moves very slowly. Then it reached near the stream of Kuroshio, strong horizontal mixing taken place near the surface layer and then, also in the layer of 200 m layer, thus formed mixed

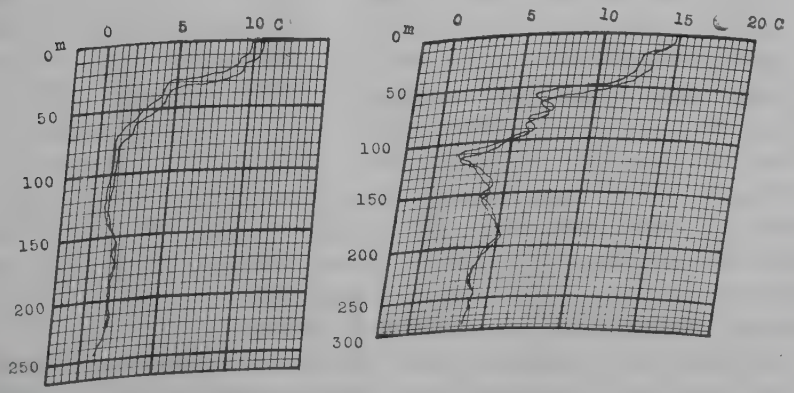

Fig. 2. Showing BT diagrams in the cold belt along the Kuroshio

* When the drogue was picked up, the parachute was still hung with music wire.

water is dragged by the Kuroshio then it begins to move rapidly.

In Fig. 2, BT records of two typical stations were reproduced. It shows that in the region of 2°C at 100 m layer, mixing process, which is revealed by zig-zag temperature-depth record, restricted near the surface, while in 4°C region, mixing process reached to the depth below 250 m.

In the region of mixed water mass, the 200 m drogue moved southeastwards with velocity of 0.9 knots. It was also found[6] that the axis of Kuroshio moved southwards with a speed of 12 miles per day. Therefore it is quite clear that the southwards component of 200 m layer is related to the southwards movement of the stream axis. But it is impossible to infer which is the cause of this phenomena only from these results of measurements.

The movement of 50 m drogue was almost similar to that of 200 m drogue although it moved southeastwards with the almost same speed from the begining of measurement, and we can consider that the water column from 50 m to 200 m layers moves simultaneously. And cold water (below 2°C in 100 m) observed in GS-1 was disappeared in GS-2 while warm water (above 6°C in 100 m) was replaced with waters of 4°C in 100 m. Thus cold water belt along the northern boundary of stream axis became very wide but the lowest temperature a little warmer. The relations between the movement of water column and the change in the temperature distribution will, however, be discussed in later.

In PD-2, both 50 m and 100 m drogues moved towards south south-east with a velocity of 2 knots and 1 knot respectively. The surface current were also 1.2—2.0 knots to south south-east, therefore the current was almost same from the surface to 100 m in direction but in magnitude, at 100 m it was about a half to the surface. The drogue were liberated in the mixed water-mass where, temperature at 100 m was above 6°C. This water-masses flowed away during the operation PD-2 and occupied by water below 4°C. In the operation GS-2, water below 4 C in 100 m had covered comparatively wide area near 38°N, therefore it seemed that these colder water-mass was following the warmer water-mass and flowed towards south south-east. The vertex of cold water-mass moved with a velocity of Ca. 1 knot and this was almost same to that of the 100 m-drogue.

The cold water belt along the northern boundary of Kuroshio was, therefore, formed by horizontal translation of cold (Oyashio) water-mass. The cold water of below 2°C in 100 m layer died away during PD-1, and this could not be explained, however, only by the horizontal translation. The most violent cyclone

during the period of survey had passed on 17th, westerly wind before the cyclone had changed into easterly wind, the former acted as to increase the velocity of Kuroshio current and the later, decrease it. Accompanied with the velocity change the thickness of the surface layer varied and resulted ascending or descending motion of discontinuous layer. Thus, the water of below 2°C formed in GS-1 was disappeared in GS-2 in 100 m layer.

4. *Summary*

1. The subsurface current was measured with parachute drogue, at the northern boundary of Kuroshio.

2. With the southward movement of stream axis, water at 200 m layer was also moved southwards.

3. The cold water belt along the northern boundary of Kuroshio was formed and flew away by the horizontal translation of Oyashio water-masses, the upwelling or sinking were also accompanied with the horizontal motion.

4. Mixing between Oyashio and Kuroshio water-masses were very remarkable at the boundary, the process of mixing was made clear.

Reference

1) Oceanographical Section, JMA: Report of Multiple ship survey in the polar front region from June to July, 1957 (Oceanographic Project for the I.G.Y.), The Oceanographical Report, J.M.A. Vol. 6(4) 43 pp., 1957.
2) The data were obtained from Oceanographic Data No. 181—196, NCIGY, JSC.
3) J. Masuzawa: This volume pp. 1—8.
4) T. Kawamoto: This volume pp. 9—12.
5) For example: The oceanographic Report C.M.O. 4(3) pp 1—10, 1955.
6) J. Masuzawa: loc. cit.

The Oceanographical Magazine
Vol. 10. No. 1 June 1958

The Response of a Stratified, Bounded Ocean to Variable Wind Stresses.*

By

Takashi Ichiye**

1. *Introduction*

One of the most interesting and important problems in physical oceanography is to know how oceanic circulation responses to variable wind stresses. The author published a theory of time-dependent wind-driven circulation in a bounded ocean about seven years ago (Ichiye, 1951), which was shown by Veronis and Morgan (1955) to be incorrect owing to the neglect of the divergence effect, and they gave a more complete theory including this effect. These works treated the problem in a homogeneous ocean. On the other hand, the density stratification is more or less important in the response problem, since in a stratified ocean internal mass adjustment may cause a different mode of motion from a homogeneous ocean. Recently two interesting papers of Charney (1955) and Veronis and Stommel (1956) have been published along this approach, treating a model of two-layered ocean without boundary, which are referred as Ch and VS hereafter. The present paper is only a trivial extension of these two works, just including a frictional force and west and east coast. The historical sketch of the problem and bibliography are given in VS.

Here we treat a two-layered ocean in β-plane with a east and west coast of straight line. As already pointed out in VS, the complete boundary condition, particularly at the west coast, should be non-linear, since inertia terms are predominant near the west coast, owing to a rapid change of vorticity in zonal direction, so that the linearized vorticity equation is no more valid there. However, such condition makes the mathematical treatment of the problem almost prohibitive. Therefore here we treat a simplified boundary condition of linear

* Woods Hole Oceanographic Institution Contribution No. 963
** Woods Hole Oceanographic Institution and also Japan Meteorological Agency

type and instead we introduce a frictional force. Such procedure might be permissible as the first step towards under-standing more realistic situation, as in the theory of stationary wind-driven oceanic circulation the frictional boundary solution still have a position as a simple picture of the first approximation about oceanic circulation instead of more reasonable inertia boundary theory.

In fact, the introduction of the frictional force seems to be inevitable, so far as we assume that the linearized vorticity equation is valid even near the west coast, because if we neglect the friction in a ocean with east and west coast the boundary conditions at these two coasts give the solution wildly oscillating as indicated in a private manuscript of Dr. Munk (1957). In such situation, only an introduction of the friction makes the physical interpretation of the solution possible by decreasing the amplitude of such solution rapidly from the coast, as will be stated later.

2. *Derivation of the vorticity equations*

The model considered here is essentially the same as that used in Ch and VS, where it consists of two layers of homogeneous water separated by a surface of discontinuity wind stresses act as a body force only in the upper layer. Then the equations of motion and continuity in two layers are given by

$$\frac{\partial u}{\partial t}-fv=-g\frac{\partial(\eta+\eta')}{\partial x}+\frac{\tau_x}{H}+F_x \tag{2.1}$$

$$\frac{\partial v}{\partial t}+fu=-g\frac{\partial(\eta+\eta')}{\partial y}+\frac{\tau_y}{H}+F_y \tag{2.2}$$

$$\frac{\partial \eta}{\partial t}+H\left(\frac{\partial u}{\partial x}+\frac{\partial v}{\partial y}\right)=0 \tag{2.3}$$

$$\frac{\partial u'}{\partial t}-fv'=-g\frac{\partial(\varepsilon\eta+\eta')}{\partial x}+F_x' \tag{2.4}$$

$$\frac{\partial v'}{\partial t}+fu'=-g\frac{\partial(\varepsilon\eta+\eta')}{\partial y}+F_y' \tag{2.5}$$

$$\frac{\partial \eta'}{\partial t}+H'\left(\frac{\partial u'}{\partial x}+\frac{\partial v'}{\partial y}\right)=0 \tag{2.6}$$

where the terms with blime define the quantities in the lower layer and x and y are the horizontal coordinates, directed eastwards and northwards, respectively; H is the equilibrium thickness of the upper layer; η is the deviation of H; τ_x, τ_y are wind stress component; ε is the density ratio ρ/ρ'; and F_x, F_y are component of frictional force: and other quantities are defined by conventional symbols.

Cross differentiating (2.1) and (2.2) and (2.4) and (2.5), we obtain the vorticity equations

$$\frac{\partial \zeta}{\partial t}-\frac{f}{H}\frac{\partial}{\partial t}\eta+\beta v=\frac{1}{H}\operatorname{curl}\boldsymbol{\tau}+\operatorname{curl}\boldsymbol{F} \tag{2.7}$$

$$\frac{\partial \zeta'}{\partial t}-\frac{f}{H'}\frac{\partial}{\partial t}\eta'+\beta v'=\operatorname{curl}\boldsymbol{F}' \tag{2.8}$$

where $\zeta=\partial v/\partial x-\partial u/\partial y$.

In Ch velocity components are assumed to be given by geostrophic relationship. However, in this paper we derive symbolic expression for velocity components from the equations of motion, by putting

$$\boldsymbol{F}=-k\boldsymbol{v},\ \boldsymbol{F}'=-k'\boldsymbol{v}';\ \left(\frac{\partial}{\partial t}+k\right)=p,\ \left(\frac{\partial}{\partial t}+k'\right)=p'$$

where k and k' may be taken as a linear operator, which indicates horizontal eddy viscosity term and/or a frictional coefficient simply proportional to the velocity itself such as $-A\nabla^2+k$ and p, p' are linear operator. Then, eliminating v or u from (2.1) and (2.2) or from (2.4) and (2.5), we obtain

$$(p^2+f^2)u=pH_x+fH_y \tag{2.9}$$

$$(p^2+f^2)v=pH_y-fH_x \tag{2.10}$$

$$(p'^2+f^2)u'=p'H_x'+fH_y' \tag{2.11}$$

$$(p'^2+f^2)v'=p'H_y'-fH_x' \tag{2.12}$$

where

$$H_x=-g\frac{\partial(\eta+\eta')}{\partial x}+\frac{\tau_x}{H},\ H_y=-g\frac{\partial(\eta+\eta')}{\partial y}+\frac{\tau_y}{H}$$

$$H_x'=-g\frac{\partial(\varepsilon\eta+\eta')}{\partial x},\ H_y'=-g\frac{\partial(\varepsilon\eta+\eta')}{\partial y}$$

When we assume that the period of the motion is longer than several days and the coefficient of friction has the similar order of magnitude to such period, then the ratio of p or p' to f is less than 0.1, since $p\sim p'<10^{-5}$. Hereafter we shall make it a rule to neglect the terms of the order less than 10^{-2} of main terms, then we can neglect p^2 and p'^2 in the left hand side of the equations (2.9) to (2.12). Thus we can obtain ζ by use of (2.9) to (2.12) as

$$\zeta=\frac{g}{fH}\left(\nabla^2\overline{\eta+\eta'}-\frac{1}{g}div\tau+\frac{p}{gf}\operatorname{curl}\tau\right)+\frac{\beta}{f^2}\left(H_y+\frac{2p}{f}H_x\right) \tag{2.13}$$

$$\zeta'=\frac{g}{fH'}(\nabla^2\overline{\varepsilon\eta+\eta'})+\frac{\beta}{f^2}\left(H_y'+\frac{2p'}{f}H_x'\right) \tag{2.14}$$

where the last two terms including β is originated from a result of taking into

account of variation of f in differentiation with y, and the ratio of these terms to the ones corresponding to the geostrophic assumption is $\frac{\beta}{f^2H}\frac{\partial(\eta+\eta')}{\partial y} : \frac{g}{fH}$

$\nabla^2\overline{\eta+\eta'}\sim\frac{\beta}{f}\left(\frac{\partial}{\partial y}\right)^{-1}$ which seems to be larger than 0.2 for a circulation with a dimension of larger than 1000 km or 10^8 cm, so that we retain them for some time.

When we put the equations for ζ and v into (2.7) and (2.8) and neglect the terms with a factor p^2/f^2, we obtain

$$\left(p\nabla^2-\frac{2p}{f}\beta\frac{\partial}{\partial y}+\beta\frac{\partial}{\partial x}\right)\overline{\eta+\eta'}-\frac{f^2}{gH}\frac{\partial}{\partial t}\overline{\eta}=\frac{f}{gH}\left(\mathrm{curl}\,\tau+\frac{p}{f}div\,\tau\right.$$
$$\left.+\frac{\beta}{f}\tau_x-\frac{2\beta p}{f^2}\tau_y\right) \qquad (2.15)$$

$$\left(p'\nabla^2-\frac{2p'}{f}\beta\frac{\partial}{\partial y}+\beta\frac{\partial}{\partial x}\right)\overline{\varepsilon\eta+\eta'}-\frac{f^2}{gH'}\frac{\partial}{\partial t}\eta'=0 \qquad (2.16)$$

These are different from the original equations of Ch in term $\frac{2p}{f}\beta\frac{\partial}{\partial y}$ in the left hand side and in the last three terms for the disturbing force, which are all originated from derivation of velocity components different from geostrophic assumption.

In order to simplify the mathematical treatment hereafter, we assume that $k=k'$ which is defined as a numerical factor, and we separate the motion into a barotropic and baroclinic mode as in Ch and Vs. Then we obtain

$$\left(\frac{\partial}{\partial t}+k\right)\left(\nabla^2-2\frac{\beta}{f}\frac{\partial}{\partial y}\right)R_j+\beta\frac{\partial R_j}{\partial x}-\lambda_j^{-2}\frac{\partial}{\partial t}R_j=\frac{f\sigma_j}{gH}F \qquad (2.17)$$

where we put $F=\mathrm{curl}\,\tau+\frac{p}{f}\,\mathrm{div}\,\tau+\frac{\beta}{f}\tau_x-\frac{2\beta p}{f_2}\tau_y$ and $j=r$ or l, and almost similar symbols are used as in Ch, except suffix r and l defines the quantities associated to barotropic and baroclinic mode, respectively and thus

$\lambda_r^2=g(H+H')/f^2$, $\lambda_l^2=g'H/f^2$, $\sigma_r=r$, $\sigma_l=-1$, $g'=g(\rho'-\rho)/\rho$, $r=H/H'$

3. *Solution for moving wind stress in a bounded ocean*

As the simplest case of variable wind stress, suppose a wind system moving at a constant speed as a sine wave given by

$$F=F_0\cos(\nu t\pm\theta x)\sin\mu x \qquad (3.1)$$

This kind of disturbing force seems to be most interesting, since any type of

wind system might be obtained by a linear combination of such harmonic wave train.

When we assume the coasts at $x=a$ and $x=-a$, velocity components u and u' should vanish there. These boundary conditions are expressed in terms of R_j as

$$\text{at } x=\pm a\,;\ \frac{\partial R_j}{\partial y}+\frac{1}{f}\left(\frac{\partial}{\partial t}+k\right)\frac{\partial R_j}{\partial x}=\frac{\sigma_j}{gH}\left\{\tau_y+\frac{1}{f}\left(\frac{\partial}{\partial t}+k\right)\tau_x\right\} \tag{3.2}$$

As seen at once, these conditions are in homogeneous type, so that we have to divide the solution into two parts, in order to satisfy both the fundamental equation and boundary conditions. Therefore, we put $R=R_{\mathrm{I}}+R_{\mathrm{II}}$, where R_{I} and R_{II} satisfy next relations, respectively $O_fR_{\mathrm{I}}=F_f$, $O_bR_{\mathrm{I}}=O$; $O_fR_{\mathrm{II}}=0$ $O_bR_{\mathrm{II}}=F_b$ in which O_f and O_b are the operational form of the left hand side of the equation (2.17) and the boundary conditions (3.2), and F_f and F_b represents symbolically the right hand side of these relations.

First, we try to obtain the solution R_{I}, and for this purpose we put $F=F_0k[\,(e^{i(\nu t+\theta x)+i\mu y}-e^{i(\nu t+\theta x)-i\mu y})/2i]$ and express the solution corresponding to the term with factor $e^{i\mu y}$ and $e^{-i\mu y}$ as R_1 and R_2, respectively. Further when we put $R_s=K_sP_s(x)e^{i\nu t\pm i\mu y}$, then we obtain the solution of $P_s(x)$ which satisfy the next relation

$$K_s\left\{(i\nu+k)\left(P_{xx}-\mu^2P\mp2\frac{\beta}{f}i\mu P\right)+\beta P_x-i\lambda^{-2}\nu P\right\}=\frac{F_0f6}{2gHi}e^{i\theta x} \tag{3.3}$$

such as

$$P_s=\frac{1}{2}(e^{i\theta x}+A_{1s}e^{i\delta_1 x}+A_{2s}e^{i\delta_2 x}),\quad s=1,2 \tag{3.4}$$

where

$$K_s=\frac{F_0f\sigma}{gH\left\{(\nu-ik)\left(\theta^2+\mu^2\pm2\frac{\beta}{f}\mu i\right)-\beta\theta+\lambda^{-2}\nu\right)} \tag{3.5}$$

and δ_1 and δ_2 are two roots of the characteristic equation

$$\delta^2-\frac{\beta}{\nu-ik}\delta+\frac{\lambda^{-2}\nu}{\nu-ik}+\mu^2\mp2\frac{\beta}{f}\mu i=0 \tag{3.6}$$

and A_{1s} and A_{2s} are constants determined by the boundary conditions at $x=\pm a$, and the suffix $s=1$ and 2 define the quantities corresponding to upper and lower sign in equations (3.3), (3.5) and (3.6), respectively. Needless to say, σ and λ have the suffix r and l indicating barotropic or baroclinic mode, which are

omitted here for avoiding confusion. The boundary conditions are now expressed by

at $x=\pm a$; $e^{i\theta x}(1\pm q\theta i)+A_{1s}e^{i\delta_1 x}(1\pm q\delta_1 i)+A_{2s}e^{i\delta_2 x}(1\pm q\delta_2 i)=0$ (3.7)

where $q=(\nu-ik)/f\mu$ and double signs correspond to suffix $s=1$ and 2.

Then the constants A_{1s} and A_{2s} are given by

$$A_{1s}=(1\pm q\theta i)\sin a(\delta_2-\theta)/(1\pm q\delta_1 i)\sin a(\delta_1-\delta_2)$$
$$A_{2s}=-(1\pm q\theta i)\sin a(\delta_1-\theta)/(1\pm q\delta_2 i)\sin a(\delta_1-\delta_2) \quad (3.8)$$

which are the same explicit form for $s=1$ and 2, since the difference is included implicitely in δ_1 and δ_2. The resultant expression for R_{I} is given by

$$R_{\mathrm{I}}=\frac{1}{2}k\{K_1P_1(x)e^{i(\nu t+\mu y)}-K_2P_2(x)e^{i(\nu t-\mu y)}\} \quad (3.9)$$

The difference between K_1 and K_2 or P_1 and P_2 exists in the term $2\frac{\beta}{f}\mu i$ in the equations (3.5) or (3.6), or in other words the ratio $2\frac{\beta}{fu}$ determines the importance of this term, which may be neglected for $\mu>10^{-7}$ or for wind stress with a dimension in y-direction smaller than $\pi\times10^2$ km according to the criterion stated above for neglecting p^2 against f^2. In such case the solution (3.9) is expressed simply by

$$R_{\mathrm{I}}=k\{iKe^{i\nu t}(e^{i\theta x}\sin\mu y+e^{i\delta_1 x}A_{11}e^{i\mu y}-A_{12}e^{-i\mu y}+e^{i\delta_2 x}A_{21}e^{i\mu y}-A_{22}e^{-i\mu y})\} \quad (3.9a)$$

In any case, as shown in the equation for Ki in (3.5), the amplitude of the response of the ocean gives a resonance for some value of θ with positive value, or for the wave moving westwards, which was also pointed out in VS.

The solution R_{II} corresponding to the homogeneous fundamental equation and inhomogeneous boundary conditions is also expressed by the combination of two proper solutions of the equation (2.17) such as

$$R_{\mathrm{II}s}=(B_{1s}e^{i\delta_1 x}+B_{2s}e^{i\delta_2 x})e^{i(\nu t\pm\mu y)} \quad (3.10)$$

assuming that

$$\frac{\sigma}{gH}(\tau_y+\frac{p}{f}\tau_x)_{x=\pm a}=i\mu T_s(\pm a)e^{i(\nu t\pm\mu y)} \quad (3.11)$$

where the suffix $s=1$ or 2 corresponds to $e^{i\mu y}$ or $e^{-i\mu y}$. The real value of the solution R_{II} may be obtained by taking the real or imaginary part of the combination of $R_{\mathrm{II}1}$ and $R_{\mathrm{II}2}$. For example, when the left hand side of the equation (3.11) is given as $\mu T\sin\nu t\cos\mu y$, then we take the imaginary part of $\frac{1}{2}(R_{\mathrm{II}1}-R_{\mathrm{II}2})$ for the real value of R_{II}. Therefore, here we give the value of the solution $R_{\mathrm{II}s}$ in

the complex form. The boundary conditions at $x=\pm a$ becomes for the function given by (3.10)

$$(1+iq\delta_1)B_{1s}e^{i\delta_1 x}+(1+iq\delta_2)B_{2s}e^{i\delta_2 x}=T(\pm a) \tag{3.12}$$

then

$$\begin{aligned} B_{1s}&=\{T_s(a)e^{-i\delta_2 a}-T_s(-a)e^{i\delta_2 a}\}/2(1+iq\delta_1)\ \sin(\delta_1-\delta_2)a \\ B_{2s}&=\{T_s(-a)e^{i\delta_1 a}-T_s(a)e^{-i\delta_1 a}\}/2(1+iq\delta_2)\ \sin(\delta_1-\delta_2)a \end{aligned} \tag{3.13}$$

thus

$$\begin{aligned} R_{IIs}=\frac{e^{i(\nu t\pm\mu y)}}{2\sin(\delta_1-\delta_2)a}\Big[&\frac{e^{i\delta_1 x}}{1+iq\delta_1}\{T_s(a)e^{-i\delta_2 a}-T_s(-a)e^{i\delta_2 a}\} \\ &+\frac{e^{i\delta_2 x}}{1+iq\delta_2}\{T_s(-a)e^{i\delta_1 a}-T_s(a)e^{-i\delta_1 a}\}\Big] \end{aligned} \tag{3.10a}$$

$$(s=1 \text{ and } 2)$$

The numerical examples of these solutions are given in the next section, and here only the estimation of the ratio of the order of R_{I} and R_{II} is stated. For complete discussion about the comparison of these two functions we have to know the behaviour of the functions regards to x, but this should be done in next section, and we cansider the ratio of the factor of $e^{i\delta_1 x}$ and $e^{i\delta_2 x}$ in both functions, which is given by

$$\begin{aligned} R_a=|B|:|KA| &\fallingdotseq \frac{\sigma|\boldsymbol{\tau}|}{|1+iq\delta||\sin(\delta_1-\delta_2)a|\mu gH}:\frac{f\sigma\ \mathrm{curl}\,\boldsymbol{\tau}|1+q\theta i||\sin a(\delta-\theta)|}{|1+iq\delta||\sin(\delta_1-\delta_2)a|IgH} \\ &\fallingdotseq |\boldsymbol{\tau}|I/\mu f\ \mathrm{curl}\,\boldsymbol{\tau} \end{aligned} \tag{3.14}$$

where

$$I_j=(\nu-ik)\left(\theta^2+\mu^2\pm 2\frac{\beta}{f}\mu i\right)-\beta\theta+\lambda_j^{-2}\nu \tag{3.15}$$

On the other hand, assuming $\boldsymbol{\tau}\sim e^{i(\mu y+\theta x)}$ then $\mathrm{curl}\,\boldsymbol{\tau}\sim\boldsymbol{\tau}(|\mu|+|\theta|)$. Thus we have $R_a\fallingdotseq I/\mu f(|\mu|+|\theta|)$. When we consider only the negative value of θ, we can avoid the resonance phenomenon and in such case I_j ranges from 10^{-19} to 10^{-21} for the range of ν from 10^{-5} to 10^{-8} and μ, θ from 10^{-7} to 10^{-8}. Thus we get the following table of R_a for μ, $\theta=10^{-8}$ and 5×10^{-8}, the former of which gives the maximum values of the ratio R_a for the range of ν between 10^{-5} and 10^{-8}.

As seen in this table, the effect of the second solution which is originated from the wind stress acting near the coast becomes more important in the baroclinic mode than in barotropic one and also for a rapidly changing wind system of a larger scale than for a slowly changing small scale wind system, although the amplitude of the second solution diminishes from the coast, as will be shown in the next section.

Table 1

ν (sec^{-1})	10^{-5}	10^{-6}	10^{-7}	10^{-8}
$R_a r1$	0.2	0.1	0.1	0.1
$R_a l1$	4.2	4.3	0.5	0.15
$R_a r2$	0.2	0.07	0.04	0.04
$R_a l2$	3.6	0.4	0.07	0.04

(Suffix r=barotropic l=baroclinic
Suffix 1 for $u=\theta=10^{-8}$(cm^{-1}), Suffix 2 for $u=\theta=10^{-7}$(cm^{-1}))

4. The amplitude of the response of the ocean.

As seen in the expression of R_I in (3.9), the order of the magnitude of the response is primarily determined by the values of K, so we discuss in this section the results of the numerical values computed by use of the physical constants shown in Table 2.

Table 2

f	β	H	H'	a	$1-\in$	λ_r^{-2}	λ_e^{-2}	r	$f\sigma_r/gH$	$f\sigma_e/gH$
10^{-4}	2.10^{-13}	6×10^4	4×10^5	3×10^8	2.10^{-3}	2.5×10^{-17}	0.83×10^{-13}	0.15	2.55×10^{-13}	1.7×10^{-12}

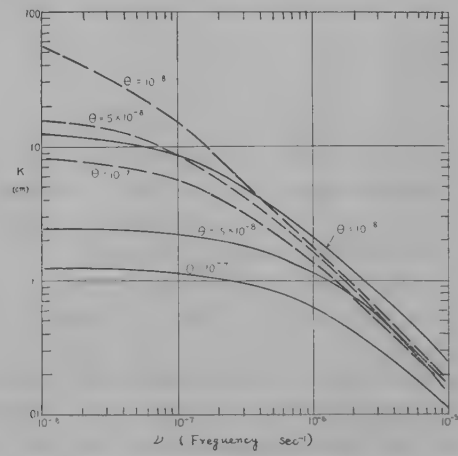

Fig. 1. K for $\mu=10^{-7}$.
(Full lines are barotropic, broken lines are baroclinic. curl $\tau=10^{-7}$)

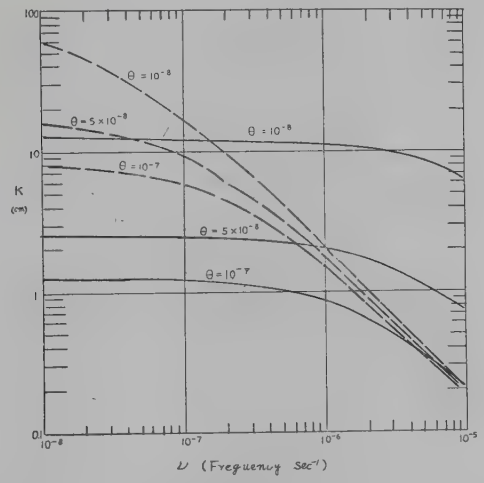

Fig. 2. K for $\mu=10^{-8}$
(Full lines are barotropic, broken lines are baroclinic. curl $\tau=10^{-7}$)

In Fig. 1 and 2 the values of K for $\mu=10^{-7}$ and 10^{-8} and for curl$\boldsymbol{\tau}=10^{-7}$ with the value of $\theta=10^{-7}$, 5×10^{-8}, 10^{-8} are shown as a function of ν. These curves indicate the interesting features of the response that the baroclinic mode increases more rapidly than barotropic as a frequency af the wind system decreases, which gives a quite measurable baroclinic amplitude of the sea surface more than 10 cm for ν less than 10^{-7} or period longer than 70 days with wave numbers less than 5×10^{-8}, although practically the value of curl of wind stress seems to decrease as decreasing frequency, so that such values as 10^{-7} is rather uncommon for longer period fluctuation of the wind system. Therefore the true values of K seems to be less than shown in these curves for smaller values of ν.

The amplitudes of both modes show the increase for constant value of curl$\boldsymbol{\tau}$ and ν as decreasing wave numbers θ and μ, the curves suggesting the changes in θ affects the values of K more than that in μ. However, this is also to be modified somewhat, since in real wind system curl$\boldsymbol{\tau}$ may be changed as according to the scale of the wind system as well as to the frequency. Therefore, as stated in the end of the last section, when we assume $\boldsymbol{\tau}\sim e^{i(\mu y+\theta x)}$, we can take curl $\boldsymbol{\tau}=|\boldsymbol{\tau}|(|\mu|+\theta|)$. Thus the values of K are computed as a function of θ and the result is shown in Fig. 3, where $|\boldsymbol{\tau}|$ is taken as 1. These curves indicate that the amplitude

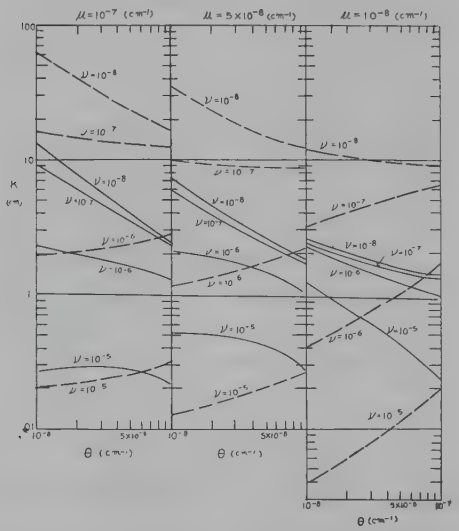

Fig. 3. K as a function of θ (wave number in y direction)
(Full lines are barotropic, broken lines are baroclinic)

of the baroclinic mode with larger frequency ν than 10^{-7} rather decreases with decreasing wave number of θ and μ and these of barotropic mode remain increasing as decreasing wave number θ, though they decrease for decreasing μ. In any way the baroclinic amplitudes have a measurable magnitude for $\nu<10^{-7}$ corresponding to morerealistic value of the curl τ, suggesting that the present problem should have close relationships to the annual change of the mean sea level.

Next the amplitudes K for westwards moving wind system are computed with the same constants, which show the resonance phenomenon for some wave number $\theta=\theta_c$, where the value of K becomes infinitive when we disregard the term $2\frac{\beta}{f}\mu i$ and frictional coefficient k in (3.5) or (3.15). We put θ_c as the value of θ making $I_0=0$, where I is taken as the expression of I_j without the term $2\frac{\beta}{f}\mu i$ and k, then the value of I_j at $\theta=\theta_c$ is given by

$$I_{jc}=-ik(\theta_c^2+\mu^2)\pm 2\frac{\beta}{f}\mu\nu i\mp 2\frac{\beta}{f}\mu k$$

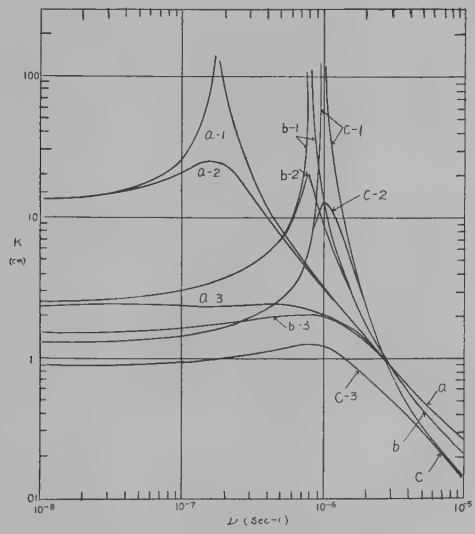

Fig. 4. K for westward moving disturbance of barotropic mode, with $\mu=10^{-7}$. (a: $\theta=10^{-8}$, b: $\theta=5\times10^{-8}$, c: $\theta=10^{-7}$, 1: $k=10^{-8}$, 2: $k=10^{-7}$, 3: $k=10^{-6}$)

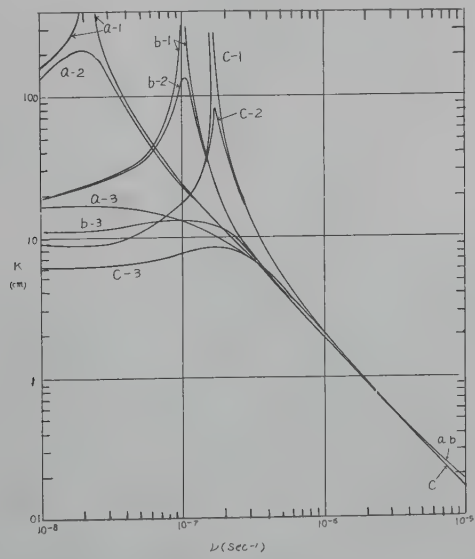

Fig. 5. K for westward moving disturbance of baroclinic mode, with $\mu=10^{-7}$ (a: $\theta=10^{-8}$, b: $\theta=5\times10^{-8}$, c: $\theta=10^{-7}$; 1: $k=10^{-8}$, 2: $k=10^{-7}$, 3: $k=10^{-6}$)

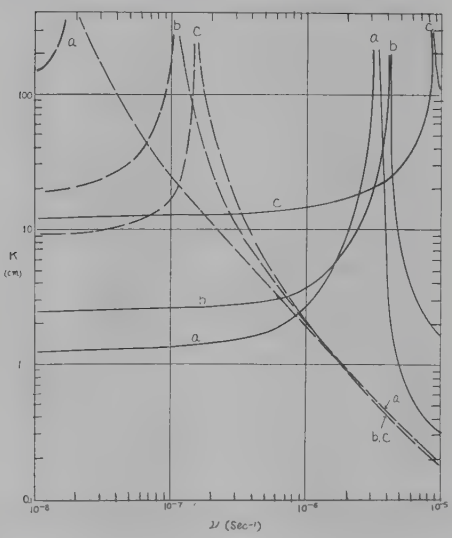

Fig. 6. K for westward moving disturbance with $\mu=10^{-8}$ and $k<10^{-8}$
(Full lines are barotropic, broken lines are baroclinic)
(a: $\theta=10^{-8}$, b: $\theta=5\times10^{-8}$, c: $\theta=10^{-7}$)

which prevent the infinitive value of K at $\theta=\theta_c$. The effect of friction and $2\frac{\beta}{f}\mu i$ term may be more or less important near the point θ_c, and in other part of the region they are almost negligible as shown in the figures 4, 5 and 6.

5. *Free waves under the influence of friction.*

The terms having a factor $e^{i\delta_1 z}$ or $e^{i\delta_2 z}$ in P_s of (3.6) or in $R_{\mathrm{II}s}$ of (3.10a) represent free waves in a stratified ocean of planetary type, which is induced by moving disturbance, not directly but rather owing to the effect of the boundaries which reflect the forced waves accompanying with the moving wave system. The wave number δ_1 and δ_2 such waves are given by the equation (3.6) or

$$\delta_s=\frac{\kappa}{1-in}\pm\left\{\left(\frac{\kappa}{1-in}\right)^2-\frac{\lambda_j^{-2}}{1-in}-\mu^2\pm2\frac{\beta\mu}{f}i\right\}^{\frac{1}{2}} \qquad (5.1)$$

where $s=1$ corresponds to the plus sign, and we put $\kappa=\beta/2\nu$, $n=k/\nu$ The relative magnitude of each term in this equation changes for differcent paysical conditions,

but when we consider the range of ν between 10^{-5} and 10^{-8} we have the following list of the order of magnitude of each term within the root sign.

ν	10^{-5}	10^{-6}	10^{-7}	10^{-8}
κ^2	10^{-16}	10^{-14}	10^{-12}	10^{-10}
$n(k=10^{-7})$	$10^{-1}0$	10	1	10

μ^2	10^{-14}	10^{-16}
$2\frac{\beta\mu}{f}$	4×10^{-16}	4×10^{-17}

$\lambda^{-2}_r=2.5\times10^{-17}$ $\lambda^{-2}_l=8.3\times10^{-14}$

This list gives the rough idea about the relative importance of each term, and we can see that the contribution from $2\beta\mu/f$ is quite small except near $\nu=10^{-5}$ and also the same value of the frictional coefficient has more effect in smaller frequency region.

When we take into account of friction δ_s is generally complex, but even when we neglect the friction and $2\beta\mu/f$ term, still we have complex values of δ_s for a certain range of ν larger than a critical value defined by $\nu_c=\beta(\lambda_j^{-2}+\mu^2)^{-\frac{1}{2}}/2$ In such range δ_1 and δ_2 has imaginary part of the same value but opposite sign and therefore we have the term $e^{i\delta_1 x}$ which decreases exponentially as spart from the western coast and the term $e^{i\delta_2 x}$ which decreases in the same manner from the eastern coast. When the imaginary part of $a\delta_s\gg1$, we obtain the following simple expression for R_I

(in the western part)

$$R_I=\Re\left[K\{-\sin(\nu t-\theta x)\ \sin\mu y-iQ_1e^{i\nu t+i\delta_1(a+x)+ia\theta}\}\right]$$

(in the eastern part)

$$R_I=\Re\left[K\{-\sin(\nu t-\theta x)\ \sin\mu y-iQ_2e^{i\nu t+i\delta_2(x-a)+ia\theta}\}\right] \qquad (5.2)$$

where $Q_s=e^{i\mu y}(1+iq\theta)/(1+q\delta_s)-e^{-i\mu y}(1-iq\theta)/(1-iq\delta_s)$

As seen from the equation (5.1), the imaginary part of δ_s increases as increasing frequency for $\nu>\nu_c$, the free waves caused by the disturbance of shorter period attenuates more rapidly as apart from the coast.

In order to give the notion about the change of the values of δ_s as variable physical constants ν, μ and k, we compute the values of δ_s both for barotropic and baroclinic mode for the range of ν between 10^{-5} and 10^{-8} and for $\mu=10^{-7}$, 5×10^{-8}, 10^{-8} and for $k=0$, 10^{-8}, 10^{-7} from the equation (5.1). The results are shown in Table 3. Especially for the range of $\nu\leqslant10^{-6}$ and $\mu\leqslant5\times10^{-8}$ of barotropic mode and also for $\nu\leqslant10^{-7}$ and $\mu\leqslant10^{-7}$ of both modes we can use the following approximate formula for δ_s

Table 3

	10^{-5}	5×10^{-6}	10^{-6}	5×10^{-7}	10^{-7}	5×10^{-8}	10^{-8}
$\nu=\mu=10^{-7}$	0.1 + i	0.2 + 0.98i	1 + 0.05i	3.732, 0.268	20, 0.05	40, 0.025	200, 0.005
	,,	,,	1.094 + 0.117i	3.732 + 0.191i	19.8 + 1.98i	38.4 + 7.68i	100 + 100i
	,,	,,	0.906 − 0.097i	0.268 − 0.111i	0.05 − 0.005i	0.025 − 0.005i	0.005 − 0.005i
δ_r	,,	0 208 + 0.981i	1.31 + 0.415i	3.530 + 0.824i	9.95 + 10.05i	7.98 + 16.05i	1.98 + 19.9i
($\times10^{-7}$)	,,	0.192 ± 0.979i	0.67 − 0.217i	0.31 − 0.056i	0.05 − 0.05i	0.025 − 0.05i	0.005 − 0.05i
	0.1 + 3.06i	0.2 ± 3.03i	1 + 2.89i	2 ± 2.31i	20, 0.417	40, 0.208	200, 0.042
	,,	,,	0.98 + 2.90i	2 + 2.35i	19.8 + 1.97i	37.9 + 4.95i	100 + 100i
			1.02 − 2.87i	2 − 2.29i	0.45 − 0.01i	0.5 − 0.005i	0.088 − 0.005i
δ_l	0.087 + 3.06i	0.17 + 3.03i	0.88 + 2.95i	1.88 + 2.74i	9.54 + 10.05i	7.78 + 16.05i	1.94 + 19.85i
($\times10^{-7}$)	0.113 − 3.06i	0.23 − 3.03i	1.10 − 2.75i	1.96 − 1.98i	0.46 − 0.05i	0.22 − 0.05i	0.05 − 0.05i
$\mu=5\times10^{-5}$	0.1 ± 0.49i	0.2 ± 0.458i	1.87, 0.13	3.94, 0.16	19.8, 0.0125	40, 6.25×10^{-3}	200, 25×10^{-4}
	,,	,,	1.87 + 0.023i	3.94 + 0.081i	19.8 + 1.98i	38.4 + 7.64i	100 + 100i
			0.13 − 0.002i	0.16 − 0.001i	$(125-25i)\times10^{-4}$	$(63-25i)\times10^{-4}$	$(25-25i)10^{-4}$
δ_r	,,	0.202 + 0.462i	1.843 + 0.225i	3.73 + 0.76i	20 + 20i	8 + 16i	1.98 + 19.8i
($\times10^{-7}$)		0.198 − 0.454i	0.157 − 0.015i	0.11 + 0.01i	$(125-125i)\times10^{-4}$	$(63-125i)\times10^{-4}$	$(125-125i)\times10^{-4}$
	0.1 ± 2.93i	0.2 ± 2.93i	1 + 2.75i	2 + 2.14i	20, 0.417	40. 0.208	200. 0.042
	,,	,,	0.99 + 2.76i	2 + 2.18i	19.4 + 1.98i	38.2 + 7.64i	100 + 100i
	,,	,,	1.01 − 2.74i	2 − 2.10i	0.4 − 0.0025i	0.2 − 0.0025i	0.042 − 0.0025
δ_l	,,	,,	0.89 + 2.85i	1.88 + 2.56i	9.57 + 10i	7.8 + 16i	1.95 + 19.8i
($\times10^{-7}$)	,,	,,	0.11 − 2.65i	1.96 − 1.80i	0.42 − 0.125i	0.21 − 0.0125i	0.04 − 0.0125i
$\mu=10^{-8}\nu$	0.1 ± 0.05i	0.366, 0.034	2.005, 0.005	4, 25×10	10, 125×10	40, 625×10^{-5}	200, 5×10^{-5}
	,,	$0.366+88i\times10^{-5}$	1.995 + 0.02i	4 + 0.08i	19.8 + 1.98i	38.4 + 7.68i	100 + 100i
		$0.034-8i\times10^{-5}$	$0.005-5i\times10^{-5}$	$(125-5i)\times10^{-5}$	$(50-5i)\times10^{-5}$	$(25-5i)\times10^{-5}$	$(5-5i)\times10^{-5}$
δ_r	0.102 + 0.05i	$0.366+88i\times10^{-4}$	1.985 + 0.2i	3.74 + 0.77i	20 + 20i	8 + 16i	1.98 + 19.8i
($\times10^{-7}$)	0.098 − 0.05i	$0.034-8i\times10^{-4}$	$(50-5i)\times10^{-4}$	$(25-5i)\times10^{-4}$	$(12.5-5i)\times10^{-4}$	$(2.5-5i)\times10^{-4}$	$(0.5-5i)\times10^{-4}$
	0.1 ± 2.89i	0.2 ± 2.88i	1 ± 2.70i	2 ± 2.14i	20, 0.417	40, 0.21	200, 0.04
	,,	,,	0 98 + 2.72i	2 + 2.12i	19.4 + 1.89i	38.2 + 7.68i	100 + 100i
			1.02 − 2.70i	2 − 2.04i	$0.5-5i\times10^{-5}$	$0.2-5i\times10^{-5}$	$0.04-5i\times10^{-5}$
δ_l			0.87 + 2.80i	1.88 + 2.52i	9.58 + 10i	7.79 + 16i	1.96 + 19.8i
($\times10^{-7}$)	,,	,,	1.11 − 2.60i	1.96 − 1.76i	$0.42-5i\times10^{-4}$	$0.21-5i\times10^{-4}$	$0.04-5i\times10^{-4}$

(1) δ_r means barotropic, δ_l baroclinic.
(2) In the first line, the values of δ for $k=0$ are shown, where δ_1 is given by the plus sign or the larger value.
(3) In the second and third lines, δ for $k=10^{-8}$ and $k=10^{-7}$ are shown, where in each line upper figure indicates δ_1 and lower one δ_2.

$$\delta_{1,2}=\frac{\kappa}{1-n_i}\pm\left\{\frac{\kappa}{1-n_i}-\frac{\mu^2}{2\kappa}(1-n_i)-\frac{\lambda_j^{-2}}{2\kappa}\pm\frac{\beta\mu}{f\kappa}(i+n)\right\} \qquad (5.1a)$$

As seen in this table or from (5.1a), the real part of δ_1 of both modes, that is, a wave number for the free waves expressed by $e^{i\delta_1 x}$ exceeds 10^{-6} for $\nu=10^{-7}$, which gives the wave length less than $63km$ and also this wave length becomes shorter as increasing period of the wind system longer than about a half year. When the friction is neglected, these waves have a constant amplitude from east to west all over the ocean. Physical interpretation of such waves is quite difficult and also the evidence of their existense seems to be doubtful. Moreover, when we neglect the friction, we cannot obtain stationary solution which satisfys boundary conditions by decreasing ν towards zero. For, when $\nu\to 0$ and $k=0$, (2.17) becomes

$$\beta\frac{\partial R}{\partial x}=\frac{f\sigma}{gH}F \qquad (5.3)$$

and the solution of this equation can satisfy the boundary condition only at one coast. The generation of the wildly oscillating waves associated with $e^{i\delta_1 x}$ is due to the situation that additional boundary condition at onother coast is impressed to the solution of the above equation which permits only one boundary condition. Therefore, the introduction of the friction is quite reasonable not only from the mathematical point of view but also from physical one because with a finite k the equation (2.17) permits two boundary conditions, even when ν approaches to zero and in fact, it gives the solution treated by Stommel (1948) in this extreme case.

Another justification of the introduction of the friction is given by the physical reasoning, because near the coast the friction should be very important rather than geostrophic effect. In reality, the linearized equation (2.17) seems to be velid only in the interior of the ocean, and as shown by recent theories of Charney (1955b) and Morgan (1956) the non linear effect may play an important role near the coast. However, the simplicity of the mathematical treatment with many results obtained in the stationary circulation problem by the theory of Stommel (1948) and Munk (1950) seems to make it reasonable to use the frictional boundary layer model as the first approximation.

When we lock at the table 3, we can find that the values of δ_1 with a large real part for the values of ν larger than ν_c become to have a large positive imaginary part, too, as a friction is introduced, suggesting that the δ_1 waves

(we call the free waves expressed by the term $e^{i\delta_2 x}$ as δ_2-waves hereafter) with small wave length attenuate rapidly as apart from the western coast. On the other hand, δ_2 waves with much larger wave length than δ_1 waves decrease from the maximum value at the eastern coast much more gradually than δ_1 waves, because δ_2 has much smaller real and imaginary part, the latter of which is negative. This is a sort of the westward intensification of the induced fluctuations in circulation, which occurs when $\beta_1 a \gg 1$, where we put $\delta_s=\alpha_s+i\beta_s$. We call this range of ν, where such condition is satisfied, as WI range, and also we define the range ν, where the solution is expressed by the equation (5.2), as SC (Subcritical) range hereafter. Then in WI range the approximate form for R_I corresponding to (5.2) becomes

$$R_I=-\Re K\{\sin(\nu t+\theta x)\sin\mu y+iQ_1 e^{i\nu t+i\delta_1(a+x)+ta\theta}(1-e^{-2a\overline{\delta_2+\theta}}) +iQ_2 e^{i\nu t+i\delta_2(x-a)-ia\theta}\} \tag{5.4}$$

This expression is valid for all range of x, though in the eastern half the term with $e^{i\delta_2 x}$ is negligible.

In order to show the effect of the friction more clearly, we plot π/β, as a

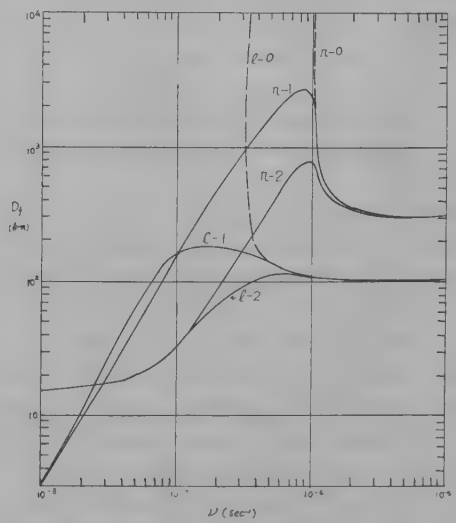

Fig. 7. $Df=\pi/\beta_1$ for $\mu=10^{-7}$
(r: Barotropic, l: Baroclinic; 0: $k=0$, 1: $k=10^{-8}$, 2: $k=10^{-7}$)

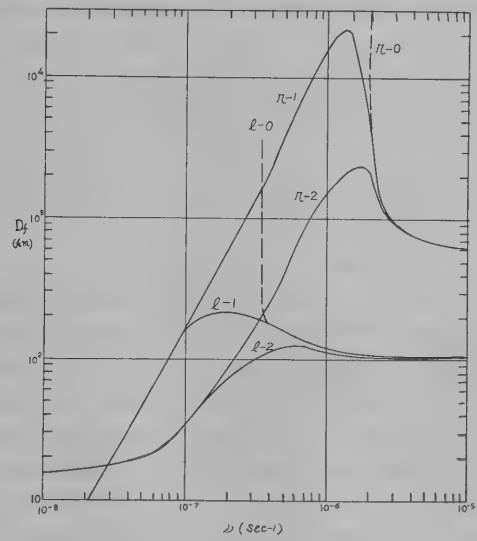

Fig. 8. $D_f=\pi/\beta_1$ for $\mu=10^{-8}$
(r: Barotropic, l: Baroclinic; 0: $k=0$, 1: $k=10^{-8}$, 2: $k=10^{-7}$)

function of frequency ν in fig. 7 and 8, which corresponds to the depth of frictional influence in the wind drift current of Ekman, since it gives the distance from the coast, where the amplitude of δ_1 waves decreases to $e^{-\pi}$ times of the value at the coast, which we shall define as D_f. In the SC range, D_f is finite even when we neglect the friction, and in fact the effect of the friction is very small as seen in Table 3 and the curves. However for $\nu<\nu_e$ this value is finite only when the friction is introduced. In the range of ν intermediate between SC and WI ranges the values of D_f of barotropic mode is much larger than those of baroclinic mode but in the range of WI, say for $\nu<10^{-7}$, they are almost equal, since $\kappa \gg \lambda_l^2$, u^2 and δ_1 is given by $2\kappa/(1-ni)$, approximately. On the other hand, the change of the values in k has much influence in the values of D_f in the WI range, and for the range $\nu<3\times10^{-8}$ the increase in k value rather increases the values of D_f, contrary to the depth of frictional influence.

Anyhow, the values of k adopted here are not so large, since Stommel (1948) gave it a value of $k=0.02/H$ or 3.3×10^{-7} in his theory of stationary circulation and Neumann (1954) gave it 3.3×10^{-6}. Therefore, the effect of friction for attenuation

of δ_1 waves is quite realistic, considering a moderate estimation of the values in k.

6. *Numerical examples for a travelling wind system*

Here we show some examples of numerical computation of the equation (3.9a) or its approximate form (5.2) or (5.4). The disturbance is considered to travel eastwards, since such one seems to be more realistic than westward moving one.

Case I. $\theta=10^{-7}$, $\mu=10^{-7}$, $\nu=5\times10^{-6}$

This model corresponds to the smallest wind system considered to give any effect on the circulation of the ocean, and in this model the effect of friction is almost negligible in the values of K and δ_s so far as k is less than 10^{-7}. The numerical values of many quantities in the equation for R_I are as follows:

$$q=5\times10^5 \quad q\theta=0.05, \quad q\delta_{sl}=0.01\pm0.049_i \quad q\delta_{sr}=0.01\pm0.152_i$$

Both barotropic and baroclinic mode lie in the range of SC and particularly for the barotropic mode the equation (5.2) can be written more simply as

(Western part)

$$R_I=K[-\sin(\nu t-\theta x)\sin\mu y+e^{-\beta(a+x)}\sin(\nu t+\alpha\overline{x+a}+a\theta)\sin\mu y-qe^{-\beta(a+x)}\cos\mu y$$
$$\{\beta\cos(\nu t+\alpha\overline{a+x}+a\theta)+(\theta+\alpha)\sin(\nu t+a\theta)\}] \qquad (6.1)$$

because $|q\theta|\ll1$, $|q\delta_{sl}|\ll1$ and also K is real.

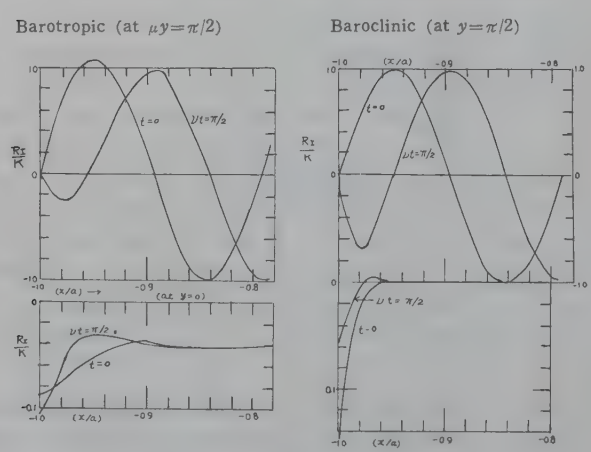

Fig. 9. R_I/K for a model I.

The wave forms of R_1 computed for this model are graphically shown in Fig. 9 for the range of χ near $-a$ or rear the western coast, and those near the eastern coast are symmetric about the point $x=0$, as seen in the equation (5.2). These curves indicate that the effect of the coast is limited within quite a narrow band from the coast, say, of about $0.08a$ for barotropic and $0.04a$ for baroclinic mode.

The condition at the coast $x=\pm a$ is $u=0$, as stated in Section 3, or

$$\frac{\partial R}{\partial y}+\frac{1}{f}\left(\frac{\partial}{\partial t}+k\right)\frac{\partial R}{\partial x}=0$$

and when we neglect the non-geostrophic term in the equation of the boundary value of u, this condition becomes simply $\partial R/\partial y=0$ and we have the solution R which vanishes at the coast. On the other hand, when we take into account of the non-geostrophic term, we have the finite value of R_1 at the coast, although the amplitude is small compared with those in the inner region. This means that the surface elevation and the depth of the upper layer show the fluctuation at the coast due to the moving wind system, and their amplitude seems to be measurable order of magnitude, which may be tested by the observation.

Case II. $\theta=5\times10^{-8}$, $\mu=5\times10^{-8}$, $\nu=5\times10^{-7}$, $k=10^{-8}$ or 10^{-7}

The quantities often used have the following values:

for $k=10^{-8}$ $q=10^5\ (1-0.02i)$, $a\delta_{1r}=118.2+2.436i$

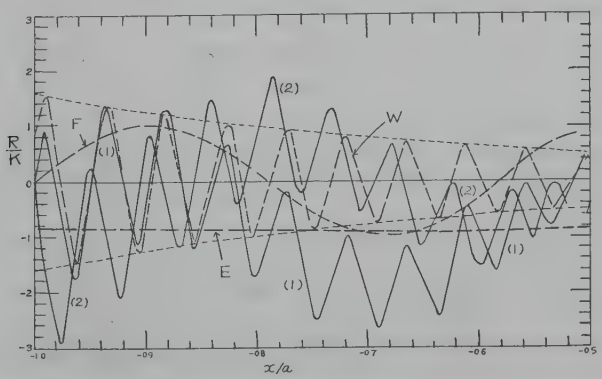

Fig. 10. R/K for model II of barotropic made with $k=10^{-8}$.
(Full lines: resultant curve at $t=0$ (1) and $\nu t=\pi/2$ (2).
Broken lines: component waves at $t=0$. Forced waves: F, δ_1—waves: W, δ_1—waves: E, Dotted lines: envelope for δ_1—waves.)

$$a\delta_{2r}=1.80-0.036i,\ a\delta_{1l}=60+65.4i,\ a\delta_{2l}=60-63i$$

for $k=10^{-7}$ $\qquad q=10^5\ (1-0.2i),\ a\delta_{1r}=111.9+22.65i$

$$a\delta_{2r}=3.3+0.39i,\ ad_{1e}=-56.3+83.4i,\ a\delta_{2l}=58.7-54.0i$$

Since $|q\theta|,\ |q\delta_1|\ |q\delta_2|\ll 1$, we can put R_1, for the barotropic mode instead of (5.4), as

$$R=K[-\sin(\nu t-\theta x)\sin\mu y-\Im\{e^{i\delta_1(\theta+x)+i\alpha\theta}(e^{-2i\overline{a\theta+\delta_2}}-1)\ (\sin\mu y-\overline{q\theta+\delta_1}\cos\mu y)$$
$$-e^{-i\alpha\theta+i\delta_2(x-a)}(\sin\mu y-\overline{q\theta+\delta_2}\cos\mu y)\}] \qquad (6.2)$$

and also for the baroclinic mode we can use the equation (6.1), since ν is larger than ν_e and $|q\delta_s|\ll 1$.

This example gives something interesting feature, since the barotropic mode is in *WI* range and the baroclinic one lies in *SC* range, so that the former is much influenced by the values of k. For $k=10^{-8}$ the value D_f is quite large and the effect of the western coast extends all over the ocean and δ_1 waves with the wave length of about 159 km are superposed till the eastern coast as shown in

$$-\sin(\nu t-\theta x+\overline{a})-1.945e^{-\beta_1(a+x)}\cos(\alpha_1\overline{a+x}+\nu t+0.004)$$
$$+2.182e^{-\beta_2(a+x)}\sin(\alpha_2\overline{a+x}+\nu t+1.099) \qquad (6.3)$$

Fig. 10 and we know no observed fact corresponding to such waves yet. On the other hand, the waves of the beroclinic mode is much more similar to case I, since they both belong to the range *SC*, so that the graphical representation is not shown

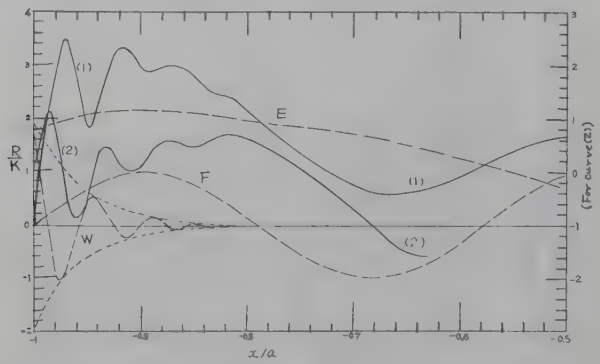

Fig. 11a. R/K for model II of barotropic mode with $k=10^{-7}$ near the western coast. (Full lines: resultant curve at $t=0$ (1) and $\nu t=\pi/2$ (2). Broken lines: component waves at $t=0$. Forced waves: *F*, δ_1—waves: *W*, δ_2—waves: *E*. Dotted lines: envelope for δ_1—waves.)

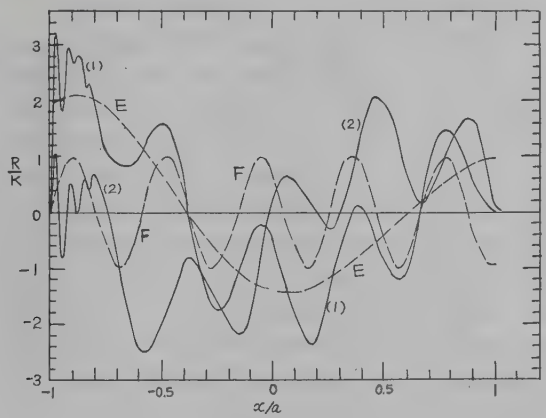

Fig. 11b. The same functions as in Fig. 11a in the whole ocean.

Then we take the frictional coefficient $k=10^{-7}$, then the pattern of barotropic waves seems to be completely changed, since the δ_1 waves become almost negligible for the values of $x>-0.08a$. The more convenient expression of the factor of $\sin \mu y$ for numerical computation is given by

$$-\sin(\nu t-\theta x+\overline{a})-1.945e^{-\beta_1(a+x)}\cos(\alpha_1\overline{a+x}+\nu t+0.004)$$
$$+2.182e^{-\beta_2(a+x)}\sin(\alpha_2\overline{a+x}+\nu t+1.099), \qquad (6.3)$$

From this equation, we can see that the effect of δ_2 waves is rather predominant, except very near to the western boundary, whose weve length is about 6900 km, almost the same as the whole length of the ocean. It is remarkable that the moving wave system with so small wave length as 1250 km can excite a relatively large amplitude of such a long waves as δ_2 waves, which are caused by the boundary condition at the eastern coast, rather than any other effects associated with the condition in the inner part of the ocean.

7. *Numerical examples for a periodically changing wind system.*

In this section we discuss the results obtained for a wind system which is stationary in its location but change periodically with annual period.

Case III. We take the wind stress as follows:

$$\operatorname{curl}\boldsymbol{\tau}=F_0\sin\nu t\sin\frac{\pi}{a}x\sin\mu y \qquad (7.1)$$

and the numerical constants as

$$\nu=2\times10^{-2}=2\pi/year,\quad k=2\times10^{-8}$$

$\mu=10^{-8}$ (IIIa), $\mu=5\times10^{-8}$ (IIIb)

This model corresponds to the change of the wind system in the Pacific Ocean, where the eastern and western half have different vorticity of surface wind as stated later. The solution of R_1 itself can be obtained very easily by combination of two solutions for the wind system moving east with a factor $e^{i(\nu t-\theta x)}$ and west with $e^{i(\nu t+\theta x)}$. The δ_1 waves and δ_2 waves in both modes lie in the range of *WI*, so that δ_1 waves are conspicuous only near the western coast.

Since the value of θ is specified as π/a, the expression for K_1 becomes somewhat more simple than (6 1). Generally K becomes different for $e^{i(\nu t-\theta x)}$ waves and $e^{i(\nu t+\theta x)}$ waves, and we put K_- for the former and K_+ for the latter, then we obtain the relation, such as (In barotropic modes) $K_+=-K_-(1+2\epsilon_r)$, (in baroclinic modes) $K_+=K_-(1+2\epsilon_i)$, where ϵ_r and ϵ_i are both positive number for the range of μ and ν considered here.

Then, for barotropic mode, we have

$$\begin{aligned}R_1=K_-[\{&\sin\nu t\cos\pi/a\,x+\epsilon_r\sin(\nu t+\pi/a\,x)+(1+\epsilon_r)e^{-\beta(a+x)}\sin\overline{\nu t+\alpha_1 a+\alpha_1 x}\\&-e^{2\beta_2 a}\sin\overline{\nu t+\alpha_1 a+\alpha_1 x-2\alpha_2 a})+(1+\epsilon_r)e^{-\beta_2(x-a)}\sin(\nu t+\alpha_2\overline{x-a})\}\sin\mu y\\&+\cos\mu y\Re\{q(\epsilon_r\pi/a+\overline{1+\epsilon_r}\delta_1)e^{i\delta_1(a+x)}-q(\epsilon_r\pi/a+\overline{1+\epsilon_r}\delta_2)e^{i\delta_2(a-x)}\}]\end{aligned}\tag{7.2}$$

Similarly, for baroclinic mode, we have

$$\begin{aligned}R_1=K_-[\{&-\cos\nu t\sin\pi/a\,x-\epsilon_i\sin(\nu t+\pi/a)+\epsilon_i e^{-\beta_1(a+x)}\\&\times(e^{2\beta_2 a}\sin\overline{\nu t+\alpha_1 a+\alpha_1 x-2\alpha_2 a}-\sin\nu t+\alpha_1 a+\alpha_1 x)\\&-\epsilon_i e^{-\beta_2(x-a)}\sin(\nu t+\alpha_2\overline{x-a})\}\sin\mu y\\&-\cos\mu y\Re\{q(\overline{1+\epsilon_i}\,\pi/a+\epsilon_i\delta_1)e^{i\delta_1(a+x)}-q(\overline{1+\epsilon_i}\,\pi/a+\epsilon_i\delta_2)e^{i\delta_2(a-x)}\}]\end{aligned}\tag{7.3}$$

IIIa $\mu=10^{-8}$ and $2\epsilon_r=0.05$, $2\epsilon_i=0.29$

The values of δ_1 and δ_2 are as follows:

(Barotropic) $a\delta_1=0.467-0.039i$ $a\delta_2=297+29.7i$

(Baroclinic) $a\delta_1=270+30i$, $a\delta_2=27-0.33i$

The expression for δ_1 waves with the factor of $\sin\mu y$ which is convenient for numerical computation becomes

(Barotropic) $0.888\,e^{-\beta_1(a+x)}\cos(\alpha_1\overline{a+x}+\nu t-0.545)$

(Baroclinic) $-0.211\,e^{-\beta_1(a+x)}\sin(\alpha_1\overline{a+x}+\nu t-0.198)$

The results of the computation are shown graphically in Fig. 12 where the functional form of R_1 at $\mu y=\pi/2$ is illustrated near the western coast and over the whole ocean separately. Since ϵ_r is almost negligible compared with 1, the forced motion becomes standing type as the wind system itself, though the

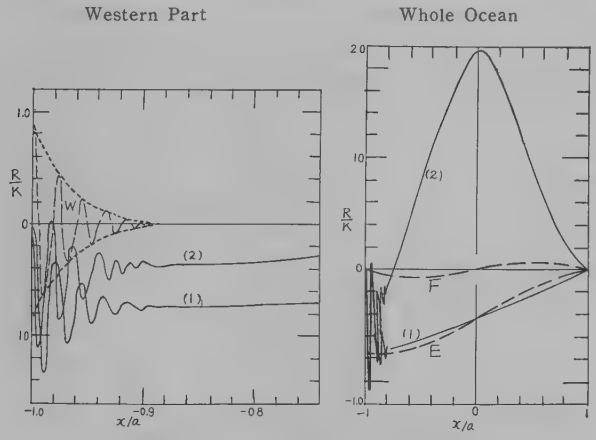

Fig. 12. R/K of barotropic mode for model III with $\mu=10^{-8}$.
(Full lines: resultant curve at $t=0$ (1) and at $t=t$ (2) Broken lines: component waves at $t=0$ Forced waves: F, δ_1—waves: W, δ_2—waves: E Dotted lines: envelope for δ_1—waves)

spatial distribution of the amplitude of the motion is displaced from that of the wind stress curl with a phase of $\pi/2$ and thus the maximum change occurs at the center, with the phase in time being the same as wind stress curl.

The effect of the δ_1 waves is almost negligible beyond $x=-0.1a$ as in Case IIb, though the frictional coefficient here is smaller (2×10^{-8}) than in the previous case (10^{-7}). It is quite interesting that the δ_1 waves with a very short wave length are excited by the large scale wave system and they are limited only in the region of the western current, because these disturbances seem to be associated with the multiple structures of the Gulf Stream which have been often observed and confirmed by Fuglister (1951a) and others.

The effects of δ_2 waves seem to retard the whole pattern with a phase lag of about 1.8 months, because they have a wave length longer than the width of the ocean and their form is expressed with the sine function such as $\sin\{0.467(x/a+1)+\nu t-0.934\}$

On the other hand, the features of baroclinic modes are quite different from the barotropic ones. First, the forced waves have a form such as $-\cos\nu t\sin\theta x$, which means that the response of the ocean to the wind system is retarded by about 1/4 period, though the spatial distribution of the motion is the same as

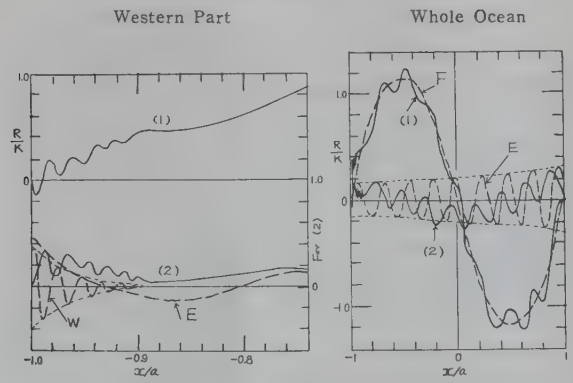

Fig. 13. R/K of baroclinic mode for model III with $\mu=10^{-8}$
(See explanation of Fig. 12 for legend)

the wind system. The δ_2 waves have a wave length of about 700 km with the amplitude almost uniform over the whole ocean, so that slight unevenness with a small wave length is recognized in the resultant pattern, although its amplitude is quite small compared with the forced motion.

IIIb $\mu=5\times10^{-8}$ and $2\epsilon_r=0.66$, $2\epsilon_i=0.285$

(Barotropic) $a\delta_1=297+29.7_i$ $a\delta_2=0.75-0.075_i$

(Baroclinic) $a\delta_1=269.7+27.0_i$ $a\delta_2=27.5-0.3_i$

The convenient expression for δ_1 waves is given by

$$1.69e^{-\beta_1(a+x)}\sin(\alpha_1\overline{a+x}+\nu t+0.739) \quad \text{(barotropic)}$$

The baroclinic waves are almost similar to the previous case, since the values of ϵ_i, δ_1, δ_2 are almost the same, so that they are not written again.

In this case, the amplitude of westward moving wave $\sin(\nu t+\pi x/a)$ is relatively large, and thus the forced motion has a pattern moving to the west as a whole. Further, both the amplitudes of δ_1 waves and δ_2 waves are larger than in IIIa, so that the difference in amplitude in each stage of phase becomes more conspicuous.

Case. IV. We consider the model discussed by Munk (1957), where the wind is zonal, with the westerly in the northern half and easterly in the southern half, such as

$$\tau_y=0 \qquad \tau_x=-T_0\cos\nu t\sin\mu y \tag{7.4}$$

in which we take $\mu=1.13\times10^{-8}$, corresponding to the distance of the ocean of about 3000 sm.

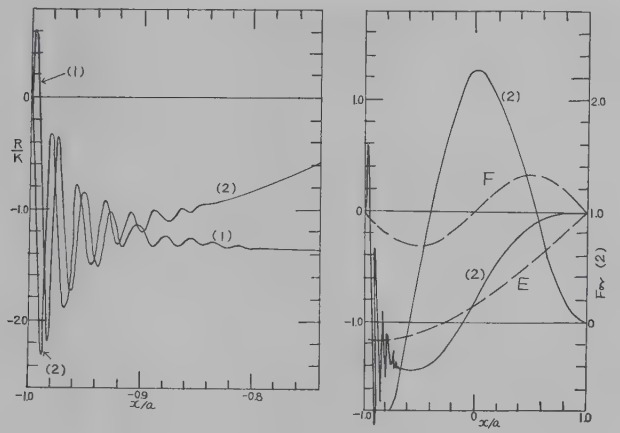

Fig. 14. R/K of barotropic mode for model III with $\mu=5\times10^{-8}$
(See explanation of Fig. 12 for legend)

In this model we retain the term $-2\frac{\beta}{f}\frac{\partial}{\partial y}R_j$ in the equation (2.17). As for the boundary conditions, we can take the exact ones given by (3.2), since the boundary values of τ are given explicitely. However, the contributions from R_{II} can be neglected with a satisfactory exactness, because from the boundary conditions

$$R_{IIy}+\frac{1}{f}\left(\frac{\partial}{\partial t}+k\right)\left(R_{IIx}-\frac{\nu}{f\mu}\frac{\sigma_j}{gH}T_0\cos\nu t\cos\mu y\right)=0$$

we obtain

$$R_{II}\sim\frac{\sigma_j}{gH}T_0\frac{\nu^2}{f^2\mu^2}$$

which gives the ratio

$$|R_{II}|/|R_I|\sim\nu^2(\mu^2\lambda_j^2)/f^2\mu^2 \qquad (j=\tau,\ l)$$
$$=4.8\times10^{-6}\quad\text{(for barotropic)}=2.7\times10^{-3}\quad\text{(for baroclinic)}$$

Therefore the exact solution of R is given by

$$R=-\frac{K}{2}(dS+\bar{d}\bar{S}-ldC+\bar{l}\bar{d}\bar{C}) \tag{7.5}$$

where

$$\begin{aligned}S=&\sin(\varphi+\nu t+\mu y)-m_1e^{-\beta_1(a+x)}\{\sin(\nu t+\mu y+\alpha_1x+\bar{a}+\varphi+{}_1\psi)\\&-e^{2\beta_2a}\sin(\nu t+\mu y+\alpha_1x+\bar{a}+\varphi+\psi_1-2\alpha_2a)\}\\&-m_2e^{-\beta_2(x-a)}\sin(\nu t+\mu y+\alpha_2x-a+\varphi+\psi_2)\end{aligned} \tag{7.6}$$

and in S, m_1, m_2, 4_1, 4_2, δ_1, δ_2 and φ are replaced with corresponding quantities with a bar and μy is taken by $-\mu y$. The terms having a factor $l=\beta/\mu f$ are produced by the condition that the wind stress function has a form such as

$$\text{curl}\,\boldsymbol{\tau}+\frac{\beta}{f}\tau x=\mu T_0\cos\nu t\,(\cos\mu y-l\sin\mu y)$$

where the second term produces the l terms in (7.5). The functions C and $\overline{C}$ are expressed by substituting cosine in functions S and $\overline{S}$, respectively. Further the quantities with a bar indicate that they are originated from the term $e^{i(\nu t-\mu y)}$, owing to the condition that $\frac{2\beta}{f}\cdot\frac{\partial}{\partial y}R$ term is taken into account of. The equation (7.5) is valid formdally in both modes, where the K, d, φ, m_l, m_t and ψ_l, $\overline{\psi_l}$ are defined as

$$K_r=\frac{f_r T_0}{\rho g H\mu\nu}=113T_0,\quad K_l=-\frac{f\mu\beta^2 T_0}{\rho g H\,(2\nu)^2}=-1.13T_0 \qquad (7.5a)$$

with r and l indicating barotropic and baroclinic as stated before, and as for d, φ, (in barotropic)

$$de^{i\varphi}=\{(1-2li)\,(1-ni)+\lambda_r^2/\mu^2\}^{-1}\bar{d}e^{i\bar{\varphi}}=\{(1+2l_t)\,(1-ni)\,(-\lambda_r^2/\mu^2\}^{-1} \qquad (7.6a)$$

(in baroclinic)

$$d=\bar{d}=1 \qquad \varphi=\bar{\varphi}=0$$

Table 4

Iva $k=2\times10^{-8}$	$\alpha_1 a$	$\beta_1 a$	$\alpha_2 a$	$\beta_2 a$	$\bar{\alpha}_2 a$	$\bar{\beta}_2 a$	d	φ	$\bar{d}$
Barotropic	297	29.7	0.460	−0.108	0.473	0.030	0.825	0.23	0.823
Baroclinic	270	30	27	−0.33	$\alpha_2 a$	$\beta_2 a$	1	0	1
Ivb $k=2\times10^{-7}$									
Barotropic	150	150	0.398	−0.458	0.535	−0.321	0.640	1.032	0.628
Baroclinic	123.5	153	26.5	−3.23	$\alpha_2 a$	$\beta_2 a$	1	0	1

Iva $k=2\times10^{-8}$	$\bar{\varphi}$	m_1	ψ_1	m_2	ψ_2	$\overline{m_1}$	$\overline{\psi_1}$	$\overline{m_2}$	$\overline{\psi_2}$
Barotropic	−0.063	0.985	−0.174	1	0	m_1	$-\psi_1$	1	0
Baroclinic	0	0.952	−0.317	1	−0.032	m_1	$-\psi_1$	1	-4_2
Ivb $k=2\times10^{-7}$									
Barotropic	0.538	0.985	−0.174	1	0	m_1	$-\psi_1$	1	0
Baroclinic	0	0.985	−0.323	0.965	−0.026	0.922	0.302	1.035	0.028

and also

$$m_l e^{i\psi_l} = (1+p\delta_s)^{-1},\ \overline{m_l e^{i\psi_l}} = (1-p\bar{\delta}_l)^{-1} \tag{7.6b}$$

Practically, $\delta_{1l}=\bar{\delta}_{1l}$, $\delta_{1r}=\bar{\delta}_{1r}$ and $\delta_{2r}=\bar{\delta}_{2r}$ Further, numerical values of these quantities are given by the Table 4.

For the baroclinic mode the expression for R becomes

$$R_l = K_l\{-\sin\nu t\cos\mu y + S_l + l\cos\nu t\cos\mu y + lC_l\} \tag{7.5b}$$

where

$$S_l = m_1 e^{-\beta_1(x+a)}\cos(\mu y+\psi_1)\{\sin(\nu t+\overline{\alpha_1 x+a}) - e^{2\beta_2 a}\sin(\nu t+\alpha_1\overline{x+a}-2\alpha_2 a) + \frac{1}{2}e^{-\beta_2(x-a)}\{m_2\sin(\nu t+\mu y+\alpha_2\overline{x-a}+\psi_2)+\overline{m_2}\sin(\nu t-\mu y+\alpha_2\overline{x-a}+\bar{\psi}_2)\} \tag{7.5c}$$

and for $k=2\times10^{-8}$ the last terms corresponding to δ_2 waves are given by

$$e^{-\beta_2(x-a)}\sin(\nu t+\alpha_2 x-a)\cos(\mu y+\psi_2)$$

and C_l is the substitution of sine in S_l by cosine terms.

Since K_r is about 100 times of K_l in this model, contribution from the baroclinic mode seems to be negligibly small Also the behavior of the function R which is associated with the sea surface and interface has been already discussed in many examples, so that we try to show the velocity distributions here instead of those of R caused by a variable wind stresses.

The western current which is given by the relationship (2.10) and (2.12) becomes very simple, because, for the barotropic mode, only the term which is produced by differentiation of δ_1 waves with x, such as $v_r = \frac{g}{f}\frac{\partial}{\partial x}e^{i\delta_1 x}$ term in R_r is predominant. Therefore it is given by

$$v_r = Ve^{-\beta_1\overline{x+a}}\{\sin\Psi_1(\cos\Psi_2+l\sin\Psi_2) - \frac{1}{2}e^{2\beta_2 a}(\sin\Phi - l\cos\Phi) - \frac{1}{2}e^{2\beta_2\bar{a}}(\sin\bar{\Phi}+l\cos\bar{\Phi})\} \tag{7.7}$$

where we put

$$V = gK_r dm_1 s/f,\ se^{i\phi} = -\beta_1+\alpha_1 i$$
$$\Psi_1 = \nu t+\alpha_1\overline{x+a}+\phi+(\varphi+\bar{\varphi})/2$$
$$\Psi_2 = \mu y+\psi_1+(\varphi-\bar{\varphi})/2$$
$$\Phi = \nu t+\alpha_1\overline{x+a}+\mu y+\psi_1+\varphi+\phi-2\alpha_2 a$$
$$\bar{\Phi} = \nu t+\bar{\alpha}_1\overline{x+a}-\mu y-\psi_1+\bar{\varphi}+\phi-2\bar{\alpha}_2 a$$

Similarly, the zonal velocity at the region apart from the western coast is also given by $u_r = \frac{1}{f}\left(-g\frac{\partial R_r}{\partial y}\right)$, because other terms in the or ginal relationship (2.9) and (2.11) are negligibly small. Therefore

$$u_r=U\{\cos\Psi_2'(\cos\Psi_1'+l\sin\Psi_1')-$$
$$-\frac{1}{2}e^{-\beta_2(x-a)}(\cos\Phi'+l\sin\Phi')-\frac{1}{2}e^{-\bar{\beta}_2(x-a)}(\cos\bar{\Phi}'-l\sin\bar{\Phi}')\} \qquad (7.8)$$

where

$$U=gK_r\mu d/f$$

and

$$\Psi'=\nu t+(\varphi+\bar{\varphi})/2,\ \Psi_2'=\mu y+(\varphi-\bar{\varphi})/2$$
$$\Phi'=\nu t+\mu y+\alpha_2(x-a)+\varphi$$
$$\bar{\Phi}'=\nu t-\mu y+\bar{\alpha}_2(x-a)+\bar{\varphi}$$

Numerical values of constants in (7.7) and (7.8) are given by

k	s	ϕ	V	U
2×10^{-8}	0.995×10^{-6}	1.67	$894T_0$	$10.3T_0$
2×10^{-7}	0.708×10^{-6}	2.35	$493T_0$	$7.9T_0$

Near the western coast, the change in amplitude and phase of δ_2 waves is very gradual compared with that of δ_1 waves, since $|\delta_2|\ll|\delta_1|$. Therefore we can put these elements of δ_2 waves almost constant and obtain much simple numerical formula for R_r near the western coast, say $-a\ll x\ll-0.9a$, when we use the values at $x=-0.95a$ for amplitude and phase of δ_2 waves. Thus we have

(for $k=2\times10^{-8}$)

$$R_r=46.6T_0[-0.817\sin(X+0.963)-0.937\sin(\bar{X}+1.281)$$
$$+e^{-\beta_1(a+x)}\{0.821\sin(Y+0.782)+0.942\sin(\bar{Y}+1.444)\}] \qquad (7.9)$$

(for $k=2\times10^{-7}$)

$$R_r=35.8T_0[-0.777\sin(X+1.245)-0.878\sin(\bar{X}+1.276)$$
$$+e^{-\beta_1(a+x)}\{0.777\sin(Y+1.086)+0.878\sin(Y+1.440)\}] \qquad (7.10)$$

where $X=\nu t+\mu y,\ \bar{X}=\nu t-\mu y\quad Y=X+\alpha_1(a+x)\quad \bar{Y}=\bar{X}+\alpha_1(a+x)$

The results of numerical computation of the equations (7.7) (7.8) (7.9) and (7.10) are shown in Fig. 15 and 16. It is rather surprising that the amplitude of the fluctuation of the western current is so large that it reaches 89.4 cm/sec for $k=2\times10^{-8}$ with $T_0=0.1$, which seems to be rather unreasonable. On the other hand, if we take the larger frictional constant $k=2\times10^{-7}$, then the decrease of the δ_1 waves apart from the western coast is so remarkable that at a distance of about 0.3a from the coast the amplitude of δ_1 waves almost become negligible.

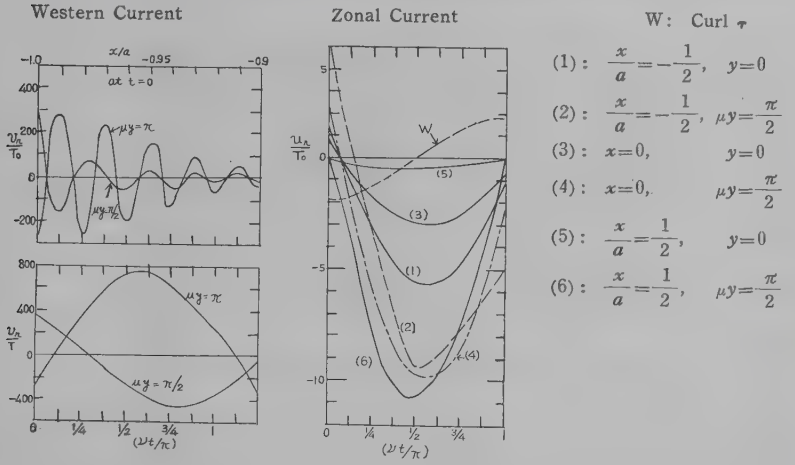

Fig. 15. U_r and V_r for model IV with $k=2\times10^{-8}$

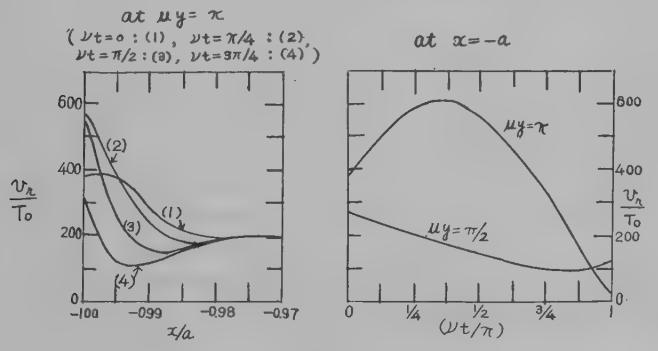

Fig. 16. v_r for model IV with $k=2\times10^{-7}$

The isopleths of R_r for $\nu t=0$ and $\pi/2$ also indicate some remarkable difference between $k=2\times10^{-8}$ and 2×10^{-7} (Fig. 17 and 18, because for a smaller friction the contours consist of some cells and for a larger friction they show only the crowdiness of the isopleths along the coast.

The change of the current both zonal and meridional (western coast $x=-a$ and $\mu y=\pi$) seems to occur with a time lag to the variation of the wind system. The zonal current, which is much smaller in magnitude than the western current has a time lag of about $\pi/2$, so that at the maximum easterly or westerly wind

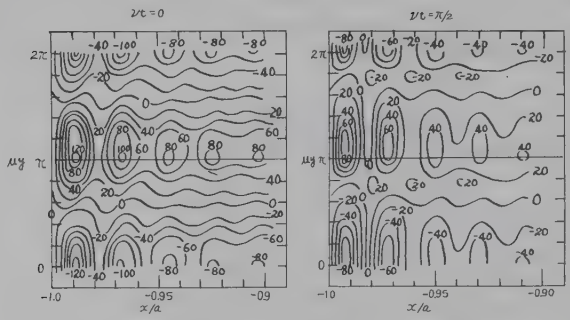

Fig. 17. Isopleths of (R_r/T_0) for $k=2\times10^{-8}$

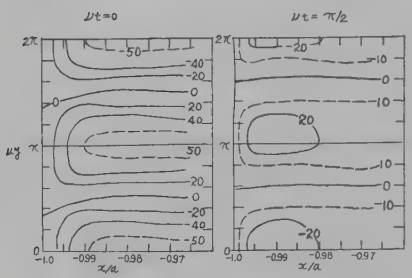

Fig. 18. Isopleths of (R_r/T_0) for $k=2\times10^{-7}$

stage the zonal current in the south or north flows to the opposite direction to the wind stress. Such situation is quite different from the results derived by Fuglister (1951a) from the statistics of the surface currents data, which says that the speed fluctuation of the north equatorial current and the trade wind are approximately the same. Further, even the western current itself shows the time lag, when we take the value at $x=-a$ and $\mu y=\pi$, which also differs from the result of Veronis and Morgan (1955), because the present model does not correspond exactly to their one.

8. *The response to an asymmetrical wind system*

When the free waves are in SC range, that is, the frequency is larger than critical values, δ_1 waves are only effective near the western coast and δ_2 waves, on the other hand, are important near the eastern coast, and their amplitude is almost symmetric about the center of the ocean, since δ_1 and δ_2 are conjugate complex number. However, in the WI range such symmetry vanishes, because δ_1 waves attenuates conspicuously as apart from the western coast, and yet the imaginary part of δ_2 is much smaller than that of δ_2. Therefore, we can expect

much difference between the SC and WI range for an asymmetric wind distribution.

The general solution of the equation (2.17) for a type of the wind stress distribution

$$F=F(x)\cos\nu t\sin\mu y \tag{8.1}$$

is given by

$$R=2\Re\{iP(x)e^{i\nu t}\sin\mu y\} \tag{8.2}$$

where

$$P(x)=J(x)+Ae^{i\delta_1 x}+Be^{i\delta_2 x} \tag{8.3}$$

and also

$$J(x)=\frac{f\sigma j}{2(i\nu+k)(\delta_2-\delta_1)gH}\int_{-a}^{x}F(\xi)\{e^{i\delta_1(x-\xi)}-e^{i\delta_2(x-\xi)}\}d\xi \tag{8.4}$$

in which the numerical constants A and B might be determined by the boundary conditions. Particularly, when we take the most simple boundary conditions, suca as $R_y=0$ at $y=\pm a$, which do not harm the general validity of the discussion here, then we obtain the solution such as

$$P(x)=J(x)+J(a)\,(e^{i\delta_2 x-i\delta_1 a}-e^{i\delta_1 x-i\delta_2 x})/2\sin(\delta_1-\delta_2)a \tag{8.5}$$

When we take into account of friction having an order of magnitude larger than 10^{-8}, we have a relation such as $|e^{i(\delta_2-\delta_1)a}|\gg|e^{i(\delta_1-\delta_2)a}|$ as seen from Table 3, so that we can put $\sin(\delta_1-\delta_2)a\fallingdotseq-e^{i(\delta_2-\delta_1)a}/2$ and the above equation becomes

$$P(x)=J(x)+J(a)e^{-i2a\delta_2}\{e^{i\delta_6(a+x)}-e^{i\delta_2(a+x)}\} \tag{8.5a}$$

In this section we assume that the function $F(x)$ is constant over a finite belt and it vanishes outside the belt, weich is called here as "wind belt". For comparison we consider two types of the wind belt, where one locates near the western coast and the other near the eastern coast. In each example the equations $F(x)$ and corresponding $J(x)$ are given as

(Va)
$$F(x)=F_0\quad(\text{in } -a<x<-a+\Delta)\quad=0\ (\text{in } -a+\Delta<x<a)$$

$$J(x)=J_0\left\{\frac{e^{i\delta_1(x+a)}(1-e^{-i\delta_1\Delta})}{i\delta_1}-\frac{e^{i\delta_2(x+a)}(1-e^{-i\delta_2\Delta})}{i\delta_2}\right\}$$

$$(\text{in } a>x>-a+\Delta)$$

$$=J_0\left\{\frac{e^{i\delta_1(x+a)}-1}{i\delta_1}-\frac{e^{i\delta_2(x+a)}-1}{i\delta_2}\right\}$$

$$(\text{in } -a+\Delta>x>-a) \tag{8.6a}$$

(Vb)
$$F(x)-F_0\ (\text{in } a-\Delta<x<a)\quad=0\ (\text{in } -a<x<a-\Delta)$$

$$J(x)=J_0\left\{\frac{e^{i\delta_1(x-a+\Delta)}-1}{i\delta_1}-\frac{e^{i\delta_2(x-a+\Delta)}-1}{i\delta_2}\right\}$$

(in $a>x>a-\Delta$)

$$=0 \quad (\text{in } a-\Delta>x>-a) \tag{8.6b}$$

where $J_0=f\sigma_i F_0/2(\iota\nu+k)(\delta_2-\delta_1)gH$

From the same assumption about the frictional coefficient we can deduce the condition $|e^{i\delta_1 a}|\ll 1$, so that the values of $J(a)$ are given by

(Va) $$J(a)=J_0e^{i\cdot\delta_2 a}(e^{-i\delta_2\Delta}-1)/(i\delta_2)$$

(Vb) $$J(a)=J_0\left(\frac{e^{i\delta_1\Delta}-1}{i\delta_1}-\frac{e^{i\delta_2\Delta}-1}{i\delta_2}\right)$$

Therefore the equation of $P(x)$ for two examples is expressed as

(Va) inside wind belt or for $-a+\Delta>x>a$

$$P(x)=\frac{J_0}{i}\left\{\left(\frac{1}{\delta_1}-\frac{1}{\delta_2}\right)(e^{i\delta_1\overline{x+a}}-1)+\frac{1}{\delta_2}e^{-i\delta_2\Delta}(e^{i\delta_1\overline{a+x}}-e^{i\delta_2\overline{a+x}})\right\} \tag{8.7a}$$

outside wind belt or for $a>x>-a+\Delta$

$$P(x)=\frac{J_0}{i}e^{i\delta_1(a+x)}\left(\frac{1-e^{-i\delta_1\Delta}}{\delta_1}-\frac{1-e^{-i\delta_2\Delta}}{\delta_2}\right) \tag{8.8a}$$

(Vb) inside wind belt or for $a>x>a-\Delta$

$$P(x)=\frac{J_0}{i}\left\{\left(\frac{1}{\delta_1}-\frac{1}{\delta_2}\right)(e^{i\delta_2(x-a)}-1)+\frac{1}{\delta_1}e^{i\delta_1\Delta}(e^{i\delta_1\overline{x-a}}-e^{i\delta_2\overline{x-a}})\right\} \tag{8.7b}$$

outside wind belt or for $a-\Delta>x>-a$

$$P(x)=\frac{J_0}{i}e^{-i2a\delta_2}(e^{i\delta_1\overline{a+x}}-e^{i\delta_2\overline{x+a}})\left(\frac{e^{i\delta_1\Delta}-1}{\delta_1}-\frac{e^{i\delta_2\Delta}-1}{\delta_2}\right) \tag{8.8b}$$

In SC range, where δ_1 and δ_2 are conjugate complex, we have a relation such that $|e^{-i\delta_2 a}|=|e^{i\delta_1 a}|\ll 1$, thus we can neglect $e^{i\delta_1 a+x}$ against $e^{i\delta_2 a+x}$ in the equation (8.8b) and we have instead

$$P(x)=-\frac{J_0}{i}e^{i\delta_2(x-a)}\left(\frac{e^{i\delta_1\Delta}-1}{\delta_1}-\frac{e^{i\delta_2\Delta}-1}{\delta_2}\right) \tag{8.8c}$$

Therefore we obtain a symmetrical distributions of a function $|P(x)|$ about the origin in SC range for the these models of (Va) and (Vb).

For the equation (8.8a) and (8.8c) are conjugate complex for the value of $x=a-x_0$ in (8.8a) and for $x=-a+x_0$ in (8.8c).

The values of (8.7a) and (8.7b) become

$$P(a-x_0)=\frac{J_0}{i}\left\{\left(\frac{1}{\delta_1}-\frac{1}{\delta_2}\right)(e^{i\delta_1 x_0}-1)+\frac{1}{\delta_2}e^{-i\delta_2\Delta}(e^{i\delta_1 x_0}-e^{i\delta_2 x_0})\right\}$$

$$P(x_0-a)=\frac{J_0}{(-i)}\left\{\left(\frac{1}{\delta_2}-\frac{1}{\delta_1}\right)(e^{-i\delta_2 x_0}-1)+\frac{1}{\delta_1}e^{i\delta_1 \Delta}(e^{-i\delta_2 x_0}-e^{-i\delta_1 x_0})\right\}$$

which are also conjugate complex, so that their absolute values are equal to each other. Further, we can see that the value of $|P(x)|$ decreases rapidly as apart from the wind belt, because it is proportional to $exp\{-\beta_1(a+x)\}$ for the case of Va and to $exp\{-\beta_1(a-x)\}$ for (Vb). When Δ is not so small and $|e^{i\delta_1\Delta}|=|e^{-i\delta_2\Delta}|\ll 1$, the equations (8.7) and (8.8) are expressed more simply as

(Va) inside wind belt

$$P(\lambda)=\frac{J_0}{i}\left\{\left(\frac{1}{\delta_1}-\frac{1}{\partial_2}\right)(e^{i\delta_1\overline{a+x}}-1)-\frac{1}{\delta_2}e^{i\delta_2(x+a-\Delta)}\right\} \tag{8.9a}$$

outside wind belt

$$P(x)=-\frac{J_0}{i\delta_1}e^{i\delta_1(a+x-\Delta)} \tag{8.10a}$$

(Vb) inside wind belt

$$P(x)=\frac{J_0}{i}\left\{\left(\frac{1}{\delta_1}-\frac{1}{\delta_2}\right)(e^{i\delta_2\overline{x-a}}-1)+\frac{1}{\delta_1}e^{i\delta_1(x-a+\Delta)}\right\} \tag{8.9b}$$

outside wind belt

$$P(x)=\frac{J_0}{i\delta_2}e^{i\delta_2(x-a+\Delta)} \tag{8.10b}$$

On the other hand in the range of *WI*, $|\delta_2|\ll|\delta_1|$, so that the relation $|e^{-i\delta_2 a}|\ll 1$ is no more valid even when $|e^{i\delta_1 a}|\gg 1$, thus we have no symmetric distribution of the absolute value of $P(x)$. In fact, from the equation (8.7a) and (8.7b) we have

(Va) outside wind belt (from eq. 8.7a)

$$|P(x)|=P_0 e^{-\beta_1(a+x)} \tag{8.11a}$$

(Vb) inside wind belt (from eq. 8.7b)

$$|P(x)|=P_0 e^{-2a\beta_2}|e^{(\alpha_1 i-\beta_1)(a+x)}-e^{(\alpha_2 i+\beta_2)(a+x)}| \tag{8.11b}$$

where

$$P_0=|J_0|\left|\frac{1-e^{-i\delta_1\Delta}}{\delta_1}-\frac{1-e^{-i\delta_2\Delta}}{\delta_2}\right|$$

The equation (8.11a) indicates that the absolute value $|P(x)|$ diminishes rapidly as apart from the wind belt the example (Va) since $\beta_1 a\gg 1$.

On the contrary, the equation (8.11b) becomes equal to a value of $P_0 exp\,\beta_2(x-a)$ as x differs only a little from $-a$, that is, at a short distance from the western coast, because $exp\{-\beta_1(a+x)\}\ll 1$ except near $x=-a$, so that the value of $|P(x)|$ for (Vb) is finite almost all over the outside region of wind belt since $\beta_2 a\ll 1$.

Summarizing above results, in the SC range or for shorter period fluctuation of the wind stress curl, the effect of wind decreases rapidly as apart from the wind belt. In the WI range or for a longer period disturbance, the effect of wind diminishes rapidly as apart from the wind belt only when the wind belt coincides with the western part of the ocean and when the wind belt locates in the eastern part, the effect reaches near the western coast and amplitude of surface fluctuation becomes finite very near the western coast.

The function $P(x)$ represents not only the fluctuation of the surface and interface but also zonal velocity, as seen from its definition. Therefore above conclusion is valid in the spatial distribution of zonal velocity. On the other hand the meridional velocity is proportional to $\partial p/\partial x$ and this quantity is more appropriate to show the situation concerning the assymmetry of the amplitude of fluctuation in SC and WI ranges for two types of wind stress distributions. The expressions for $\partial p/\partial x$ for the same wind stress distribution are given by

(Va) inside wind belt $(-a+\Delta>x>-a)$

$$P_x=J_0\{e^{i\delta_1(x+a)}(1-\frac{\delta_1}{\delta_2}+\frac{\delta_1}{\delta_2}e^{-i\delta_2\Delta})-e^{i\delta_2(x+a-\Delta)}\} \tag{8.12a}$$

outside wind belt $(a>x>-a+\Delta)$

$$P_x=J_0e^{i\delta_1(x+a)}\{1-e^{-i\delta_1\Delta}-\frac{\delta_1}{\delta_2}(1-e^{-i\delta_2\Delta})\} \tag{8.13a}$$

(Vb) inside wind belt $(a>x>a-\Delta)$

$$P_x=J_0\{e^{i\delta_1(x-a+\Delta)}-e^{i\delta_2(x-a)}(1-\frac{\delta_2}{\delta_1}+\frac{\delta_2}{\delta_1}e^{i\delta_1\Delta})\} \tag{8.12b}$$

outside wind belt $(a-\Delta>x>-a)$

$$P_x=J_0e^{-i2\delta_2a}\left\{\delta_1e^{i\delta_1(a+x)}-\delta_2e^{i\delta_2(a+x)}\right\}\left(\frac{1-e^{i\delta_2\Delta}}{\delta_2}-\frac{1-e^{i\delta_1\Delta}}{\delta_1}\right) \tag{8.13b}$$

where we can consider $|e^{i\delta_1a}|\ll 1$.

In *SC* range with moderate value of Δ, we have

$|e^{-i\delta_2a}|=|e^{i\delta_1a}|\ll 1, \quad |e^{i\delta_1\Delta}|=|e^{-i\delta_2\Delta}|\ll 1$

so the equations (8.12) and (8.13) have more simple form such as

(Va) inside wind belt

$$P_x=J_0\{e^{i\delta_1(x+a)}(1-\frac{\delta_1}{\delta_2})-e^{i\delta_2(x+a-\Delta)}\} \tag{8.14a}$$

outside wind belt

$$P_x=-J_0e^{i\delta_1(x+a-\Delta)} \tag{8.15a}$$

(Vb) inside wind belt

$$P_x=J_0\{e^{i\delta_1(x-a+\Delta)}-e^{i\delta_2(x-a)}(1-\frac{\delta_1}{\delta_2})\} \tag{8.14b}$$

outside wind belt

$$P_x=J_0e^{i\delta_2(x-a+\Delta)} \tag{8.15b}$$

The equation (8.14) and (8.15) indicate similar features as those (8.9) and (8.10) and the amplitude distribution for two types of wind stress is symmetrical about the origin as the absolute valve of $P(x)$ itself.

In the WI range where $|\delta_1|\gg|\delta_2|$ and $|e^{i\delta_1\Delta}|\ll 1$, we obtain

(Va) inside wind belt

$$P_x=-J_0\{e^{i\delta_2(x+a-\Delta)}+\frac{\delta_1}{\delta_2}e^{i\delta_1(x+a)}(1-e^{-i\delta_2\Delta})\} \tag{8.16a}$$

outside wind belt

$$P_x=-J_0e^{i\delta_1(x+a)}\{e^{-i\delta_1\Delta}+\frac{\delta_1}{\delta_2}(1-e^{-i\delta_2\Delta})\} \tag{8.17a}$$

(Vb) inside wind belt

$$P_x=J_0\{e^{i\delta_1(x-a+\Delta)}-(1-\frac{\delta_2}{\delta_1}e^{i\delta_2(x-a)}\} \tag{8.16b}$$

ouside wind belt

$$P_x=J_0e^{-2i\delta_2a}(1-e^{i\delta_2\Delta})\{\frac{\delta_1}{\delta_2}e^{i\delta_1(a+x)}-e^{i\delta_2(x+a)}\} \tag{8.17b}$$

It is remarkable that the value of P_x does not vanish at the coast and as symmetry of the distribution of the value of $|P_x|$ between Va and Vb in WI range is clearly shown by the comparison of the value at the western and eastern coast. In fact, in SC range these values are expressed by

(Va)
$$P_x(a)=J_0e^{i\delta_1(2a-\Delta)}$$
$$P_x(-a)=J_0(1-\frac{\delta_1}{\delta_2})$$

(Vb)
$$P_x(a)=J_0(1-\frac{\delta_1}{\delta_2})$$
$$P_x(-a)=J_0e^{-i\delta_2(2a+\Delta)}$$

Therefore the value of $P_x(-a)$ in (Va) is the same as that of $P_x(a)$ in (Vb) and also $P_x(a)$ in (Va) is the same as $P_2(-a)$ in Vb, where the latter is almost zero. On the other hand, these boundary values in WI range become

(Va)
$$P_x(a)=-J_0e^{2i\delta_1a}\{e^{-i\delta_1\Delta}+\frac{\delta_1}{\delta_2}(1-e^{-i\delta_2\Delta})\}$$

$$P_x(-a) = J_0\left(1-\frac{\delta_1}{\delta_2}\right)\ (1-e^{-i\delta_2 A})$$

(Vb)
$$Px(a) = J_0\left(1-\frac{\delta_2}{\delta_1}\right)$$

$$P_x(-a) = J_0 e^{-i2a\delta_2}\left\{\frac{\delta_1}{\delta_2}(1-e^{i\delta_2 A})-1\right\}$$

Therefore, in the example (Va) $|P_x(a)| \ll 1$, since $|e^{i\delta_1(2a-A)}| \ll 1$ but in (Vb) the western current $P_x(-a)$ is not so small, because in this case the relation $|e^{-i2a\delta_2} \ll 1$ is not valid.

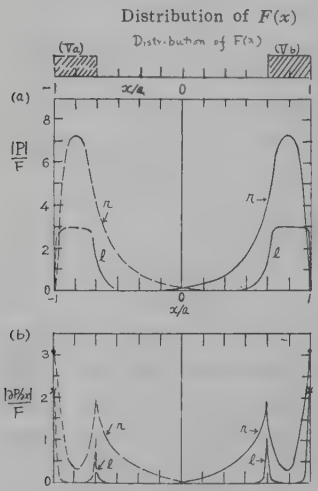

(The scale of ordinates is 10> for r-curves, 10^5 for l-curves.)

(The scale of ordinates is 1 for r-curves, 10^{-3} for l-curves.)

Fig. 19. $|P(x)|$ and $|P_x(x)|$ for SC range.
(Broken lines: V_a model, r: barotropic mode, Solid lines: V_b model, l: baroclinic mode)

In Fig. 19 (*a*) we show the distribution of $|P(x)|$ about x for two types of wind stress distribution by taking $\mu = 5\times10^{-8}$, $\nu = 5\times10^{-6}$, $A = 10^8$, which corresponds to the SC range. We can see that the amplitude $|P(x)|$ is finite only within and near the wind belt and also its spatial distribution is symmetrical about the origin for the case (Va) and (Vb), as stated before. Further, the values of $|P(x)|$ for barotropic mode is far larger than that of baroclinic mode, since $J_{0r}/J_{0l} \fallingdotseq (\delta_2-\delta_1)_l/(\delta_2-\delta_1)_r \gamma$. This is true even in WI range, because $|J_{0r}/J_{0l}| \fallingdotseq \frac{1}{\gamma}$ since $|(\delta_2-\delta_1)_l| \fallingdotseq |(\delta_2-\delta_1)_r|$ in this range.

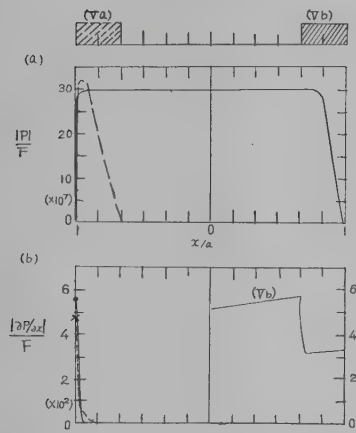

(Scale for V_b curve in east section. Note that the values in east section is 10^{-2} of those at western coast and that these of V_a are so small that the curve almost coincides with the abscissa)

Fig. 20. $|P(x)|$ and $|P_x(x)|$, of barotropic mode for WI range ($\nu=10^{-7}$, $k=10^{-8}$, $\Delta=10^{8}$)
(Broken lines: V_a model, Solid lines: V_b model)

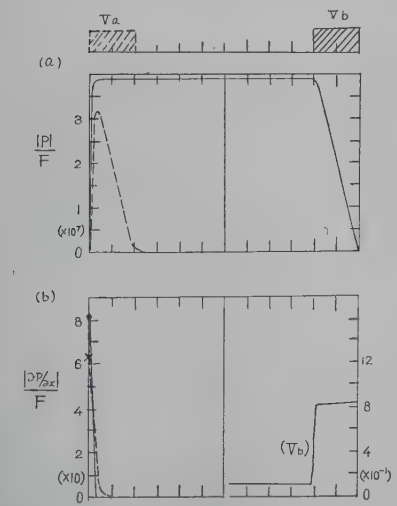

(Scale for V_b curve in east section. The same remark as in Fig. 20b)

Fig. 21. $|P(x)|$ and $|P_x(x)|$ of baroclinic mode for WI range
($\nu=10^{-7}$, $k=10^{-8}$, $\Delta=10^{8}$)

In Fig. 20(a) and 21(a) we indicate the similar distribution of $|P(x)|$ for WI range, by taking the numerical constant such as $\mu=5\times10^{-8}$, $\nu=10^{-7}$, $k=10^{-8}$, Δ

$=10^8$. These figures indicate clearly the difference between WI and SC, since in (Va) the amplitude $|P(x)|$ is finite only in the wind belt which locates in the western part and it dminishes rapidly as apart from it. On the other, hand, the value of $|P(x)|$ has almost constant, equal to $|J_0||1-e^{-i\delta_2\Delta}|/|\delta_2|$ all over the ocean outside wind belt, except at $x=-a$. Especially for barotropic mode this constant has approximate value of $|J_0|\Delta$, since $|i\delta_2\Delta|\ll 1$.

When we compare the values of $|P(x)|$ between SC and WI range, we can see generally that the value in WI is larger than in SC range. When we exress the maximum value of $|P(x)|$ in each range, they are proportional to $|J_0/\delta_2|$ or to $|/\nu|\delta_2(\delta_2-\delta_1)|$ for both range (in SC range we might take this as $|J_0/\delta_1|$ since $|\delta_1|=|\delta_2|$) and in WI range $\nu|\delta_2|$ is quite smaller than that in SC range, and $|\delta_2-\delta_1|$ has a most the same order of magnitude in both ranges.

In Fig. 19(b) we show the similar distribution of $|P_x|$ for (Va) and (Vb) with same numerical constants as In Fig. 19(a), which indicates that the meridional velocity is finite only near the coast and the boundary of the wind belt and its spatial distribution is symmetrical about the origin as in the distribution of P shown in Fig. 19(a).

In Fig. 20(b) and 21(b) the distribution of $|P_x|$ in WI range is shown by taking the same numerical constants as in Fig. 20(a) and 21(a) which indicate that in both types of wind distribution almost the same amount of westeward meridional current is produced notwithstanding the condition that in (Va) the wind acts only near the eastern coast. Especially it is interesting to note that in (Vb) model the meridional current in the wind belt which is near the eastern coast is much weaker than the western coast current. In fact the value of P_x in and near wind belt is expressed as

(inside wind belt or $a>x>a-\Delta$)

$$P_2=J_0\{e^{i\delta_1(x-a+\Delta)}-e^{i\delta_2(x-a)}\} \tag{8.18}$$

(outside wind belt and not near the western coast)

$$P_x=J_0(1-e^{-i\delta_2\Delta})e^{i\delta_2(x-a+\Delta)}$$

where the contribution of the first term in (8.18) becomes negligible except very close to $x=a-\Delta$. Therefore, in this type of wind stress distribution the meridional current in the wind belt near the eastern coast has an order of magnitude J_0 or $J_0\ 1-e^{-i\delta_2\Delta}$ which is far smaller than the western current of the order of about $|J_0\delta_1/\delta_2|e^{B_2(\Delta-2a)}$.

It is somewhat worthwhile to examine the mode of the western current caused

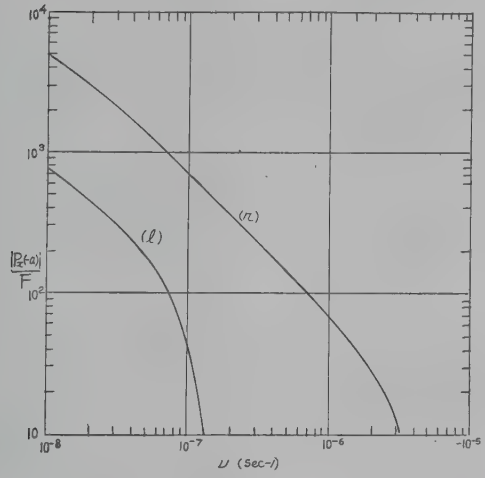

Fig. 22. $P_x(-a)$ as a function of ν (r): Barotropic (l): Baroclinic

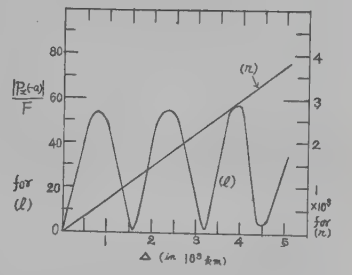

Fig. 23. $P_x(-a)$ as a function of Δ (r): Barotropic (l): Baroclinic

by the wind stress of type (Vb). Here we show two of such relationships, one is Fig. 22, which gives the value of $|P_x(-a)$ as a function of ν by taking $k=10^{-8}$ $\mu=5\times10^{-8}$ and $\Delta=10^8$. We can see that the value of $|P_x(-a)|$ increases as ν decreases or the period of the fluctuation increases. When ν approaches to the critical value between SC and WI range the value of $|P_x(-a)|$ rapidly decreases, since in SC range it has an order of magnitude of $e^{-2\beta_1 a}$. Further, we can see that the value is always larger for barotoropic mode.

As another example we show the change of $|B_x(-a)|$ as a function of Δ with numerical constants $k=10^{-8}$, $\mu=5\times10^{-8}$, $\nu=10^{-7}$ or in WI range of course. In this example we have a very simple relation for the barotropic mode, since $|i\delta_2\Delta|\ll1$ and $|P_x(-a)|$ increases almost linearly with Δ. On the other hand, for the baroclinic mode

$$|P_x(-a)|\sim|1-e^{i\delta_2\Delta}|$$

and also when we put $\Delta=\frac{a}{3}\Delta_0$, then we have $i\delta_2\Delta=(\Delta i+0.025)\Delta_0$ and thus the value of $|R_x(-a)|$ shows spectral distribution about Δ_0 or there exists some resonance phenomenon.

The difference in the response to the wind stress between two cases of western wind belt and eastern wind belt in WI range is due to the fundamental property of β-plane and this situation can be explained more simply by stationary circulation pattern in a rectangular β-plane of homogeneous ocean with friction proportional to velocity which was treated by Stommel (1948) to prove the westward intensification of oceanic circulation.

In such model the vorticity equation becomes

$$\beta v+k\zeta=\frac{1}{h}\left(\frac{\partial \tau_y}{\partial x}-\frac{\partial \tau_x}{\partial y}\right)$$

where k is friction coefficient, ζ relative vorticity, τ_x, τ_y are stress component, h is depth. Assuming geostrophic relation for velocity, we put

$$u=-\partial P/\partial y \qquad v=\partial P/\partial x$$

$$F(x)\sin \mu y=\frac{1}{kh}\left(\frac{\partial \tau_y}{\partial x}-\frac{\partial \tau_x}{\partial y}\right)$$

then we have

$$P_{xy}+\frac{\beta}{k}P_x-\mu^2 P=F(x)$$

Therefore the general solution of $P(x)$ is given by

$$P(x)=J(x)+J(a)\,e^{-2\lambda_1 a}\{e^{\lambda_2(a+x)}-e^{\lambda_1(a+x)}\}$$

as in (8.5a), where

$$J(x)=\frac{1}{(\lambda_1-\lambda_2)}\int_{-a}^{x}F(\xi)\{e^{\lambda_1(x-\xi)}-e^{\lambda_2(x-\xi)}\}d\xi$$

and

$$\lambda_1=-(\beta/2k)+\sqrt{(\beta/2k)^2+\mu^2}$$

$$\lambda_2=-(\beta/2k)-\sqrt{(\beta/2k)^2+\mu^2}$$

and also $|e^{\lambda_2 a}|\ll 1$, unless μ is large and if $k<10^{-5}$, or in other words, when the north-south pattern of the system is larger than the order of magnitude of 1000 km and friction is not so large.

When we assume the same wind belt as in (Va) and (Vb), we obtain the special solution, corresponding to (8.16) and (8.17), such as

(V'a) inside wind belt $(-a+\Delta>x>-a)$

$$P(x)=\frac{F_0}{(\lambda_1-\lambda_2)}\left\{\left(\frac{1}{\lambda_1}-\frac{1}{\lambda_2}\right)(e^{\lambda_2\overline{a+x}}-1)+\frac{e^{-\lambda_1\Delta}}{\lambda_1}(e^{\lambda_1\overline{(a+x)}}-e^{\lambda_2\overline{a+x}})\right\}$$

outside wind belt $(a>x>-a+\Delta)$

$$P(x)=\frac{F_0 e^{\lambda_2(a+x)}}{(\lambda_1-\lambda_2)}\left(\frac{e^{-\lambda_2\Delta}}{\lambda_2}+\frac{1-e^{-\lambda_1\Delta}}{\lambda_1}\right)$$

(V'b) inside wind belt $(a>x>a-\Delta)$

$$P(x)=\frac{F_0}{(\lambda_1-\lambda_2)}\left\{\left(\frac{1}{\lambda_1}-\frac{1}{\lambda_2}\right)(e^{\lambda_1\overline{x-a}}-1)+\frac{e^{\lambda_2(x-a+\Delta)}}{\lambda_2}\right\}$$

outside wind belt $(a-\Delta>x>-a)$

$$P(x)=\frac{F_0}{\lambda_1-\lambda_2}\left(\frac{1}{\lambda_2}-\frac{1}{\lambda_1}+\frac{e^{\lambda_1\Delta}}{\lambda_1}\right)e^{-2\lambda_1 a}\{e^{\lambda_2(a+x)}-e^{\lambda_1(a+x)}\}$$

where we assume that Δ is of a moderate magnitude or $e^{\lambda_2\Delta}\ll 1$. In order to give some idea about the magnitude of λ_1 and λ_2 we show the next table which corresponds to Table 3.

$\mu=$		10^{-7}	5×10^{-8}	10^{-8}
$k=10^{-6}$	$\lambda_1(\times10^{-7})$	0.41	0.12	0.005
	$\lambda_2(\times10^{-7})$	−2.41	−2.12	2.005

$k=10^{-7}$	$\lambda_1(\times 10^{-9})$	5.0	1.25	0.05
	$\lambda_2(\times 10^{-8})$	2.005	2.000	2.000

Therefore these equations have the same features as the equations (8.16) and (8.17), because in (V'a) model $|P(x)|$ diminishes to zero quite rapidly as apart from the wind belt owing to the exponential factor $\exp\lambda_2(a+x)$. On the other hand, in the model (V'b) in which the wind belt lies near the eastern coast, the function $P(x)$ has a factor $\exp\lambda_1(x-a)$ outside wind belt, which remains finite as we can see from above table.

This similarity between the condition in the stationary circulation and in the range of WI in a text exists also in the spatial distribution of $\partial P/\partial x$. This is quite obvious, because in non-stationary solution we get stationary circulation when we put $\nu=0$ which belongs certainly to WI range as seen in Table 3.

Generally speaking, the absolute values of $P(x)$ and $\partial P/\partial x$ are larger in barotropic mode than in baroclinic mode for both range of *SC* and *WI* and the ratio of these quantities of barotropic to baroclinic mode becomes larger for small values of ν or in *SC* range, so that barotropic mode becomes more predominent as frequency increases as in case of various kinds of wind stress distributions discussed above.

Moreover, it seems to be worthwhile to remark that in certain ranges of ν between very low and high frequencies, for example between $\nu=10^{-6}$ and 5×10^{-7} for $\mu=5\times10^{-8}$ as seen in Table 3, the barotropic mode belongs to *WI* range whereas baroclinic mode belongs to *SC* range. In other words, in such range of ν when wind belt is located near eastern coast the excitation of westward intensification occurs only in barotropic mode.

Summarizing above results, we can conclude that

(1) For a disturbance of a period shorter than a couple of weeks the respons of the ocean is limited only near wind belt, no matter where it is located in the ocean.

(2) For a disturbance of a period longer than half a year, in case wind belt is near the western coast, the response is limitted near wind belt, but in case it is near eastern coast, the response reaches western coast and particularly amplitude of meridional current along the western coast is larger than that along the eastern coast, even though wind belt is near eastern coast. This is true for both modes.

(3) For a disturbance of a period between these two values the response of barotropic mode has the same feature as described in (2), whereas that of baroclinic mode indicates the feature of shorter period as described in (1), so

that when the wind belt is near the eastern coast, strong west coast current is generated only in barotropic mode.

(4) For all periods considered here the amplitude of the response of the ocean is larger for barotropic mode than for baroclinic mode, and such difference in amplitude becomes larger as the period of disturbance decreases.

9. *Application of theoretical models and concluding remarks.*

In this paper we have no space to discuss the application of the models to practical problems in detail, partly because we have not had enough observed facts concerning the response of the ocean to variable wind stresses. However, it seems to be better to show some examples, even though they are very poor as an example of application of the theoretical models, rather than not to mention them.

In Fig. 24 annual variations of the total mass transport of the Kuroshio south off Cape Shionomisaki (Ichiye, 1957) and that of the Gulf Stream in the section between Montauk Pt. and Bermuda (Iselin, 1940) are shown. These two curves are not so adequate to be compared with each other, since the reference level

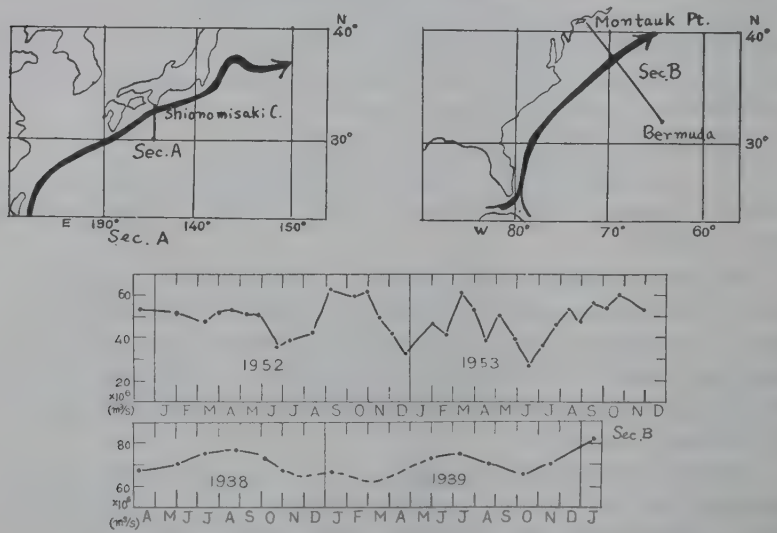

Fig. 24. Annual variations of mass transport in the Kuroshio and the Gulf Stream.

for dynamic computation is different (in the Kuroshio 1000 db, and in the Gulf Stream 2000 db), and also the year of observation, the distances between succesive stations are not the same in two curves. Neverthless, if we examine these curves closely, we can recognize some characteristic features between two current systems. The annual range of fluctuation in the Kuroshio reaches about 20×10^6 m^3/s, whereas that of the Gulf Stream is only about half of it, although the mean transport of the Kuroshio is less than that of the Gulf Stream by about 30×10^6 m^3/s. The difference in the mean values may be partly due to the condition that the reference level in the Kuroshio is more shallow than in the Gulf Stream. Further, the maximum transport seems to occur in spring and autumn in the former, whereas it occurs in summer and winter in the latter, though it is too early to conclude by use of so incomplete data.

The data concerning wind stress distribution over the ocean are also insufficient in the present stage, since such data are given only in the average state, as far as the author knows. However, the voritcity distribution of the

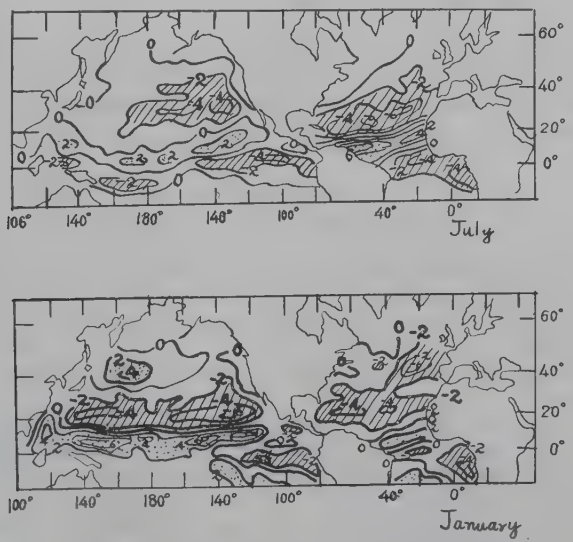

Fig. 25. Vorticity of mean surface wind over the ocean in 10^{-6} S^{-1} after MINTZ and DEAN (1952). (The stippled pattern indicates positive, and the diagonal ruling negative vertical vorticity greater than 2×10^{-6} s^{-1})

surface wind in July and January prepared by MINTZ and DEAN (1952) which is reproduced in Fig. 25 indicates interesting features of the difference of wind stress condition over the north Atlantic and the north Pacific. When we pay attention to the region between N40° and N20° which corresponds roughly to the rectangular basin considered here, the difference in the vorticity of wind between in winter and summer is more conspicuous over the Pacific than over the Atlantic. Further, the absolute value of negative vorticity in the considered region is higher in summer than in winter over the Atlantic, whereas the condition over the Pacific is reverse. Unfortunately we have no chart of spring and autumn, so that we cannot say about the difference in phase of the annual variation of the transport in two oceans. However, the larger annual fluctuation of the transport of the Kuroshio seems to be associated with the larger annual range (or winter-summer difference) of wind vorticity over the Pacific, particularly over the eastern half of the Pacific, as exlpained in the theoretical model, because the variable wind of annual or semi-annual period can cause a large fluctuation of the western current, even when it is applied to the eastern part of the ocean.

Acknowledgement: The author wishes his thanks to Mr. H. STOMMEL for his encouragement and advices and also to Dr. G. VERONIS, Dr. W. MALKUS and Mr. F. FUGLISTER for their discussions about the present paper.

References

CHARNEY, J.G., 1955 (a) The generation of ocean currents by wind Journ. Mar. Res. 14(4) pp 477-498

CHARNEY, J.G., 1955 (b) The Gulf Stream System as an inertial boundary layer. Proc. N.A.S. (USA) 41(10) pp 731-740

FUGLISTER, E.C., 1951. (a) Annual variations in current speeds in the Gulf Stream System. Journ. Mar. Res. 10(1) pp 119-127

FUGLISTER, F.C., 1951 (b) Multiple currents in the Gulf Stream System. Tellus, 4, pp 230-233

ICHIYE, T., 1951 On the variation of ocean circulation (1) Oceanog. Mag. 3(2) pp 79-82

ICHIYE, T., 1957 On the Hydrography of the Western North Pacific and its seasonal variation. (To be published. The paper was read at the meeting of Ass. d'Ocean. Phys. of IUGG at Toronto in September of 1957)

ISELIN, C,O'D., 1940 Preliminary report of long-period variations in the transport of the Gulf Stream. Pap. phys. Oceanog. Met. 3(1) pp 1-40

MINTZ, Y. and DEAN, G., 1952 The observed mean field of motion of the atmosphere. Geophys. Res. Papers no. 17, (Geophys. Res. Dir. Air Force Cambridge Res. Center)

MORGAN, G.w., 1956 On the wind-driven ocean circulation. Tellus, 8(3) pp 301-320

MUNK, W.H., 1950 On the wind-driven ocean circulation. Journ. Met. 7(2) pp 79-93

MUNK, W.H., 1957 Note on Charney's calculations. (Unpublished manuscript)

NEUMANN, G., 1954 Note on the wind-driven ocean circulation New York University, College of Engineering, Research Division. pp 1-54

STOMMEL, H., 1948 The westward intensification of wind-driven ocean currents. Trans. Amer. Geophys. Un., 29(2) pp 202-207

STOMMEL, H., 1955 Why do our ideas about the ocean circulation have such a peculiarly dream-like quality? (Private printing)

VERONIS, G. and G.W. MORGAN, 1955 A study of the time-dependent wind-driven ocean circulation. Tellus 7(2) pp 232-242

VERONIS, G. and H. STOMMEL, 1956 The action of variable wind stresses on a stratified ocean. Journ. Mar. Res. 15(1) pp 43-75

The Oceanographical Magazine
Vol. 10. No. 1. June 1958

A Method for the Harmonic Analysis of Tides

By

Masamori Miyazaki

Japan Meteorological Agency

1. *Introduction*

Since the first proposal of Laplace, many methods have been tried for the harmonic analysis of tides. Certain of them, such as those of G. H. Darwin (sammarized in Darwin 1907) and A. T. Doodson (T. I. Method, 1928), are thought to be excellent for the hand analysis and widely used throughout the world. Making use of these methods, the tidal constants were already computed at many important harbours, and the tide tables have been published annually from many countries and authorities.

There remains, however, an important practical problem. With all these excellent methods, workers are often disgusted with the labour involved in the harmonic analysis of tides. For instance, two skilled workers require two months or more for the tidal analysis of the one-year records. So, they will be not so much blamed for the incompleteness of the network of the constants and the check of their timely variations.

The recent development of the electric or electronic computors will fairly decrease the labour of us. But above methods are essentially of the hand-work type, and the processes are often very confused when we carry out the analysis by these computors.

In this manuscript, the author intends to show a new, simple method which computes the constituents from the tidal records of about one year. We shall easily obtain the final results in two or three days by hand, when the continuous records are given and the corrections of the time and datum line are already made before the work. The electronic computors would obtain the results in decimals of an hour or more rapidly.

2. *Choice of the constituents*

The constituents here considered are first given from the harmonic expansion

of the tide-generating potential (DOODSON 1921), and some constituents are added which are caused by the meteorological origins or by the interaction of important constituents. 63 constituents are here chosen, but all of them will be not necessary. The constituents of small amplitudes are to be ignored by the statistical tests, and the tide predictor only counts some definite constituents whose amplitudes are large in general.

We now consider the following constituents from the expansion of the potential:

Long-period constituents	Mf, Mm, Ssa, Mt.
Diurnal constituents	O_1, K_1, P_1, Q_1, M_1, J_1, OO_1, ρ_1 σ_1, π_1, $2Q_1$, ϕ_1, x_1, θ_1, ψ_1, γ_1, α_1, β_1.
Semi-diurnal constituents	M_2, S_2, N_2, K_2, ν_2, μ_2, L_2, T_2, $2N_2$, δ_2, λ_2, η_2, R_2, ε_2, ζ_2.
Ter-diurnal constituents	M_3

The arguments of these constituents are shown in Table 1.

Table 1. Argumments of normal constituents chosen by us.

Name	Argument		Coefficient*	Name	Argument		Coefficient*
	s	h			s	h	
Mf	2	0	0.15642	M_2	−2	2	0.90812
Mm	1	0	8254	S_2	0	0	42286
Ssa	0	2	7287	N_2	−3	2	17387
Mt	3	0	2995	K_2	0	2	7857
				ν_2	−3	4	3303
O_1	−1	1	0.37689	μ_2	−4	4	2777
K_1	0	1	− 36233	L_2	−1	2	− 2567
P_1	0	−1	17554	T_2	0	−1	2479
Q_1	−3	1	7216	$2N_2$	−4	2	2301
M_1	−1	1	− 2964	δ_2	−5	4	671
J_1	1	1	− 2964	λ_2	−1	0	− 620
OO_1	2	1	− 1623	η_2	1	2	643
ρ_1	−3	3	1371	R_2	0	1	− 354
σ_1	−4	3	1153	ε_2	−2	1	− 314
π_1	0	−2	1029	ζ_2	−2	3	276
$2Q_1$	−4	3	955				
ϕ_1	0	3	− 756	M_3	−3	3	− 0.01188
χ_1	−1	3	− 566				
θ_1	1	−1	− 560				
ψ_1	0	2	− 423				
γ_1	3	1	− 311				
α_1	−5	3	278				
β_1	−1	−1	− 278				

* Those of the principal constituents (after DOODSON).

We have chosen the constituents whose coefficients in the expansion of the potential are more than 0.003 or so except for the long period ones. For the long period constituents, the limit is taken at 0.02, since the relative importance of the equilibrium amplitudes against the observed ones will be fairly large for these slow motions.

The following constituents are chosen as the meteorological tides:

Sa, S_1.

They are the annual and daily variations, which are mainly caused by the meteorological or oceanographical origins.

The following constituents are also taken as the shallow water tides or the compound tides:

Long-period constituents	Msf
Diurnal constituents	MP_1, SO_1.
Semi-diurnal constituents	OP_2, OQ_2, $2SM_2$.
Ter-diurnal constituents	MK_3, MO_3, SK_3, SO_3, SP_3, MQ_3, K_3.
Quarter-diurnal constituents	M_4, MS_4, MN_4, MK_4, S_4, SN_4 SK_4.
Sixth-diurnal constituents	$2MS_6$, M_6, $2SM_6$.

They are the constituents whose relative importances seem to be significant.

Two constituents δ_2 and η_2 have the same speed with the compound tides MNS_2 and KJ_2, respectively. Doodson considered these constituents as the compound tides. But they are not likelv to become more remarkable than the normal ones. The coefficients of the normal constituents are both nearly equal to that of λ_2 in the expansion of the potential, while the relative importance of the compound ones seems to be fairly smaller than that of $2SM_2$ and OP_2, respectively. It will be rather natural to consider that the normal constituents will be more important in general cases.

We take only four from the shallow water constituents given by the interaction of three normal ones. These constituents will be generally small except for very special cases.

3. *Method of analysis*

We now take the period 355 days as the unit of the analysis. This period will be very convenient for us because the period of each constituent chosen above is closely proximate with a certain, corresponding harmonic wave in it, respectively. The corresponding speeds of constituents and harmonics per mean solar hour are shown in Table 2.

Table 2. Speeds of the constituents (σ_c) and the corresponding harmonics (σ_n) per mean solar hour, k being the number of harmonics for the 240-term analysis.

n	σ_n	σ_c		k	cos	sin
0	0.000	0.000	A_0	0	$A_{0,0}$	—
1	0.042	0.041	Sa	1	$(A_{1,1}-b_{1,1})/2$	$(a_{1,1}+B_{1,1})/2$
2	0.085	0.082	Ssa	2	$(A_{2,2}-b_{2,2})/2$	$(a_{2,2}+B_{2,2})/2$
13	0.549	0.544	Mm	13	$(A_{13,2}+b_{13,2})/2$	$(a_{13,2}-B_{13,2})/2$
24	1.014	1.016	Msf	24	$A_{24,1}$	$B_{24,1}$
26	1.099	1.098	Mf	26	$(A_{22,1}+b_{22,1})/2$	$(-a_{22,1}+B_{22,1})/2$
39	1.648	1.642	Mt	39	$(A_{13,1}-b_{13,1})/2$	$(-a_{13,1}-B_{13,1})/2$
293	12.380	12.373	α_1	53	$(A_{5,2}+b_{5,2})/2$	$(a_{5,2}-B_{5,2})/2$
304	12.845	12.854	$2Q_1$	64	$(A_{16,1}+b_{16,1})/2$	$(a_{16,1}-B_{16,1})/2$
306	12.930	12.927	σ_1	66	$(A_{18,1}-b_{18,1})/2$	$(a_{18,1}+B_{18,1})/2$
317	13.394	13.399	Q_1	77	$(A_{19,2}+b_{19,2})/2$	$(-a_{19,2}+B_{19,2})/2$
319	13.479	13.472	ρ_1	79	$(A_{17,1}-b_{17,1})/2$	$(-a_{17,1}-B_{17,1})/2$
330	13.944	13.943	O_1	90	$A_{6,0}$	$-a_{6,0}$
332	14.028	14.025	MP_1	92	$(A_{4,2}+b_{4,2})/2$	$(-a_{4,2}+B_{4,2})/2$
341	14.408	14.410	β_1	101	$(A_{5,1}-b_{5,1})/2$	$(a_{5,1}+B_{5,1})/2$
343	14.493	14.492	M_1	103	$(A_{7,2}+b_{7,2})/2$	$(a_{7,2}-B_{7,2})/2$
345	14.577	14.570	χ_1	105	$A_{9,0}$	$a_{9,0}$
353	14.915	14.918	π_1	113	$(A_{17,2}+b_{17,2})/2$	$(a_{17,2}-B_{17,2})/2$
354	14.958	14.959	P_1	114	$(A_{18,1}+b_{18,1})/2$	$(a_{18,1}-B_{18,1})/2$
355	15.000	15.000	S_1	115	$A_{19,0}$	$a_{19,0}$
356	15.042	15.041	K_1	116	$(A_{20,1}-b_{20,1})/2$	$(a_{20,1}+B_{20,1})/2$
357	15.085	15.082	ψ_1	117	$(A_{21,2}-b_{21,2})/2$	$(a_{22,2}+B_{21,2})/2$
358	15.127	15.123	ϕ_1	118	$(A_{22,2}+b_{22,2})/2$	$(a_{22,2}-B_{22,2})/2$
367	15.513	15.513	θ_1	113	—	—
369	15.592	15.585	J_1	111	$(A_{5,1}-b_{5,1})/2$	$(a_{5,1}-B_{5,1})/2$
380	16.056	16.057	SO_1	100	$A_{4,0}$	$-a_{4,0}$
382	16.141	16.139	OO_1	98	$(A_{2,2}+b_{2,2})/2$	$(-a_{2,2}+B_{2,2})/2$
395	16.690	16.683	γ_1	85	$A_{11,0}$	$a_{11,0}$
647	27.338	27.342	OQ_2	73	$(A_{23,2}-b_{23,2})/2$	$(a_{23,2}+B_{23,2})/2$
649	27.423	27.424	δ_2	71	$(A_{23,1}-b_{23,1})/2$	$(-a_{23,1}-B_{23,1})/2$
660	27.887	27.895	$2N_2$	60	$A_{12,0}$	$-a_{12,0}$
662	27.972	27.963	μ_2	58	$(A_{10,2}+b_{10,2})/2$	$(-a_{10,2}+B_{10,2})/2$
673	28.437	28.440	N_2	47	$(A_{1,2}+b_{1,2})/2$	$(a_{1,2}-B_{1,2})/2$
675	28.521	28.513	ν_2	45	$A_{3,0}$	$a_{3,0}$
684	28.901	28.902	OP_2	36	$(A_{12,1}+b_{12,1})/2$	$(a_{12,1}-B_{12,1})/2$

n	σ_n	σ_c		k	cos	sin
685	28.944	28.943	ε_2	35	$A_{13,0}$	$a_{13,0}$
686	28.986	28.984	M_2	34	$(A_{14,1}-b_{14,1})/2$	$(a_{14,1}+B_{14,1})/2$
687	29.028	29.025	ζ_2	33	$(A_{15,2}-b_{15,2})/2$	$(a_{15,2}+B_{15,2})/2$
697	29.451	29.456	λ_2	23	$(A_{23,2}+b_{23,2})/2$	$(-a_{23,2}+B_{23,2})/2$
699	29.535	29.528	L_2	21	$(A_{21,1}-b_{21,1})/2$	$(-a_{21,1}-B_{21,1})/2$
709	29.958	29.959	T_2	11	$(A_{11,1}-b_{11,1})/2$	$(-a_{11,1}-B_{11,1})/2$
710	30.000	30.000	S_2	10	$A_{10,0}$	$a_{10,0}$
711	30.042	30.041	R_2	9	$(A_{9,1}+b_{9,1})/2$	$(-a_{9,1}+B_{9,1})/2$
712	30.085	30.082	K_2	8	$(A_{8,2}+b_{8,2})/2$	$(-a_{8,2}+B_{8,2})/2$
725	30.634	30.627	η_2	5	$A_{5,0}$	$a_{5,0}$
734	31.014	31.016	$2SM_2$	14	$(A_{14,1}+b_{14,1})/2$	$(a_{14,1}-B_{14,1})/2$
1003	42.380	42.377	MQ_3	43	$(A_{5,2}-b_{5,2})/2$	$(-a_{5,2}-B_{5,2})/2$
1016	42.930	42.927	MO_3	56	$(A_{8,1}-b_{8,1})/2$	$(a_{8,1}+B_{8,1})/2$
1029	43.479	43.476	M_3	69	$(A_{21,1}+b_{21,1})/2$	$(a_{21,1}-B_{21,1})/2$
1040	43.944	43.943	SO_3	80	$A_{16,0}$	$a_{16,0}$
1042	44.025	44.025	MK_3	82	$(A_{14,2}+b_{14,2})/2$	$(-a_{14,2}+B_{14,2})/2$
1064	44.958	44.959	SP_3	104	$(A_{8,1}+b_{8,1})/2$	$(a_{8,1}-B_{8,1})/2$
1066	45.042	45.041	SK_3	106	$(A_{10,1}-b_{10,1})/2$	$(a_{10,1}+B_{10,1})/2$
1068	45.127	45.123	K_3	108	$(A_{12,2}+b_{12,2})/2$	$(a_{12,2}-B_{12,2})/2$
1359	57.432	57.424	MN_4	81	$(A_{15,1}+b_{15,1})/2$	$(a_{15,1}-B_{15,1})/2$
1372	57.972	57.968	M_4	68	$(A_{20,2}+b_{20,2})/2$	$(-a_{20,2}+B_{20,2})/2$
1383	58.437	58.440	SN_4	57	$(A_{9,2}-b_{9,2})/2$	$(-a_{9,2}-B_{9,2})/2$
1396	58.986	58.984	MS_4	44	$(A_{4,1}-b_{4,1})/2$	$(-a_{4,1}+B_{4,1})/2$
1398	59.070	59.066	MK_4	42	$(A_{8,2}+b_{8,2})/2$	$(-a_{8,2}-B_{8,2})/2$
1420	60.000	60.000	S_4	20	$A_{20,0}$	$a_{20,0}$
1422	60.085	60.082	SK_4	18	$(A_{18,2}+b_{18,2})/2$	$(-a_{18,2}+B_{18,2})/2$
2058	86.958	86.952	M_6	102	$(A_{6,2}-b_{6,2})/2$	$(-a_{6,2}-B_{6,2})/2$
2082	87.972	87.968	$2MS_6$	78	$(A_{18,2}-b_{18,2})/2$	$(a_{18,2}+B_{18,2})/2$
2106	88.986	88.984	$2SM_6$	54	$(A_{6,1}+b_{6,1})/2$	$(-a_{6,1}+B_{6,1})/2$

This table clearly shows us that these sixty harmonics can be completely separated by the analysis of 35.5 hourly observations (240 terms), except for two relatively small constituents π_1 and θ_1. The latter two will be separated by two assumptions, which will be expressed later.

The following 15 constituents (which are used in the tide-predictor of the Kelvin type) will be also separated by the analysis of 71 hourly values, when two

small constituents ϕ_1 and OQ_2 are neglected.

Sa, *Ssa*, O_1, K_1, P_1, Q_1, M_2, S_2, N_2, K_2, ν_2, μ_2, L_2, MS_4, M_4.

The last method is less precise than the former, but will be sometimes useful as it is quicker at figures.

The KOBAYASHI's method (KOBAYASHI 1953) will be useful for the hand analysis in these cases. We now assume that a large integer r is the product of two integers p and q, which are prime with each other. Then, the r-term harmonic analysis can be given by the q-sets of p-term analysis and the q-term analysis of these results.

When the electric or electronic computors are available, the direct harmonic analysis will be more useful than this method.

The harmonic constants thus obtained are close to the corresponding tidal constants, but small corrections are to be made which are caused by the slight differences of the periods. When the analysis is made for a constituent (frequency $\sigma+\varepsilon$) with a harmonic frequency σ, we have

$$A' = \frac{2}{T}\int_0^T \{A\cos(\sigma+\varepsilon)t + B\sin(\sigma+\varepsilon)t\}\cos\sigma t\, dt$$

$$\approx \frac{2\sin\frac{\varepsilon T}{2}}{\varepsilon T}\left\{A\cos\frac{\varepsilon T}{2} + B\sin\frac{\varepsilon T}{2}\right\}, \qquad (1)$$

$$B' \approx \frac{2\sin\frac{\varepsilon T}{2}}{\varepsilon T}\left\{-A\sin\frac{\varepsilon T}{2} + B\cos\frac{\varepsilon T}{2}\right\},$$

provided that $\sigma \gg \varepsilon$, where T is the period of analysis.

(1) shows that a constituent (say C) is response to the neighbouring constituents as much as $\dfrac{2\sin\frac{\varepsilon T}{2}}{\varepsilon T}$ times its magnitude. The phase corrections are not necessary when we use the uncorrected results of the harmonic analysis for C in this case.

After these corrections are all made,

the amplitude correction $a = \dfrac{\varepsilon_0 T}{2} \Big/ \sin\dfrac{\varepsilon_0 T}{2}$, and

the phase correction $\Delta = \dfrac{\varepsilon_0 T}{2}$

are to be made for each constituent, where ε_0 is taken as the frequency difference between the constituent and the corresponding harmonic wave.

4. *Practical processes of the computation*

i) *Preparation of the data*

At first, we must read the 35.5 hourly values from the tidal records. When we make use the hourly records, not the mareogram itself, half of these readings are to be given by the interpolation. The formula

$$\zeta_0=\frac{9}{16}(\zeta_{-1}+\zeta_1)-\frac{1}{16}(\zeta_{-3}+\zeta_3) \qquad (2)$$

will be useful in such a case, where ζ_{-3}, ζ_{-1}, ζ_1, and ζ_3 are the hourly values. We shall denote these 35.5 hourly values by h_0, h_1, h_2, ..., h_{239}. It will be convinient to tabulate these values as follows;

$$\left.\begin{array}{ccccc} h_0, & h_1, & h_2, & h_3, & h_4, \\ h_5, & h_6, & h_7, & h_8, & h_9, \\ \vdots & \vdots & \vdots & \vdots & \vdots \\ h_{235}, & h_{236}, & h_{237}, & h_{238}, & h_{239}. \end{array}\right\} \qquad (3)$$

ii) *Harmonic analysis of the first step*

Prepare five analysis forms given in Table 3. In the first two columns in these forms, the numerical values of

$$\left.\begin{array}{l} \left\{\begin{array}{llll} h_0, & h_5, & h_{10}, & \cdots\cdots, h_{115}, \\ h_{120}, & h_{125}, & h_{130}, & \cdots\cdots, h_{235}; \end{array}\right. \\ \left\{\begin{array}{llll} h_{48}, & h_{53}, & h_{58}, & \cdots\cdots, h_{163}, \\ h_{168}, & h_{173}, & h_{178}, & \cdots\cdots, h_{43}; \end{array}\right. \\ \left\{\begin{array}{llll} h_{96}, & h_{101}, & h_{106}, & \cdots\cdots, h_{211}, \\ h_{216}, & h_{221}, & h_{226}, & \cdots\cdots, h_{91}; \end{array}\right. \\ \left\{\begin{array}{llll} h_{144}, & h_{149}, & h_{154}, & \cdots\cdots, h_{19}, \\ h_{24}, & h_{29}, & h_{34}, & \cdots\cdots, h_{139}; \end{array}\right. \\ \left\{\begin{array}{llll} h_{192}, & h_{197}, & h_{202}, & \cdots\cdots, h_{67}, \\ h_{72}, & h_{77}, & h_{82}, & \cdots\cdots, h_{187}; \end{array}\right. \end{array}\right\} \qquad (4)$$

are to be entered, respectively. The final results computed in these five forms will be now denoted by

$$\left.\begin{array}{llllll} p_{0,0}, & p_{1,0}, & p_{2,0}, & \cdots\cdots, & p_{24,0}; & q_{1,0}, q_{2,0}, \cdots\cdots, q_{23,0}; \\ p_{0,1}, & p_{1,1}, & p_{2,1}, & \cdots\cdots, & p_{24,1}; & q_{1,1}, q_{2,1}, \cdots\cdots, q_{23,1}; \\ \vdots & \vdots & \vdots & & \vdots & \vdots \\ p_{0,4}, & p_{1,4}, & p_{2,4}, & \cdots\cdots, & p_{24,4}; & q_{1,4}, q_{2,4}, \cdots\cdots, q_{23,4}. \end{array}\right\} \qquad (5)$$

iii) *Harmonic analysis of the second step*

We next analyse each column in (5) such as

$$p_{14,0},\ p_{14,1},\ p_{14,3},\ p_{14,2},\ p_{14,4},$$

harmonically. The type of analysis forms is shown in Table 4. The harmonic constants thus obtained are generally denoted by

$$A_{i,j},\ B_{i,j},\ a_{i,j},\ \text{and}\ b_{i,j},$$

where i is the order of harmonic in the first step, and j that in the second step. $A_{i,j}$ and $B_{i,j}$ are the cosine and sine terms in the analysis of $p_{i,j}$, and $a_{i,j}$ and $b_{i,j}$ are those in the analysis of $q_{i,j}$, respectively.

The harmonics corresponding to the tidal constituents will be then given by the combinations of $A_{i,j}$ and $b_{i,j}$ or $a_{i,j}$ and $B_{i,j}$, which are shown in Table 2. Only 64 of 121 harmonics (including the constant term) will be necessary in our analysis.

iv) *The correction terms*

Prepare five pairs of forms similar to that shown below, the multipliers in the correction terms being in Table 5—Table 9.

Constituent		Correction terms			Corrected value
Name	Value	Q_1	O_1	P_1	
α_1		−0.0042	0.0004	−0.0005	
$2Q_1$		−0.0078	0.0006	−0.0006	
σ_1		−0.0092	0.0006	−0.0006	
Q_1			0.0011	−0.0006	

The cosine and sine terms of the harmonics computed above are to be entered in the lefter blank columns, and the important ones are also to be entered in the upper blank rows of the correction terms. The computations are easily made in these forms.

v) *Final process*

Prepare the forms of the following type. First enter the corrected cosine and sine terms of constitutents in the first two blank rows. The coefficients a and A are given from Table 10. The arguments V, u, and f are given from s, h, P, P_1, and N by using the Table 11. Numerical values of these astronomical ele-

	α_1	$2Q_1$	
A			
B			
R			
a			
f			
$H=afR$			
δ			
V			
u			
Δ			
æ=sum			

ments are shown in many tables, such as those in SHUREMAN's manual (1924). After these factors are obtained, they are to be entered in the corresponding space of this table.

The amplitude and phase lag will be easily computed in this table, where

$$R=\sqrt{A^2+B^2},$$
$$æ=V+u+\Delta+\delta. \qquad (6)$$

The tidal constants of π_1 and θ_1 constituents are both given from the terms of 113-th harmonics, which will be separated by the following two assumptions:

$$\frac{æ(\theta_1)-æ(\pi_1)}{æ(K_1)-æ(O_1)}=0.542 \quad \text{(ratio of the corresponding frequency differences)},$$
$$H_\theta/H_\pi=0.550 \quad \text{(ratio of the equilibrium amplitudes)}.$$

Then we easily obtain

$$\left.\begin{aligned} H_\pi &= \frac{1.005R}{\sqrt{1.288+1.074\cos(S_\pi-S_\theta-d)}},\\ æ_\pi &= \delta+\tan^{-1}\frac{\sin S_\pi+0.537\sin(S_\theta+d)}{\cos S_\pi+0.537\cos(S_\theta+d)},\\ H_\theta &= 0.550H_\pi,\\ æ_\theta &= æ_\pi+d. \end{aligned}\right\} \qquad (7)$$

where $S=V+u+\Delta$, and $d=0.542\{æ(K_1)-æ(O_1)\}$, respectively.

vi) *Analysis by the calculating punch*

When the culculating punch is available, the time of analysis will be fairly decreased. The direct analysis will be sometimes more useful in this case.

For this purpose, multipliers for the constituents (three-figure values)

$$m_{i,k}=\frac{\delta}{240}\cos\frac{2\pi ik}{T} \quad \text{or} \quad \frac{1}{120}\sin\frac{2\pi ik}{T}$$

are first to be punched on cards (and read into tapes, if necessary), where

$$i=0,\ 1,\ 2,\ \cdots\cdots,\ 239;\ \delta=1 \text{ for } i=0,\ =2 \text{ for } i\neq 0,$$

respectively. Each term to be analysed (three-figure values) h_i is next to be punched on each blank card. Then the analysis

$$\sum_i m_{i,k}\cdot h_i$$

will be easily obtained by the machine.

The time of computation is about 1 hour (15 constituents) and 4 hours (all constituents) when we make use the type 602A calculating punch. If the EDPM of the type 704 is available, the time of computation will be within a few minutes.

vii) *Analysis for 120 terms*

The odd order terms of h_t are absent in this case, and the hand analysis of the first step will be replaced by the 24-term analysis. Computations of l_t and m_t are not necessary in the forms shown in Table 3. The divisors in the second step of analysis are then one half those for 240-term analysis. The time and labour will be fairly decreased in this case, but the results will be somewhat less accurate than the former results.

5. *Example of the practical analysis*

As an example of the analysis by this method (240 terms), we have computed the tidal constants for Sumoto (Awaji Is., Hyōgo Pref.) by using the data for 1949. The tide gauge of OKADA's type is set at this station, and the continuous records are given with the sufficient accuracy. The analysis was already made by us (MIYAZAKI 1952) according to the T.I. method by using the same records. The harmonic constants for 15 constituents given by two methods are shown in Table 12.

The tide on January, 1949, are predicted on trial by both series of constants, and they are compared with the observation. A part of these curves will be shown in. Fig. 1.

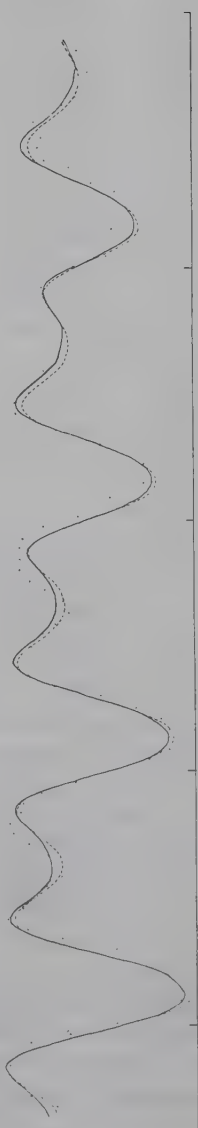

Fig. 1. Predicted and observed curves.

Two predicted curves are in good agreement with the observed ones, and it will be difficult to discriminate which is better than another.

Thus, in conclusion, the present method will be very useful, since the time and labour involved is trivial and the accuracy of results will be similar to those given by the usual, labourous methods.

The author here wishes to express his hearty thanks to Prof. K. HIDAKA, Dr. M. NAKANO, Dr. Y. TAKENOUCHI, for their kind advices and encouragement. He is also greatly indebted to the staff of tidal subsection, *JMA*, who kindly operate the tide predictor for him.

References

DARWIN, G.H., 1907: "Scientific Paper, Part I (Oceanic tides)", Art. 1-7, p. 1-327, Cambridge.

DOODSON, A. T., 1921: The Harmonic Development of the Tide-generating Potential. Proc. Roy. Soc. London, **A 100** (704), p. 305-329.

DOODSON, A. T., 1928: The Analysis of Tidal Observations. Phil. Trans. Roy. Soc. London, **A 227**, p. 223-279.

KOBAYASHI, T., 1953: On the Multipi-harmonic Analysis (1). Jour. Met. Soc. Japan, **31** (11-12) p. 370-

MIYAZAKI, M., 1952: Harmonic Analysis of Tide at Several Ports in the Western Part of Japan. Mem. Kobe Mar. Obs. **10**, p. 46-52.

SCHUREMAN, P., 1924: "A Manual of the Harmonic Analysis and Prediction of Tides" U. S. Coast and Geod. Survey. Sp. Publ. 98, Washington.

Table 3. Harmonic analysis of the first step.

I	II	III	IV	V	VI	VII	Multipliers											
							1	991	1	924	1	793	1	609	1	383	1	131
							966	924	707	383	259	−383	−259	−924	−707	−924	−966	−383
							866	793	0	−383	−866	−991	−866	−131	0	924	866	609
							707	609	−707	−924	−707	−131	707	991	707	−383	−707	−793
							500	383	−1	−924	500	924	500	−383	−1	−383	500	924
							259	131	−707	−383	966	609	−966	−793	707	924	−259	−991
							k_1	l_1	k_3	l_3	k_5	l_5	k_7	l_7	k_9	l_9	k_{11}	l_{11}
						VI	p_1		p_3		p_5		p_7		p_9		p_{11}	
							p_{23}		p_{21}		p_{19}		p_{17}		p_{15}		p_{13}	
							131	259	383	707	609	966	793	966	924	707	991	259
							383	500	924	1	924	500	383	−500	−383	−1	−924	−500
							609	707	924	707	−131	−707	−991	−707	−383	707	793	707
							793	866	383	0	−991	−866	131	866	924	0	−609	−866
							924	966	−383	−707	−383	259	924	259	−924	−707	383	966
							991	1	−924	−1	793	1	−609	−1	383	1	−131	−1
							m_1	n_1	m_3	n_3	m_5	n_5	m_7	n_7	m_9	n_9	m_{11}	n_{11}
VIII	IX	X	XI				q_1		q_3		q_5		q_7		q_9		q_{11}	
							q_{23}		q_{21}		q_{19}		q_{17}		q_{15}		q_{13}	
							1	966	1	707	1	259	0	259	0	707	0	966
							866	707	0	−707	−866	−707	500	707	1	707	500	−707
							500	259	−1	−707	500	966	866	966	0	−707	−866	259
							0	−259	0	707	0	−966	1	966	−1	−707	1	259
							−500	−707	1	707	−500	707	866	707	0	707	−866	−707
							−866	−966	0	−707	866	−259	500	259	1	707	500	966
							k_2	l_2	k_6	l_6	k_{10}	l_{10}	n_2	m_2	n_6	m_6	n_{10}	m_{10}
						X	p_2		p_6		p_{10}		q_2		q_6		q_{10}	
							p_{22}		p_{18}		p_{14}		q_{22}		q_{18}		q_{14}	
							1	1	1	866	1	500	1	0	0	500	0	866
							1	1	500	0	−500	−1	−1	866	1	866	0	500
							1	1	−500	−866	−500	500	1	866	500	−866	−866	0
							1	1	−1	−866	1	500	−1	0	−500	0	866	500
							1	1	−500	0	−500	−1	1	−866	866	−1	0	866
							1	1	500	866	−500	500	−1	−866	−866	−500	−866	0
							k_0	l_0	k_4	l_4	k_8	l_8	k_{12}	n_4	m_4	n_8	m_8	
							$2p_0$		p_4		p_8		p_{12}	q_4		q_8		
							p_{24}		p_{20}		p_{16}			q_{20}		q_{16}		

Turn the latter half of IV

(IV+V)

(IV−V)

(I−II)

(I+II)

Former half of III

Latter half of III

(VIII+IX)

(VIII−IX)

Remarks:

(1) $\begin{cases} \delta p_i = k_i + l_i & (i-0\,;\,\delta=2 \\ p_{24-i} = k_i - l_i & i \neq 0\,;\,\delta=1) \end{cases}$

(2) $\begin{cases} q_i = m_i + n_i \\ q_{24-i} = m_i - n_i \end{cases}$

(3) Decimal points are understood before the numerical values of multipliers except for ±1. For instance,
868 means 0.866,
−1 means −1.000.

Table 4. Harmonic analysis of the second step.

	Multipliers				
$p_{t,0}$	1.00000	0.00000	1.00000	0.00000	
$p_{t,1}$	0.30902	0.95106	−0.80902	0.58779	
$p_{t,2}$	−0.80902	0.58779	0.80902	−0.95106	
$p_{t,3}$	−0.80902	−0.58779	0.80902	0.95106	
$p_{t,4}$	0.30902	−0.95106	−0.80902	−0.58779	
					Sum
120	60	60	60	60	Divisor
$A_{t,0}$	$A_{t,1}$	$B_{t,1}$	$A_{t,2}$	$B_{t,2}$	
$q_{t,0}$	1.00000	0.00000	1.00000	0.00000	
$q_{t,1}$	0.30902	0.95106	−0.80902	0.58779	
$q_{t,2}$	−0.80902	0.58779	0.80902	−0.95106	
$q_{t,3}$	−0.80902	−0.58779	0.80902	0.95106	
$q_{t,4}$	0.80902	−0.95106	−0.80902	−0.58779	
					Sum
120	60	60	60	60	Divisor
$a_{t,0}$	$a_{t,1}$	$b_{t,1}$	$a_{t,2}$	$b_{t,2}$	

Table 5. Multipliers in the correction terms (long-period constituents).

	Sa	*Ssa*
A	0.0288	0.0289
Sa	—	594
Ssa	− 273	—
Mm	− 23	− 51
Msf	− 12	− 25
Mf	− 11	− 24
Mt	− 7	− 15

Table 6. Multipliers in the correction terms (diurnal constituents).

	Q_1	O_1	M_1	P_1	K_1	J_1
α_1	− 0.0042	0.0004	0.0004	−0.0005	0.0004	0.0020
$2Q_1$	− 78	6	6	− 6	5	22
σ_1	− 92	6	6	− 6	6	23
Q_1	—	11	8	− 8	7	28
ρ_1	533	13	9	− 8	8	29
O_1	79	—	17	− 12	11	37
MP_1	68	− 74	20	− 13	12	39
β_1	43	− 13	108	− 22	19	52
M_1	39	− 11	—	− 25	22	56
χ_1	36	− 10	− 106	− 31	26	61
π_1	28	− 6	− 21	− 273	94	91
P_1	28	− 6	− 19	—	142	97
S_1	27	− 6	− 18	288	288	104
K_1	26	− 6	− 16	142	—	112
ψ_1	26	− 5	− 15	94	− 273	122
ϕ_1	25	− 5	− 14	71	− 138	133
θ_1	20	− 4	− 9	22	− 25	779
J_1	20	− 4	− 8	19	− 22	—
SO_1	16	− 3	− 6	11	− 12	− 130
OO_1	16	− 3	− 5	10	− 11	− 110
γ_1	13	− 2	− 4	7	− 7	− 55

Table 7. Multipliers in the correction terms (semi-diurnal constituents).

	$2N_2$	μ_2	N_2	ν_2	M_2	L_2	T_2	K_2
OQ_2	— 0.0145	0.0058	— 0.0028	0.0073	0.0011	0.0031	— 0.0005	0.0009
δ_2	— 171	66	— 31	78	12	32	— 6	9
$2N_2$	—	448	— 56	139	17	41	— 6	11
μ_2	1050	—	— 67	158	18	43	— 6	11
N_2	150	— 77	—	1125	33	62	— 8	14
ν_2	129	— 66	382	—	39	67	— 8	15
OP_2	81	— 39	67	— 220	219	107	— 11	20
ε_2	77	— 37	62	— 198	448	115	— 12	21
M_2	74	— 36	57	— 181	—	124	— 12	22
ζ_2	72	— 34	53	— 166	— 411	135	— 13	22
λ_2	52	— 24	31	— 91	— 39	866	— 23	37
L_2	49	— 23	28	— 84	— 33	—	— 28	43
T_2	39	— 18	20	— 59	— 19	— 157	—	191
S_2	38	— 18	20	— 57	— 18	— 143	289	289
R_2	37	— 17	19	— 56	— 17	— 131	142	594
K_2	37	— 17	19	— 54	— 16	— 121	95	—
η_2	29	— 14	14	— 40	— 11	— 61	18	— 43
$2SM_2$	26	— 12	14	— 34	— 9	— 45	11	— 25

Table 8. Multipliers in the correction terms (quarter-diurnal constituents).

	M_3
MQ_3	0.0012
MO_3	25
M_3	—
SO_3	— 29
MK_3	— 25
SP_3	— 9
SK_3	— 9
K_3	— 9

Table 9. Multipliers in the correction terms (quarter-diurnal constituents).

	M_4	MS_4
MN_4	0.0066	0.0012
M_4	—	18
SN_4	— 77	33
MS_4	— 36	—
MK_4	— 33	— 210
S_4	— 18	— 18
SK_4	— 17	— 16

Table 10. Numerical values of a and Δ.

	a	Δ		a	Δ
A	1.0000	0.00	OQ_2	1.0129	— 15.87
Sa	0015	— 5.05	δ_2	0016	5.53
Ssa	0052	— 10.10	$2N_2$	0620	34.21
Mm	0227	— 20.97	μ_2	0122	— 15.43
Msf	0030	7.72	N_2	0090	13.25
Mf	0003	— 2.38	ν_2	0706	— 36.40
Mt	0282	— 23.34	OP_2	0003	2.38
			ε_2	0003	— 2.59
α_1	1.0057	10.58	M_2	0030	— 7.72
$2Q_1$	0828	39.26	ζ_2	0084	— 12.85
σ_1	0055	— 10.38	λ_2	0227	20.96
Q_1	0172	18.30	L_2	0430	— 28.68
ρ_1	0517	— 31.35	T_2	0013	5.06
O_1	0004	— 2.67	S_2	0000	0.00
MP_1	0083	— 12.26	R_2	0013	— 5.06
β_1	0352	26.01	K_2	0052	— 10.10
M_1	0008	— 3.86	η_2	0507	— 31.01
χ_1	0602	— 33.73	$2SM_2$	0030	7.72
π_1	0052	10.10			
P_1	0015	5.05	MQ_3	1.0057	10.58
S_1	0000	0.00	MO_3	0055	— 10.38
K_1	0015	— 5.05	M_3	0068	— 11.57
ψ_1	0052	— 10.10	SO_3	0004	— 2.67
ϕ_1	0117	— 15.14	MK_3	0083	— 12.26
θ_1	0293	— 23.63	SP_3	0015	5.05
J_1	0352	— 26.01	SK_3	0015	— 5.05
SO_1	0004	2.67	K_3	0117	— 15.14
OO_1	0028	— 7.43	MN_4	1.0016	5.53
γ_1	0421	— 28.39	M_4	0122	— 15.43
			SN_4	0090	13.25
			MS_4	0030	— 7.72
			MK_4	0135	— 16.21
			S_4	0000	0.00
			SK_4	0052	— 10.10
			M_6	1.0277	— 23.15
			$2MS_6$	0122	— 15.43
			$2SM_6$	0030	— 7.72

Table XI. *V*, *u*, and *f*.

Constituent	*V*					*f*, *u*	Constituent	*V*					*f*, *u*
	s	*h*	*p*	p_1				*s*	*h*	*p*	p_1		
Sa	0	1	0	0		—	δ_2	−5	4	3	0		M_2
Ssa	0	2	0	0		—	$2N_2$	−4	2	2	0		M_2
Mm	1	0	−1	0		*Mm*	μ_2	−4	3	0	0		M_2
Mf	2	0	0	0		*Mf*	N_2	−3	2	1	0		M_2
Mt	3	0	0	0		*Mf*	ν_2	−3	4	−1	0		M_2
							ε_2	−2	1	0	1	180°	—
α_1	−5	3	1	0	270°	O_1	M_2	−2	2	0	0		M_2
$2Q_1$	−4	1	2	0	270	O_1	ζ_2	−2	3	0	−1		—
σ_1	−4	3	0	0	270	O_1	λ_2	−1	0	1	0	180	M_2
Q_1	−3	1	1	0	270	O_1	L_2	−1	2	−1	0	180	L_2
ρ_1	−3	3	−1	0	270	O_1	T_2	0	−1	0	1		—
O_1	−2	1	0	0	220	O_1	S_2	0	0	0	0		—
β_1	−1	−1	1	0	90	O_1	R_2	0	1	0	−1	180	—
M_1	−1	1	0	0	90	M_1	K_2	0	2	0	0		—
χ_1	−1	3	−1	0	90	J_1	η_2	1	2	−1	0		*Mf*
π_1	0	−2	0	1	270	—							
P_1	0	−1	0	0	270	—	M_3	−3	3	0	0	180	*
S_1	0	0	0	0	180	—							
K_1	0	1	0	0	90	—							
ψ_1	0	2	0	−1	90	—							
φ_1	0	3	0	0	90	—							
θ_1	1	−1	1	0	90	J_1							
J_1	1	1	−1	0	90	J_1							
OO_1	2	1	0	0	90	OO_1							
γ_1	3	1	−1	0	90	OO_1							

* $f(M_3)=\{f(M_2)\}^{\frac{3}{2}}$,

$u(M_3)=\frac{3}{2}u(M_2)$.

Msf	S_2-M_2	MQ_3	M_2+Q_1	MN_4	M_2+N_2	M_6	M_4+M_2
MP_1	M_2-P_1	MO_3	M_2+O_1	M_1	M_2+M_2	$2MS_6$	M_4+S_2
SO_1	S_2-O_1	SO_3	S_2+O_1	SN_4	S_2+N_2	$2SM_6$	S_4+M_2
		MK_3	M_2+K_1	MS_4	M_2+S_2		
OQ_2	O_1+Q_1	SP_3	S_2+P_1	S_1	S_2+S_2		
OP_2	O_1+P_1	SK_3	S_2+K_1	SK_4	S_2+K_2		
$2SM_2$	S_4-M_2	K_3	K_2+K_1				

Table 12. Harmonic constants for Sumoto (34° 20′ N, 134° 54′ E).

Constituent	Present method		T.I. method	
	H	æ	*H*	æ
Sa	20.1cm	163.5°	19.3cm	160.2°
Ssa	2.9	52.1	1.9	68.9
Q_2	3.6	171.7	3.5	180.2
O_2	17.4	181.9	17.4	186.0
P_2	7.9	209.3	7.5	203.4
K_2	23.8	206.4	23.3	207.4
μ_2	3.2	147.3	3.3	176.3
N_2	6.4	208.3	6.5	202.9
ν_2	1.7	109.7	0.4	167.5
M_2	31.1	197.9	29.6	196.1
L_2	2.8	336.3	0.1	200.8
S_2	18.0	228.1	16.4	222.8
K_2	6.3	228.3	4.3	214.0
MS_4	2.2	127.2	1.1	96.8
M_4	1.3	73.5	1.0	54.5

The Oceanographical Magazine
Vol. 10. No. 1 June 1958

On the fluctuation of the Kuroshio south of Honshū (3)
(A short note on the computation of the relative volume transport)

By

Shigeo Moriyasu

Kōbe Marine Observatory

1. *Introduction*

We need to find the fluctuation in the intensity of the Kuroshio when we analyze the oceanographic conditions in the sea south of Honshū. But, it is very difficult to choose the factor indicating the intensity of the Kuroshio most pertinently. And the many factors are used for that purpose, for instance, the transport, the mean current velocity, the maximum current velocity, the width of the current etc. Though each factor is thought to be able to indicate the intensity of the current, the volume transport seems to be most suitable factor from the dynamical viewpoint.

As the computation of the absolute volume transport is troublesome, the relative volume transport is commonly utilized for convenience' sake. Masuzawa (1951) computed the volume transport in the sea south of Shiono-misaki in this manner and studied its distribution in detail, and Sugiura (1955, a, b) discussed the fluctuation in the eastern sea of Honshū by using the volume transport. Their works present very interesting results and show that the volume transport is useful for the analysis of the oceanographic conditions. However, we think that there are some problems which must be taken care of. In this note, they should be considered based on the recent data in the sea south of Shiono-misaki. Moreover, it should be discussed how great significance we can find in computing the relative volume transport up to the large depth in the considered sea area.

2. *The influence of the depth upon the volume transport*

It seems to be most convenient to use the dynamic computation for the estimation of the volume transport, though some methods can be applied. The

outline of the method is as follows (Sverdrup, 1942). Assuming the geostrophic current, we can compute the volume transport per unit width from the surface to the reference surface (d db) by means of the following equations:

E-component: $U=\frac{10}{f}\frac{\partial Q}{\partial y}$,

N-component: $V=-\frac{10}{f}\frac{\partial Q}{\partial x}$,

where $Q=\int_0^d \Delta D dz$. Here, f is the Coriolis parameter and ΔD the dynamic depth anomaly referred to the d db surface. The volume transport between two stations A and B (A lying to the right), at the distance L, is represented by

$$T_d=L\int_0^d v dz=\frac{10}{f}\int_0^d(\Delta D_A-\Delta D_B)dz=\frac{10}{f}(Q_A-Q_B)=\frac{10}{f}\delta Q,$$

where Q_A and Q_B is the value of Q at A and B, respectively. Hence, the volume transport is proportional to the difference between the values of Q at both ends of the considered section and independent of the distance between both ends. Consequently, we can easily estimate the volume transport between two arbitrary oceanographic stations, if the Q-chart is given.

Table 1 shows the volume transport on the meridian of 135°40′E (south of Shiono-misaki) for three values of d, that is, d=600, 800 and 1000 m. Here, $f=7.73\times10^{-5}$ ($\varphi=32°$N) is used for simplicity and therefore, $T=6.60\times10^6$m³/sec corresponds to $\delta Q=50$ m³/sec². The section is wider than 100 nautical miles in general. Since the oceanographic conditions fluctuated remarkably from 1954 to 1956, the results in the table are those under various conditions, say, when there is a eddy, accompanied by the cold water region in Enshū-nada, on the section or not. Furthermore, the main current of the Kuroshio is not within the section in some cases because the observations can not be made up to the sufficient depth north of the main current. Accordingly, it is of no significance to regard these values as the volume transports of the Kuroshio in every case. However, the fluctuation of δQ and so T for each value of d has the tendency similar to each other. For instance, δQ_{1000} T_{1000} for d =1000, and δQ_{600} T_{600} become larger when δQ_{800} T_{800} becomes larger. The relations are shown in Fig. 1, from which a linear relation seems to exist among them. By means of the method of least squares, the following relations are obtained:

$\delta Q_{600}=0.668\delta Q_{800}$ $\varepsilon=\pm29.5$m³/sec²,

Table 1. The value of the volume transport for d=600, 800 and 1000 m on the meridian of 135°40′E. A and B is the southern and northern end of the considered section. Remark is as follows:

A: the main current is included within the section and the counter-clockwise eddy does not appear on the meridian,

B: the main current is included within the section and the counter-clockwise eddy appears on the meridian,

C: the main current is not included within the section and the counter-clockwise eddy does not appear.

The unit of δQ and T is m^3/sec^2 and $10^6 m^3/sec$, respectively.

The positive value of T means the eastward transport.

	1954			1955				1956			
	May	Aug.	Oct.	Mar.	May	Aug.	Nov.	Mar.	May	Aug.	Nov.
A	31°—10′N	30°—35′N	31°—10′N	31°—00′N	30°—30′N	30°—30′N	31°—00′N	31°—00′N	31°—30′N	30°—40′N	31°—00′N
B	33—20	33—20	33—20	33—20	33—20	33—20	33—20	33—20	33—20	32—40	33—00
δQ_{600}	232	216	149	187	186	248	274	183	166	43	59
T_{600}	30.01	27.94	19.28	24.19	24.06	32.08	35.45	23.67	21.48	5.56	7.63
δQ_{800}	323	323	219	264	270	360	421	281	264	99	129
T_{800}	41.79	41.79	28.33	34.15	34.93	46.58	54.46	36.35	34.15	12.81	16.69
δQ_{1000}	377	370	255	318	315	396	520	353	336	135	183
T_{1000}	48.77	47.87	32.99	41.14	40.75	51.23	67.27	45.67	43.47	17.46	23.67
Remark	A	A	B	B	A	B	A	A	A	C	C

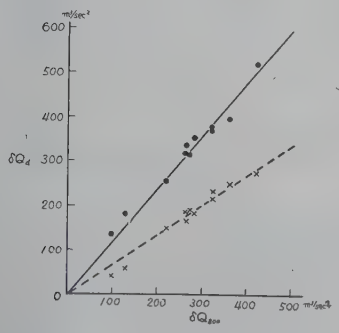

Fig. 1. The relations among δQ_{600}, δQ_{800} and δQ_{1000}.
× and • is the observed value for d=600 and 1000 m, respectively. Full and broken line is obtained by the method of least squares for d=600 and 800m, respectively.

$\delta Q_{1000}=1.195\delta Q_{1000}$ $\varepsilon=\pm 41.4\ m^3/sec^2$.

From this, we have

$T_{600}=0.668T_{800}$,

$T_{1000}=1.195T_{800}$.

Here, ε is the probable error. Therefore, the linear relation may be found among them, and it may be concluded that T_{1000} and T_{600} is about 120% and 70% of T_{800}, respectively. In the Oyashio region adjacent to Hokkaido, it was reported by Sugiura (1957) that T_{1000} was equal to $1.3T_{800}$ on the average. So, the relation between T_{1000} and T_{800} may be nearly common to both the Kuroshio and Oyashio region.

When the total volume transport of the

current is computed, the following conditions must be satisfied:

(1) the zone with main strong current is situated within the section;

(2) the depth of the reference surface is larger than that of the main current.

However, it is clear that the value of the transport depends remarkably upon how the reference surface is taken even when the above conditions are satisfied. Furthemore, it is not reasonable to make the depth of the reference surface constant everywhere. In the shallow water, some methods are used for the estimation, but they yield no little errors. Thus, it is very difficult to obtain the most reasonable value of the transport till these questions will be solved.

We adopt the volume transport as a measure to know the intensity of the Kuroshio. And, in practice, we estimate the fluctuation of the transport from the relative one computed in the manner stated above. This procedure itself is considered very suitable. But, the fluctuation of the transport is more significant than the value itself in forecasting the oceanographic conditions. If we use such relative volume transport based on the dynamic calculation to know its fluctuation, it seems that the depth of the reference surface is not an essential factor. Because, the tendency of the fluctuation may be found independent upon the depth as stated above. Therefore, we can make the depth of the reference surface any of 600, 800 and 1000 m for the purpose. However, a linear relation will not be found if the depth is smaller than the depth of the main strong current. Though this is useful for practical purposes in the sea south of Honshū, it should be studied whether the result is applicable to the other sea area.

3. *The relation between the volume transport at the surface and that from the surface to the depth of 800 m*

It is shown in the preceding section that there are linear relations among T_{600}, T_{800} and T_{1000}. In this section, we will consider whether the volume transport at the surface is connected with that from the surface to the depth of 800 m.*

The latter is represented by

$$T_{800}=\frac{10}{f}\delta Q_{800}.$$

As Q_{800} is the integral of ΔD from the surface to the depth of 800 m, Q_{800} is

* This came into question in the conference for the oceanographic forecast near Japan held on March, 25, 1958 in Tokyo.

represented by the mean of ΔD within the considered layer, $\overline{\Delta D}_{800}$, as follows:

$$Q_{800}=800\overline{\Delta D}_{800}$$

And so, we have

$$T_{800}=-\frac{10\times800}{f}\{(\overline{\Delta D}_{800})_A-(\overline{\Delta D}_{800})_B\}=-\frac{10\times800}{f}\delta\overline{\Delta D}_{800}.$$

As the relation between $\overline{\Delta D}_{800}$ and the mean velocity $\overline{u}_{800}$ within the layer is identical with that between ΔD and the velocity corresponding to it, we have

$$T_{800}=\int_A^B\overline{u_{800}}dy$$

from the above equation, that is, the volume transport is represented also by the integral of the mean velocity within the layer. On the other hand, the volume transport at the surface per unit depth is

$$T_0=\int_A^B u_0dy=\frac{10}{f}\{(\Delta D_0)_A-(\Delta D_0)_B\}=\frac{10}{f}\delta\Delta D_0.$$

Therefore, T_{800} will be represented by T_0 if $\delta\overline{\Delta D}_{800}$ is connected with ΔD_0. As Ichiye (1954) has shown that the mean velocity from the surface to the depth of 800 m is a quadratic function of the current velocity at the surface in the considered sea area, and T_{800} and T_0 is the integral of $\overline{u}_{800}$ and u_0 between A and B, respectively, T_{800} may be expected to be in close relation with T_0. The relation of $\delta\overline{\Delta D}_{800}$ to $\delta\Delta D_0$ is shown in Fig. 2, where the values are based on the same data as those in Table 1. From this, we find the following relation by means of the method of least squares:

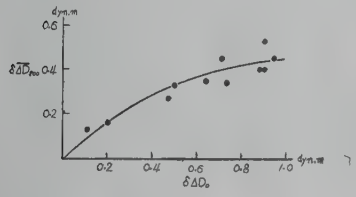

Fig. 2. The relation between $\delta\overline{\Delta D}_{800}$ and $\delta\Delta D_0$.

$$\delta\overline{\Delta D}_{800}=0.915\delta\Delta D_0-0.485(\delta\Delta D_0)^2,$$

$$\varepsilon=\pm0.035\text{dyn m}.$$

Accordingly we have

$$T_{800}=800(0.915T_0-\frac{f}{10}\times0.485T_0^2),$$

which seems not to contradict the result derived by Ichiye. Namely, the volume transport from the surface to the depth of 800 m is approximated by the quadratic function of that at the surface with sufficient accuracy. We consider that this relation is due to the vertical distribution of the current velocity in the considered sea area.

Comparing the geopotential topography at the surface with the Q-chart. (Fig. 3), we find that there is a resemblance between them. This is caused by the

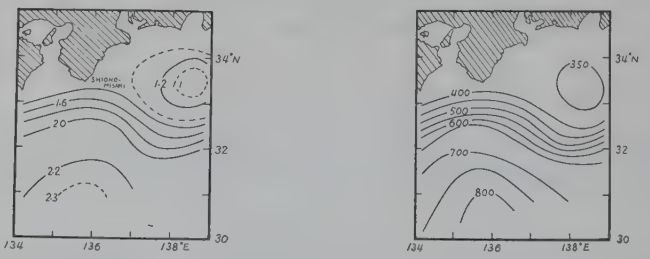

(a) the geopotential topography at the surface in November, 1955.

(b) the Q-chart in November, 1955. (unit: m^3/sec^2)

Fig. 3. The comparison of the geopotential topography at the surface with the Q-chart.

result mentioned above. In the considered sea area, it is reported that the current axis is situated more off-shore a little in the lower layer than in the upper layer, and then the difference between them appears on the geopotential topography. Accordingly, the position of the current axis on the Q-chart coincides not always with that on the geopotential topography at the surface, but the difference is not so conspicuous. Thus the mean position of the current axis from the surface to the depth of 800 m may be decided approximately from the geopotential topography instead of from the Q-chart. Hence, it seems to be sufficient for the purpose of discussing the general pattern of the current only to make the geopotential topography at the surface. Furthermore, the volume transport at the surface may be used for estimating the fluctuation of the relative volume transport from the surface to the depth of 800 m.

4. *The influence of the horizontal distance upon the volume transport*

In the preceding sections, we have discussed the influence of the depth on

Table 2. The value of the volume transport for d=800 m on the meridian of 135°40′E in March, 1955. A and B is the southern and northern end of the considered section. The unit of δQ and T is m^3/sec^2 and $10^6 m^3/sec$, respectively. The positive value of T means the eastward transport.

A	31°—00′N	31°—30′N	32°—00′N	32°—30′N	33°—00′N
B	31—30	32—00	32—30	33—00	33—20
δQ_{800}	72	216	58	−45	−37
T_{800}	9.3	28.0	7.5	−5.8	−4.8

the relative volume transport. However, the distance of the section is also thought a important factor.

Table 2 shows the relative volume transport from the surface to the depth of 800 m on the meridian of 135°40′E in March, 1955. Here, the width of each section is 20～30 nautical miles. At that time, the cold water region extended westward and the current, accompanied by the counter-clockwise eddy, appeared on the meridian, while the current axis was situated nearly at 31°20′N. From Table 2, we obtain the following values:

total eastward transport $44.8\times10^6 m^3/sec$,
total westward transport $10.6\times10^6 m^3/sec$,
total transport $34.2\times10^6 m^3/sec$.

The large value of the westward tansport means that the transport produced by the eddy has large quantity. In such a case, the volume transport between 31°N and 33°20′N contains the following ones:

(1) the eastward transport of the main strong current of the Kuroshio,
(2) the eastward and weastward transport of the eddy,
(3) the eastward transport south of the main current of the Kuroshio.

It is not proper to regard the total eastward transport as the transport of the Kuroshio, because the former indicates not only the transport of the Kuroshio but of the eddy. Therefore, the latter must be taken off from the total eastward transport so that we may find the transport of the main current of the Kuroshio. Since the eddy may be considered symmetric and the eastward transport compensates the westward one, the total transport between 31°N and 33°20′N does not include the transport produced by the eddy and indicates nearly the transport of the Kuroshio.

As the current velocity is not large south of the main current in general, we apt to think that the transport in the region is not important when the transport of the Kuroshio is computed. However, the width of the main strong current is not large (about 40～50 nautical miles) and that of the region is large. And so the influence of the transport in the region becomes remarkable if the width of the off-shore region is made much larger than that of the main current. For instance, if the mean current from the surface to the depth of 800 m is 10 cm/sec and the width of the region is 100 nautical miles, its transport amounts to $14.4\times10^6 m^3/sec$ which is equivalent to about a third or half of the transport of the main current. As an example, Table 3 shows the values of the

Table 3. The value of the volume transport for d=800 m on the meridian of 135°40′E in November, 1955. A is the southern end of the considered section, and the northern end is 33°20′N. The unit of δQ and T is m^3/sec^2 and $10^6 m^3/sec$, respectively. The positive value of T means the eastward transport.

A	31°—00′N	31°—30′N	32°—00′N	32°—30′N
δQ_{800}	421	379	308	275
T_{r00}	54.5	48.9	41.1	35.6

transport for various southern ends on the meridian of 135°40′E in November, 1955, when the main current flowed north of 32°30′N and the weak eastward current was found south of it. This indicates that the value of the transport north of 31°N is larger by about 50% than that north of 32°30′N and will be much larger than that produced by the main current of the Kuroshio alone. Thus, even when the total eastward transport is large, we should not conclude that the transport of the main current is large in such a case. Consequently, it is important what to regard as the volume transport of the main current of the Kuroshio and then how to decide the horizontal section in computing the relative volume transport.

5. *Summary*

We discuss the influence of some factors upon the relative volume transport by using the data in the sea south of Shiono-misaki. When the fluctuation of the relative volume transport from the surface to the depth d is considered, the depth may take any value of 600, 800 and 1000 m. And then a simple relation is found between the transport from the surface to the depth of 800 m and that at the surface, and so the geopotential topography may be substituted for the Q-chart for practical purposes. Furthermore, it is indicated that the section must be taken carefully in computing the relative volume transport.

Acknowledgements—The author wishes to express his hearty thanks to Dr. K. Yoshida and Dr. J. Masuzawa for their suggestions and to Dr. K. Hidaka, Dr. Y. Shibata, Dr. K. Hishida and Dr. T. Nan'niti for their encouragements. He is also indebted to Dr. J. Masuzawa for the publishment of this note.

References

Ichiye, T. (1954): On the variation of oceanic circulation (VII). *Oceanogr. Mag.* **6**, 1.

MASUZAWA, J. (1951): On the transport of Kuroshio current south off Shionomisaki. *Oceanogr. Rep. of C. M. O.* **2**, 2. (in Japanese)

SUGIURA, J. (1955a): On the transport in the eastern sea of Honshū (Part 1). *Oceanogr. Mag.* **6**, 4.

SUGIURA, J. (1955b): On the transport in the eastern sea of Honshū (Part 2). *Oceanogr. Mag.* **7**, 1.

SUGIURA, J. (1957): On the Oyashio current in the sea adjacent to Hokkaido. *Oceanogr. Mag.* **9**, 1.

SVERDRUP, H. U. and others (1942): The oceans. New York.

The Oceanographical Magazine
Vol. 10. No. 1. June 1958

Studies on the Inter-relationship between the Sea and the Atmosphere (Part 3)

By

Masao HANZAWA

Japan Meteorological Agency

Abstract: Anomalies of sea surface temperature at coastal stations along the Pacific coast of Japan and of North and South America are compared in connection with simultaneous atmospheric circulation over the North Pacific. When a single negative pressure anomaly pattern over the North Pacific is a dominant feature, the intensity of the Aleutian Low is believed to be above normal and that of the Pacific High is believed to be below normal. In such case, water temperature anomalies on the American side show large positive values and those on the Japanese side show large negative values.

The opposite situation occurs when a single positive pressure anomaly prevails over the Pacific. The circulation and temperature anomalies of 1926 are analysed as a good example of the former case while those of 1955 are analysed as an example of the latter.

1. Introduction

In his previous reports (HANZAWA and INOUE 1952, HANZAWA 1956 and 1957), the author studied the relationship between the anomalies of sea water temperatures and weather circulation over the North Pacific. One of the interesting facts found is that in the North Pacific, anomalies of sea water temperature along the eastern and western sides show opposite signs when a prevailing circulation situation is simple and the pressure anomaly values are large. Namely, in the case of a negative atmospheric pressure anomaly, the sea water temperatures were negative on the west and positive on the east side. With a positive pressure anomaly, the opposite was found.

In 1955, we experienced very cold water temperatures along the coast of the east side of the Pacific. In the same year, considerably warm water temperatures were observed along the west side of the Ocean namely along Japan and the Philippine Islands.

Recently, RIEHL (1956), REID and RODEN (1958), and RODEN (1958), of the United States, studied the inter-relationship between the weather circulation and the water temperature situation in the Pacific. RODEWALD (1957 a,b), of Germany, analysed in detail the unusual cold water temperature of the east side of the Pacific as it occurred in 1955.

Temperatures from coastal stations along the Pacific have been compiled in Japan and in the U.S. recently (Coast and Geodetic Survey, 1956). Therefore, comparison of temperature anomalies along both coasts became possible. Using these data, we can make simultaneous comparison of monthly mean water temperatures of both sides of the Ocean in connection with the monthly mean weather and circulation situations. The present investigation confirms the author's theory which was previously advanced.

2. *Weather and atmospheric circulation of 1955 and 1926*

(*a*) *Synopsis of weather and atmospheric circulation of 1955*

The dynamic climatological feature of 1955 was, in short, a 'high index type'. This weather feature was analysed in detail by KLEIN (1956) and SUDA (1956) from aerological view points. The most prominent feature of the general circulation over the North Pacific, according to KLEIN, is a large center of positive 700-mb height anomaly, some 200 feet above normal, which is situated over the central part of the Ocean. The positive height anomaly in the mid-Pacific is found almost all through the year on monthly mean chart. The yearly mean pressure anomaly chart for 1955 is shown in Fig. 1. This shows that the intensity

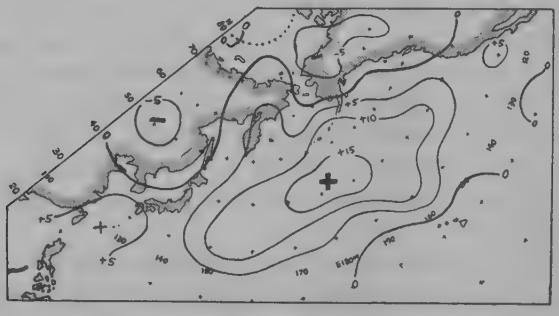

Fig. 1. Yearly mean 700-mb height departures from normal in tens of feet for 1955.

of the Pacific High was above normal that year, therefore there was reason to expect the transport of water due to atmospheric circulation to be above normal from the south along the western side and above normal from the north along the eastern side of the ocean.

It is evident that, in a climatological sense, the excess of water transportation from the south would bring about an 'above normal' temperature condition in the western side and a 'below normal' temperature condition in the eastern side in the same manner.

The detailed analysis of the aerological weather situation over the Far East was carried out by SUDA (1956) with emphasis on the explanation of the abnormally hot weather in Japan during July of 1955. The analysis showed that in July 1955, a prominent 'ridge' was seen on the 500-mb monthly mean chart. However, the westward extension of the Pacific High was nearly normal that year, but the High became more pronounced as its height increased. Isolines of surface pressure anomaly ran from SW to NE in that month, and such a situation was very favorable to bring about a warm southerly air current to the said area. The position of the climatological jet stream was shifted northward over the North Pacific that year.

(*b*) *Synopsis of weather and circulation of 1926*

The synoptic weather and circulation condition of 1926 (and 1925) was studied in detail by RODEWALD (1952). In the years 1925 and 1926, aerological observations were sparse and we can not construct the global upper air circulation pattern from available data. However, judging from available surface observations, the year of 1926 can be considered as a 'low index' year and we can see prominent negative surface pressure anomalies in the Pacific and in the Atlantic.

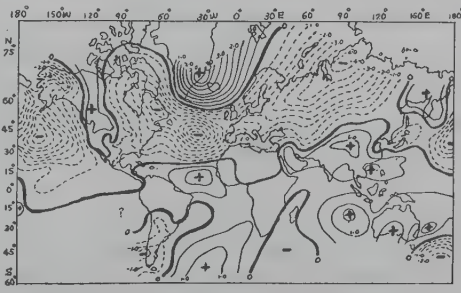

Fig. 2. Yearly mean surface atmospheric pressure departure (mm) from normal, 1926. Contours are drawn for every 0.5mm. (Afer RODEWALD, 1952)

This shows that the Aleutian Low was stronger than normal (the Pacific High below normal)

during 1926. And a warm ocean current from the south was not well developed that year in the eastern side. On the contrary, it is natural to think that the cold current from the north such as the Oyashio was accelerated getting energy from the atmospheric circulation. This circulation condition brings about cold surface water (below normal) in the western side of the Ocean (Japan) and, conversely, warm surface water (above normal) on the U.S. coast.

3. *Water temperatures at coastal stations in 1926 and 1955*

Water temperatures in 1926 were abnormally high on the western coast of North America. (Data of South America at that time are not available). Yearly mean anomaly of temperature for Seattle, Wash. was +2.7°F, and that for Port Hueneme, Calif. was +2.5°F in 1926. The water temperatures in 1955 were remarkably low along the North and South American coasts. For example, temperatures of Neah Bay, Wash. in 1955 was lowest in recent 17 years, those of San Francisco, Calif. were second lowest in recent 29 years. In the same year, water temperatures were above normal in the western side of the Pacific. For example, yearly mean anomaly of temperature was +2.5°F at Shioyazaki in 1955. To clarify this relationship, several diagrams are presented. In Figs. 3 and 4, the relationship is shown. The *y*-axis represents the anomaly of monthly mean water temperatures of the Japanese coast, Shioyazaki as a representative one. The *x*-axis represents the same factor obtained on eastern side of the Pacific, say, of La Jolla etc. In the 1926 case, if the America side anomalies are plotted on the *x*-axis and the Japanese side anomalies are plotted on the *y*-axis, the points will be found to fall in quadrant IV.

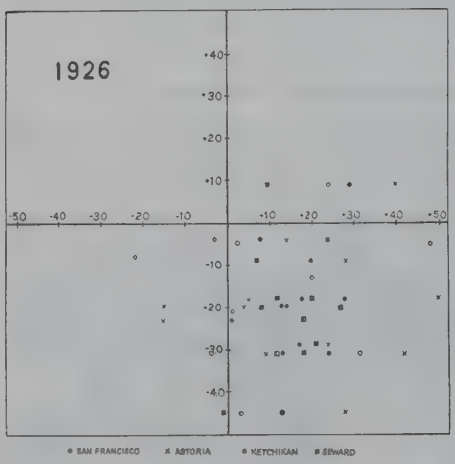

Fig. 3. Monthly mean sea surface temperature anomalies for 1926 Shioyazaki (Coordinate) vs. San Francisco (Calif.), Astoria (Ore.), Ketchikan (Alaska), and Seward (Alaska) (Abscisa). Anomalies in °F.

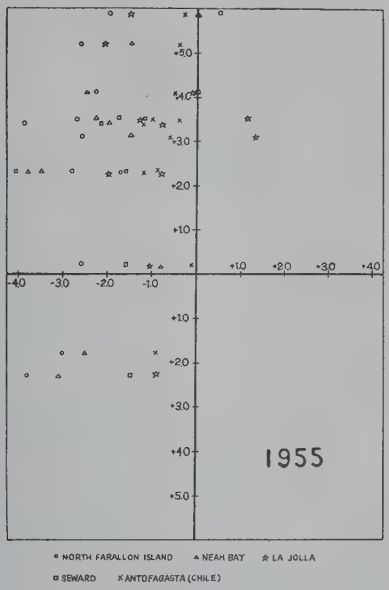

Fig. 4. Monthly mean sea surface temperature anomalies for 1955, Shioyazaki (Coordinate) vs. North Farallon Island (Calif.), Neah Bay (Wash.), La Jolla (Calif.), Seward (Alaska), and Antofagasta (Chile) (Abscisa). Anomalies in °F.

On the contrary, in 1955 case the points fall in quadrant II. Of course, since such a relationship is of a climatological nature, the points scatter and are not situated on a distinct straight line. However, we can still trace a close relationship between anomalies of the both sides of the Ocean.

4. *Conclusion*

Although we have investigated the period from 1922 to 1956, in this report only two representative abnormal years (1926, 1955) are shown. It becomes evident that when abnormally high (or low) water temperatures are seen in one side of the Pacific, their opposite is likely to occur on the other side simultaneously. As RODEWALD (1957 a) stated, the years of 1926, 1931, 1941 and 1942 were 'warm years' for the American coast, but among them, the years of 1931 and 1941 were 'cold years' for the Japanese coast. In the years of 1931 and 1941, bad rice crop due to cool summer because of lowering of sea water temperatures in the seas adjacent to Japan took place. On the contrary, the years of 1922, 1933, 1935, 1949 and 1955 were 'cold years' for the American coast, but among them 1922 and 1955 were rather 'warm years' for the Japanese coast.

The fact is due to the abnormal state of the weather circulation, namely excessive intensity of the Aleutian Low or the Pacific High. As RODEWALD (1957 b) has already pointed out, the yearly mean anomaly rotated clockwise in the North Pacific and anti-clockwise in the South Pacific in 1955. This is a good evidence that in 1955 the Pacific High got stronger and the anomaly rotated clockwise (anticyclonic) in the North Pacific starting from the Gulf of Alaska, having a

maximum off the northern Californian coast and decreasing its intensity as it reached to the South Pacific Islands and became positive in the Philippine Islands and Japan. In the succeeding report, some theoretical considerations on the author's rule will be given.

Acknowledgements—The author wishes to express his sincere thanks to Dr. Y. TAKENOUTI of the Japan Meteorological Agency for valuable advice of this paper. He is also indebted to Mr. J. FUKUOKA of the Meteorological Research Institute for furnishing him compiled data of water temperatures obtained at several light houses along the coast of Japan, and to Drs. G.I. RODEN, M. ROBINSON, J. REID, Jr. of the Scripps Institution of Oceanography and to Dr. M. RODEWALD of the Deutscher Wetterdienst, Seewetteramt for furnishing him valuable data and documents.

References

Coast and Geodetic Survey (1956): Surface water temperatures at tide stations, Pacific Coast, North and South America and Pacific Ocean Islands. *Special Publication* No. 280, 5th Ed.

HANZAWA, M. and T. INOUE (1952): Relation between oceanic and atmosgheric state in the North Pacific Ocean for the years of bad and good rice crop. (In Jap.) *Oceanogr. Rep. C.M.O.*, **2** (3), 65-70.

HANZAWA, M. (1956): Preliminary report on a close relationship between surface water temperatures at the two separated ocean weather stations, Papa and Tango. *Oceanogr. Mag.*, **8** (2), 157-160.

HANZAWA (1957): Studies on the inter-relationship between the sea and the atmosphere (Part 2). *Oceanogr. Mag.*, **9** (1), 87-93.

KLEIN, W.H. (1956): The weather and circulation of 1955. *Weatherwise*, **9** (1), 5-10.

RIEHL, H. (1956): Sea surface temperatures of the North Atlantic 1887-1936. Dept. Met., Univ. Chicago, Contract N6 ori-02036; Project NR 082-120, Office of Naval Research.

RODEN, G.I. and J.L. REID, Jr. (1958): On a relationship between the variations in atmospheric pressure and sea surface temperatures in the North Pacific Ocean. (Unpublished manuscript)

RODEN, G.I. (1958): Spectral analysis of a sea-surface temperature and atmospheric pressure record off Southern California. (To be published)

RODEWALD, M. (1952): Das meteorologisch merkwürdige Jahr 1925. *Ann. Meteorol.*, Band 5, Heft 3-5, 122-129.

RODEWALD, M. (1957 a): Beiträge zur Klimaschwankung in Meere. Die Temperaturen der pazifischen Küstengewässer Nordamerikas von 1920 bis 1955. *D.H.Z.*, Band 10. Heft 4, 147-151.

RODEWALD, M. (1957 b): Beiträge zur Klimaschwankung in Meere. Das kalte pazifische Jahr 1955. *D.H.Z.*, Band 10, Heft 4, 151-157

SUDA, K. (1956): On the unusual hot summer of 1955. (In Jap.) *J. Met. Res.*, **8** (8), 463-472.

The Oceanographical Magazine
Vol. 10. No. 1 June 1958

On Convective Circulation and Density Distribution in a Zonally Uniform Ocean*

By

Takashi Ichiye**

1. *Introduction*

Many oceanographers have worked on oceanic circulation from point of view of wind driven theory since a pioneer work of Henry Stommel in 1948 and it is generally accepted that the primary cause of upper circulation of the ocean may be wind stresses. However, the importance of thermal or convective circulation, particularly as a main driving force of deep sea circulation, has become confirmed recently (Stommel 1957, Veronis 1957) and also some theoretical works on the subject were published (Fofonoff 1954, Lineykin 1955), though the complete understanding of the problem seems to be still difficult, chiefly owing to non-linearity accompanying with the analysis of the motion.

The present study aims at obtaining the relationships between circulation and density distribution, considering a simple model of circulation in a meridional section.

2. *Fundamental equations*

In this paper the condition in the midst of the ocean far from the coast is discussed, since the existence of coastal barriers just adds an analytical difficulty which is not an essential part of convective circulation. By such assumption we can neglect east-west difference of all quantities and thus the motion can be fully described only on a meridional section. When we take y-axis as northwards and z-axis as upwards, equations of motion, continuity and mass flux are written as follows :

---

* Woods Hole Oceanographic Institution Contribution No. 981.
** Woods Hole Oceanographic Institution.

$$-fv=A\frac{\partial^2 u}{\partial z^2} \quad (1) \qquad fu=-\frac{1}{\rho}\frac{\partial p}{\partial y}+A\frac{\partial^2 v}{\partial z^2} \quad (2)$$

$$g\rho=-\partial p/\partial z \quad (3) \qquad \partial v/\partial y+\partial w/\partial z=0 \quad (4)$$

$$v\frac{\partial \rho}{\partial y}+w\frac{\partial \rho}{\partial z}=K\frac{\partial^2 \rho}{\partial z^2} \quad (5)$$

where u, v and w are zonal, meridional and vertical component of velocity and A and K are eddy viscosity and diffusivity. From (4) we can introduce current function φ which gives

$$v=\partial\varphi/\partial z, \qquad w=-\partial\varphi/\partial y$$

By differentiating (2) with z and substituting $\partial p/\partial z$ from (3) we have

$$f\frac{\partial u}{\partial z}=\frac{g}{\rho}\frac{\partial \rho}{\partial y}+A\frac{\partial^4 \varphi}{\partial z^4} \quad (6)$$

We put $v=\partial\varphi/\partial z$ into (1) and integrate it with z under the boundary conditions at the surface

$$\varphi=0, \qquad A\partial u/\partial z=T(y)$$

where $T(y)$ is zonal wind stress, we have

$$f\varphi=-A\partial u/\partial z+T \quad (7)$$

We eliminate $\partial u/\partial z$ from (6) and (7), then we have

$$A^2\frac{\partial^4 \varphi}{\partial z^4}+A\frac{g}{\rho}\frac{\partial \rho}{\partial y}+f^2\varphi-fT=0 \quad (8)$$

and also from (5)

$$\frac{\partial \varphi}{\partial z}\frac{\partial \rho}{\partial y}-\frac{\partial \varphi}{\partial y}\frac{\partial \rho}{\partial z}=K\frac{\partial^2 \rho}{\partial z^2} \quad (9)$$

These two equations (8) and (9) are basic equations for unknown functions ρ and φ.

For convenience of further computation we introduce non-dimensional variables such as

$$\varphi=\varphi_0\Psi, \quad \rho=\rho_0\sigma, \quad y=aY, \quad z=hZ, \quad T=T_0\tau$$

where a and h are meridional distance and depth of the ocean and we assume that CORIOLIS' parameter is linear function of y such as

$$f=f_0+\beta y=f_0(1+\gamma Y) \quad \text{with} \quad \gamma=\beta a/f_0$$

Then we have next equations from (8) and (9)

$$\epsilon^2\frac{\partial^4 \Psi}{\partial Z^4}+(1+\gamma Y)^2\Psi=-\alpha\frac{\partial \sigma}{\partial Y}+(1+\gamma Y)\delta\tau \quad (10)$$

$$\frac{\partial^2 \sigma}{\partial Z^2}=\kappa\left(\frac{\partial \Psi}{\partial Z}\frac{\partial \sigma}{\partial Y}-\frac{\partial \Psi}{\partial Y}\frac{\partial \sigma}{\partial Z}\right) \quad (11)$$

where $\kappa=h\varphi_0/aK$, $\quad \in=A/h^2f_0$

$\alpha=gA/f_0^2\varphi_0 a$, $\quad \delta=T_0/f_0\varphi_0$

3. *Boundary layers and interior region*

Now the whole prolem is to solve the two equations (10) and (11) for unknown quantities Ψ and σ under suitable boundary conditions. The wind stress τ is given as a function of Y, but for a while we disregard this term for simplicity and we consider only convective circulation caused by the density field.

As suitable and yet simple boundary conditions, we assume that the density at the top and bottom of the ocean is given and further the density at the bottom is constant. This condition corresponds to the situation in the ocean that some meteorological condition maintains the surface density variable only in latitudes and also at the bottom (or more properly the lower boundary where the present dynamic model is valid) the density is kept constant by some dynamic process of the deep sea. As for the conditions for velocity field, we can assume that at the surface $Z=1$, $W=0$ or $\Psi=0$ and at the bottom $Z=0$, $V=W=0$ or $\Psi=0$, $\partial\Psi/\partial Z=0$, which seems to be more reasonable than the boundary conditions for density.

Then, as easily seen, the equation (10) is of boundary layer type, so that we can obtain seperate solutions for upper and lower boundary layers and interior region (Foronoff, 1954). Especially for the boundary condition that the bottom density is constant, the lower boundary layer vanishes, since the value of $\partial\sigma/\partial Y$ is equal to zero and also $\partial^2\sigma/\partial Y\partial Z$ is small near the bottom as shown in later analysis.

The solution of the equation (10) in the upper boundary layer is obtained by neglecting the change of $\partial\sigma/\partial Y$ with the depth in this layer and it is similar to the solution of Ekman (1905), given by

$$\Psi=-\alpha\frac{\partial\sigma}{\partial Y}[1-\exp\{-k(1-Z)\}\cos k(1-Z)]/(1+\gamma Y)^2 \qquad (13)$$

where $k=[(1+\gamma Y)/2\in]^{\frac{1}{2}}$. The thickness of the boundary layer is given by $Z_0=3\pi/4k$, which is the same as the depth of friction of Ekman. This quantity is very small compared with 1 in the present non-dimentional form, since $k\gg 1$.

In the interior region below this boundary layer, we can neglect the term with the coefficient $\in^2$ and we get

$$(1+\gamma Y)^2\Psi=-\alpha\partial\sigma/\partial Y \qquad (14)$$

When we substitute this into (11) we have

$$\frac{\partial^2\sigma}{\partial Z^2}=\frac{\alpha\kappa}{(1+\gamma Y)^2}\left(\frac{\partial^2\sigma}{\partial Y^2}\frac{\partial\sigma}{\partial Z}-\frac{\partial^2\sigma}{\partial Y\partial Z}\frac{\partial\sigma}{\partial Y}\right)-\frac{2\alpha\kappa\gamma}{(1+\gamma Y)^3}\frac{\partial\sigma}{\partial Y}\frac{\partial\sigma}{\partial Z} \tag{15}$$

which contains only one unknown variable σ and when we give boundary values at the top (or at the upper boundary layer) and the bottom of the ocean we can get the distribution of σ which in turn gives the velocity field by the equation (14).

4. *Uniformly rotating system*

As the first step we consider a simple model of uniformly rotating system, where CORIOLIS' coefficient is constant or $\gamma=0$ in the equation (15). In this model, a solution which is mathematically simple and yet represents the actual condition of the ocean in some way is expressed by a power series of Y. The solution can be obtained by equaling the coefficients of the same power of Y in the equation (15), so that only the solution of less than the second power of Y is possible.

When we put

$$\sigma=F_0(Z)+F_1(Z)Y+F_2(Z)Y^2 \tag{16}$$

then the ordinary differential equations for $F_i(Z)$ become

$$F_0''=p(2F_2F_0'-F_1'F_1) \tag{17}$$

$$F_1''=-2pF_1F_2' \tag{18}$$

$$F_2''=-2pF_2F_2' \tag{19}$$

where $p=\alpha\kappa$,

whereas the boundary conditions that the density at the surface is a function of Y and that at the bottom is constant are expressed as

$$\text{at } Z=1,\ F_0=\sigma_0,\ F_1=\sigma_1,\ F_2=\sigma_2;\ \text{ at } Z=0,\ F_0=\sigma_b,\ F_1=F_2=0 \tag{20}$$

In this solution, we cannot demand another condition at the bottom corresponding to the condition that $V=0$ or $\partial\psi/\partial Z=0$, since this leads to additional requirement such as $\partial^2\sigma/\partial Y\partial Z=0$ or $F_1'=F_2'=0$ at $Z=0$ so far as we use the relation (14) near the bottom instead of (10). This additional boundary condition can be satisfied only when we introduce the lower boundary layer, in which the stream function ψ is expressed by a similar equation to (13), with the term including the coefficient k replaced by $\exp(-kZ)(\cos kZ+\sin kZ)$ (FOFONOFF, 1954). However, since $\partial\sigma/\partial Y=F_1+2F_2Y$ is small near the bottom so long as we adopt the boundary condition $F_1(0)=F_2(0)=0$, the introduction of the lower boundary layer does not much affect the values of σ and Ψ near the bottom.

On the other hand, we cannot take the boundary condition for $F_2(Z)$ such that $F_2'=0$ at $Z=0$, regardless of any other boundary conditions. For, when we expand F_2 in power series of Z near $Z=0$, such as

$$F_2=C_0+C_1Z^s+C_2Z^{s+1}+\cdots\cdots$$

then $s>1$, if we demand the condition that $F_2'(0)=0$. Substituting this series in the equation (19), we have

$$F_2''=s(s-1)C_1Z^{s-2}+s(s+1)C_2Z^{s-1}+\cdots\cdots$$
$$F_2F_2'=C_0C_1Z^{s-1}+C_0C_2(s+1)Z^s+C_1^2Z^{2s-1}+\cdots\cdots$$

Therefore, by equaling the coefficient of the same power of Z, we have $C_1=0$, since the lowest power of Z in F_2F_2' is $Z^{s-1}(s>1)$. Then we get succesively $C_2=C_3=\cdots\cdots=0$.

The solutions of the equation system (17)—(19) is obtained by integrating first the equation (19), which gives

$$F_2'=-p(F_2^2\pm C^2) \tag{21}$$

where C is a positive integration constant, and plus sign corresponds to a negative value of σ_2 and minus to a positive σ_2. For by integrating (21) again we get

$$\left.\begin{aligned} F_2&=c\tanh cpZ \quad (\text{for } \sigma_2>0) \quad (\text{A})\\ F_2&=-c\tan cpZ \quad (\text{for } \sigma_2<0) \quad (\text{B})\end{aligned}\right\} \tag{22}$$

where the constant C is determined by the boundary condition at $Z=1$, which gives

$$c\tanh cp=\sigma_2 \quad (\text{A}), \qquad c\tan cp=-\sigma_2 \quad (\text{B}) \tag{23}$$

The equation (18) becomes

$$\left.\begin{aligned} F_1''&=-(2p^2c^2\operatorname{sech}^2 cpZ)F_1 \quad (\text{A})\\ F_1''&=(2p^2c^2\sec^2 cpZ)F_1 \quad (\text{B})\end{aligned}\right\} \tag{24}$$

These equations cannot be integrated by use of elementary functions, so that we have to resort to numerical integration or approximate integration.* However, as shown later, numerical value of cp is generally small compared with 1 for reason-

* More exact approximate solution of the equation (24) is expressed by use of Bessel functions. First, we change a variable Z to $\xi=mZ+n$ by a linear transformation. Then we can express the coefficient of F_1 in the equation (24) by some power or ξ such as

$$d^2F_1/d\xi^2+\beta\xi^sF_1=0$$

for the interval of $Z=0$ to 1 by taking suitable numerical constants m, n, β and s, so that $\beta\xi^s$ may give the value as close to the original coefficient of F_1 as possible. Then this equation has a solution of a type

$$F_1(\xi)=C_1\sqrt{\xi}\,J_{\frac{1}{s+2}}\left(\frac{2\sqrt{\beta}}{s+2}\xi^{\frac{s+2}{2}}\right)+C_2\sqrt{\xi}\,Y_{\frac{1}{s+2}}\left(\frac{2\sqrt{\beta}}{s+2}\xi^{\frac{s+2}{2}}\right)$$

where C_1 and C_2 are integration constant to be determined from the boundary conditions.

able physical constants in the ocean, we can consider $\mathrm{sech}^2 cpZ$ or $\sec cpZ$ almost constant between $Z=0$ and 1 and replace them by their mean value in this interval, then we have

$$F_1'' \fallingdotseq -2p\sigma_2 F_1 \quad \text{(A) and (B)} \tag{25}$$

as easily verified by use of the condition (23). Thus the solution satisfying the boundary condition (20) is given by

$$F_1=\frac{\sigma_1 \sin\sqrt{2p\sigma_2}\,Z}{\sin\sqrt{2p\sigma_2}} \quad \text{(A)}, \qquad F_2=\frac{\sigma_1 \sinh\sqrt{-2p\sigma_2}\,Z}{\sinh\sqrt{-2p\sigma_2}} \quad \text{(B)} \tag{26}$$

The solution F_0 of the equation (17) is also given by a simple integration which is

$$F_0'=A\exp(2p\int_0^z F_2dz)-p\exp(2p\int_0^z F_2dz)\int_0^z F_1F_1'\exp(-2p\int_0^{z_1}F_2dz)\,dz_1 \tag{27}$$

or

$$\left.\begin{aligned} F_0'&=A\cosh^2 cpZ-B\cosh^2 cpZ\int_0^z \sin 2\sqrt{2p\sigma_2}\,Z\cosh^{-2} cpZdz \quad \text{(A)}\\ F_0'&=A\cos^2 cpZ-B\cos^2 cpZ\int_0^z \sinh 2\sqrt{-2p\sigma_2}\,Z\cos^{-2} cpZdz \quad \text{(B)}\end{aligned}\right\} \tag{28}$$

where A is an integration constant determined by the boundary condition and B represents

$$B=\frac{\sigma_1^2\sqrt{2\sigma_2 p}}{\sin^2\sqrt{2\sigma_2 p}} \quad \text{(A)}, \qquad B=\frac{\sigma_1^2\sqrt{-2\sigma_2 p}}{\sinh^2\sqrt{-2\sigma_2 p}} \quad \text{(B)}$$

Since the function $F_0(z)$ represents the vertical profile of the density at $Y=0$ or, so to speak, at the reference station, we had better state physical explanation of each term of (27) or (28). When we consider the equation (14), the function F_2 represents the vertical current, as easily seen from the relationship

$$W=-\frac{\partial \Psi}{\partial Y}=\alpha\frac{\partial^2\sigma}{\partial Y^2}=2\alpha F_2$$

Therefore we can consider that the first term represents the effect of vertical current upon the density profile. On the other hand, even when F_2 vanishes, or there is no vertical motion, the second term gives the distribution of density different from constant, if F_1' is not zero, so that this term may be interpreted as giving the effect of horizontal current. Thus we call these two terms convective and advective term, respectively. The advective term vanishes at the bottom, and when we demand the flux of mass to vanish at the bottom at $Y=0$, $A=0$ or only the advective term remains.

The complete solution of (17) satisfying the boundary condition (20) is thus written as

$$\left.\begin{aligned} F_0 &= (J(1) - \sigma_b + \sigma_0)\tanh cpZ/\tanh cp + \sigma_b - J(Z) \quad \text{(A)} \\ F_0 &= (J(1) - \sigma_b + \sigma_0)\tan cpZ/\tan cp + \sigma_b - J(Z) \quad \text{(B)} \end{aligned}\right\} \tag{29}$$

where $$J(z) = B\int_0^z \cosh^2 cpZ_1 \int_0^{z_1} \sin 2\sqrt{2p\sigma_2}Z_2 \cosh^{-2} cpZ_2 dz_1 dz_2 \quad \text{(A)}$$

$$J(z) = B\int_0^z \cos^2 cpZ_1 \int_0^{z_1} \sinh 2\sqrt{-2p\sigma_2}Z_2 \cos^{-2} cpZ_2 dz_1 dz_2 \quad \text{(B)}$$

Numerical Computation: The parameter p is given by $p=\alpha\kappa=gAh/Kaf_0^2$, and we give next geometrical and physical constants corresponding to the ocean (here we have to remind that we assume that CORIOLIS' coefficient is constant, so that we cannot discuss the condition of the whole scale ocean)

$$f_0=10^{-4}, \quad a=10^8, \quad h=10^5, \quad g=10^3$$

then we have $p=A/K$. As stated before, cp must be small compared with 1, so that the approximation (20) may be valid, and this condition is satisfied so long as $p<10^3$, when we determine c from the condition (23) for a reasonable value of $\sigma_2=10^{-3}$. Actually we have no conclusive knowledge about the magnitude of eddy viscosity and eddy diffusivity in the ocean, but there are many evidences (for example, SVERDRUP *et al*, Ocean) that the ratio A/K is larger than 1 and smaller than 10^3. Therefore we compute the density distribution expressed by (22), (26) and (29) with $p=10^3$ and $p=10$. Further, we take $\sigma_0-\sigma_b=3\times10^{-3}$, $\sigma_1=2\times10^{-3}$, $\sigma_2=\pm10^{-3}$ where these values of σ_t can be given in σ_t values instead density itself.

In Fig. 1 we indicate vertical profiles of F_0, F_1 and F_2 for model (A) ($\sigma_2=10^{-3}$) and (B) ($\sigma_2=-10^{-3}$) by use of these numerical values. As stated in the beginning of this section, these curves represent the values of functions F_0, F_1 and F_2 only in the interior region of the ocean where $\epsilon^2\psi^{(IV)}$ can be neglected, so that we might avoid additional

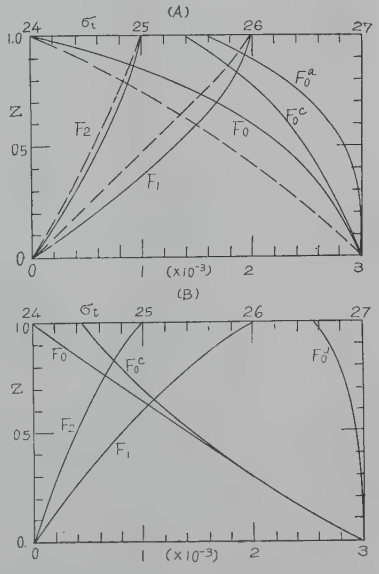

Fig. 1. Profiles of F_i, in two models for $A/K=10^3$ (In (A), broken lines are curves for $A/K=10^2$).

complication. Therefore, in order to obtain complete pictures of the distribution of the density in the whole depth of the ocean we have to add upper and lower boundary layer outside the considered region, where F_i is constant with the depth.

When we look at the curves, we can see that all F_i are linear function of Z for $p=10$, which means that in the present model the water mass is almost thoroughly mixed in a vertical direction already for a eddy diffusivity of about one tenth of an eddy viscosity. When the ratio A/K increases, the effect of convection also increases, since the whole system of current on meridional section in this model is produced by frictional force even in the interior region (as seen in the equation (1) menidional velocity V is caused by frictional force) and thus the increase of A produces stronger current on this section. The difference between (A) and (B) is clearly seen in the profile of $F_0(z)$ for $p=10^3$, where in (A) vertical current is upwards and thus it brings the heavy water towards surface, resulting in producing more shaliow thermocline than in the model (B). Further, in this figure we show the advective (F_0^a) and convective term (F_0^c, the first

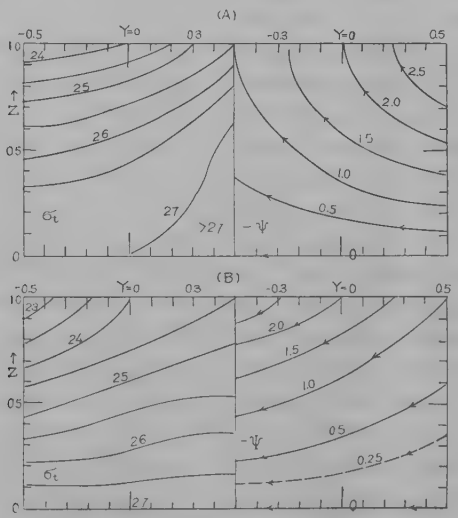

Fig. 2. Density field (in σ_t) and stream function (in A/φ_0).

term including $\tanh c\not{p}Z$ or $\tan c\not{p}Z$) in the equation (29). We can see that the relative magnitude of these two terms are different in two models and in the model (A) they are almost of the same order, whereas in the model (B) the advective term F_0^a is quite small compared with F_0^e. The reason of this difference is more clearly illustrated by vertical sections of density and stream pattern which are shown in Fig. 2. (Stream function Ψ is shown with a unit of $\frac{A}{\varphi_0}$.) We can see at once that in the model (A) stream lines cross isopicnals, whereas in (B) they are almost parallel. Moreover, in the model (A) thermocline becomes more shallow towards north, but in (B) in it is almost the same, slightly deeper towards north. (In this numerical example the density decreases downwards in the layer of about $0.4>Z>0$ at $Y=0.5$, so that in this layer instability occurs. However, the present model is only a schematical one and we are not concerned with stability problem).

As one more simple model, we show the density distribution for $\sigma_2=0$, where there is no vertical motion since $F_2=0$ and thus

$$F_1=\sigma_1 Z, \quad F_0=(\sigma_0-\sigma_b)Z+\sigma_b+p\sigma_1^2(Z-Z^3)/\sigma \tag{30}$$

The density field is rather similar to that of the model (B), because, as seen from the distribution of $F_0(z)$ in Fig. 1. $F_0(z)$ is almost the same in these two models.

5. *Circulation produced by a density field increasing uniformly polarwards in β plane.*

In a uniformly rotating system we have an exact solution for a given distribution of density at the surface expressed by up to the square equation of Y. On the other hand, in a β— plane, the solution of (15) is expressed exactly with finite series of Y only when the surface density is given as a linear function of Y. In fact, we may assume that

$$p=\alpha\kappa(1+\gamma Y)^{-2}=\text{const.}, \quad q=2\alpha\kappa\gamma(1+\gamma Y)^{-3}=\text{const.} \tag{31}$$

in β=plane, since p is proportional to f^{-2} and q is to βf^{-2}. Then when we put (16) into

$$\frac{\partial^2\sigma}{\partial Z^2}=p\left(\frac{\partial^2\sigma}{\sigma Y^2}\frac{\partial\sigma}{\partial Z}-\frac{\partial^2\sigma}{\partial Y\partial Z}\frac{\partial\sigma}{\partial Y}\right)-q\frac{\partial\sigma}{\partial Y}\frac{\partial\sigma}{\partial Z} \tag{15'}$$

equations which are obtained by equaling the same degree of Y in both side of (15') are as follows:

$$F_0''=p(2F_0'F_2-F_1'F_1)-qF_1F_0' \tag{32}$$

$$F_1''=-2pF_1F_2'-q(F_1'F_1+2F_0'F_2) \tag{33}$$

$$F_2''=-2pF_2F_2'-q(2F_2F_1'+F_1F_2'') \tag{34}$$

and also there exists a term $-qF_2F_2'Y^3$ in the right hand side of the equation (15'), which should vanish. However, this is impossible, so that we have to express σ in infinite series of Y or if we want to have finite form of the solution, we should put $F_2=0$. In this section we follow the second approach and we shall compare the results with those of the previous model.

By taking the type of solution $\sigma=F_0+YF_1$, we have the ordinary differential equations for F_0 and F from (32) and (33) such as

$$F_0' = -pF_1'F_1-qF_1F_0' \tag{35}$$

$$F_1'' = -qF_1'F_1 \tag{36}$$

where the second equation is integrated at once by the same process described in the previous section and the solution is

$$F_1 = c\tanh(qcZ/z) \tag{37}$$

in which the integration constant c is determined from the relation such as $\sigma_1=c\tanh(qc/2)$ for the boundary condition that $F_1(0)=0$, $F_1(1)=\sigma_1$.

The solution of the first equation F_0' is also given by

$$F_0' = \operatorname{sech}^2(qcZ/2)\,(A-pc^2\log\cosh(qcZ/2)) \tag{38}$$

where A is an integration constant. Further, when we take the same boundary condition as given in (20), we have

$$F_0 = (\sigma_0-\sigma_b+I(1))\tanh\frac{qcZ}{2}\Big/\left(\tanh\frac{qc}{2}\right)-I(Z)+\sigma_b \tag{39}$$

where $$I(Z) = pc^2\int_0^z \operatorname{sech}^2(qcZ/2)\log\cosh(qcZ/z)\,dz$$

Numerical computation. For numerical computation of these equations, we use the following constants

$$\beta=2\times10^{-13},\quad \gamma=0.4$$

in addition to the physical and geometrical constants already introduced in the previous section. Since the analysis of this section include the effect of β, we can assume that the present model is valid for larger range of Y than the previous model, so that we shall compute the distribution of σ and Y from $Y=-1$ to 1. Then the average values of p and q in this range of Y are

$$p=1.774\,A/K,\qquad q=1.872\,A/K$$

Here we should remind that the solution (37) and (39) are valid only in the interior region, therefore we have to take the upper boundary of the solutions as $1-Z_0$ instead of 1. However, this only contributes to make the mathematical form more complicated, so that we keep the mathematical formula simple and yet in numerical computation of the distribution of σ and ψ

we introduce the upper boundary layer. This layer is located from $Z=1-Z_0$ to $Z=1$ as stated in section 3, and the distribution of ψ is computed from the equation (13).

The results are shown in Fig. 3 and 4, where meridional section of σ and ψ are indicated for the ratio $A/K=10$ and 10^3. As stated in the previous section, the vertical profile of $F_0(z)$ and $F_1(z)$ approaches to linear function of depth Z as the ratio A/K decreases, so that they are almost expressed by linear function of Z for $A/K=10$. On the other hand, in the interior region

$$\psi=-\alpha F_1(Z)/(1+\partial Y)^2$$

and $F_1(z)>0$ in this model, we have a downwards vertical motion throughout the interior region from the relation $W=-\partial\Psi/\partial Y$, even though in case of $F_2=0$, which gives no vertical current in an uniformly rotating system. Therefore, in the previous model the density profiles show deeper thermocline generally than in the previous model, owing to the sinking motion.

However, the response of the density distribution for such vertical movement is different for different values of A/K, and indeed for $A/K=10^3$, the isopicnals are more horizontal than for $A/K=10$, indicating that the depth of maximum

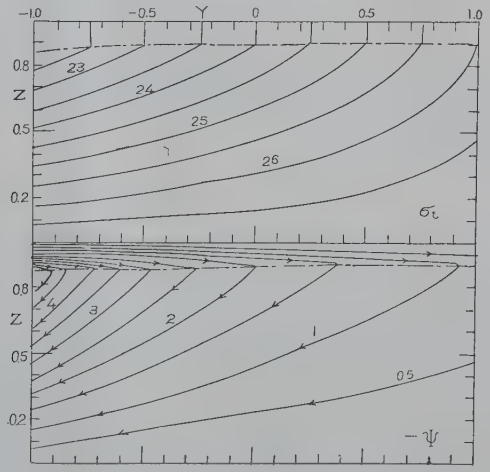

Fig. 3. Density field (in σ_t) and stream function (in A/φ_0) for $A/K=10$. (Chain lines indicate a limit of upper boundary layer).

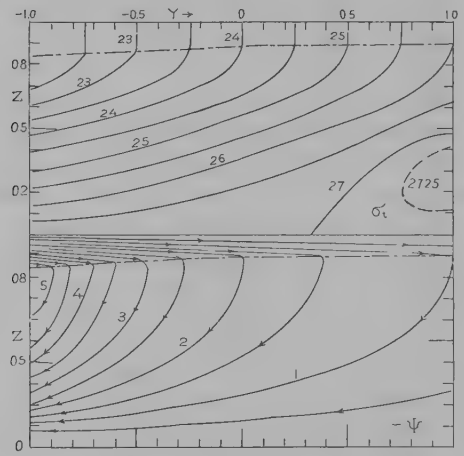

Fig. 4. Density field and stream function for $A/K=10^3$.

gradient becomes deeper towards low latitude. On the other hand, current pattern indicated by the distribution of ψ shows that in low latitudes sinking motion is stronger for $A/K=10^3$ than for $A/K=10$. Therefore, in the former case the streamlines and isopicnals cross each other, whereas in the latter they are almost parallel, which is explained by considering the relative magnitude of the advective effect and diffusion effect.

6. *Circulation produced by the uniformly increased surface density in a variable p, q.*

In the previous section we assume that p and q are constant throughout the domain $-1\leqslant Y\leqslant 1$, which is rather bold assumption, because they are variable in this range of Y such as $2.78\geqslant p(K/A)\geqslant 0.51$, $3.70\geqslant q(K/A)\geqslant 0.29$. In order to improve this approximation, we divide this range of Y into small intervals, where p and q are safely assumed to be constant. Then in each of such intervals we apply the procedure described in the previous section to obtain the solution. The values of the solutions at a boundary of successive intervals which are computed by use of the formula (37) and (39) in each interval are not equal to each other mathematically. However, so long as we consider the boundary condition that the surface density is linear function of Y, these two values are almost

the same practically by taking the distance of such interval to be small enough. Therefore, we can consider such procedure gives an accurate solution numerically. Here we divide the whole range of $-1 \leqslant Y \leqslant 1$ into 10 intervals of equal distance of 0.2, and compute the values of σ and Ψ for the ratio $A/K=10^3$ and same physical constants as in the previous section.

The result which is shown in Fig. 5 indicate us that the isopicnals and streamlines become more vertical in the lower latitudes than in the previous model shown in Fig. 3 and 4, suggesting that vertical current in the lower latitudes is stronger than in the model of constant p and q, as easily verified by the relation of Ψ and p. When the ratio A/K decreases and is equal to about 10, the distributions of σ and ψ are almost the same as in the previous model, so that they are not shown here.

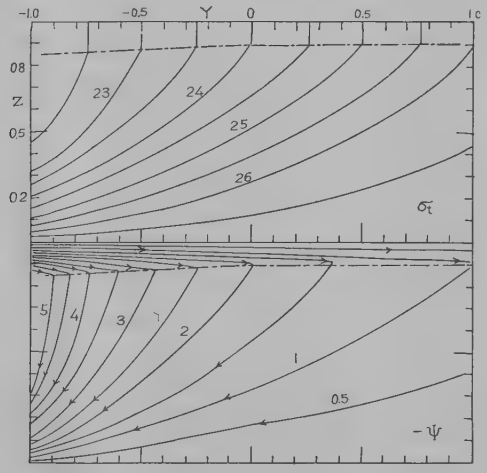

Fig. 5. Density field (in σ_t) and stream function (in A/φ_0) with varying p and q for $A/K=10^3$.

On the other hand, in an interval where Y is variable within a small fraction of 1, we can assume $p=\alpha\kappa/(1+\gamma Y)^2=-q_1Y+p_1$. Then equations for F_0 and F_1 become

$$F_0''=-p_1F_1'F_1-qF_0'F_1 \tag{40}$$

$$F_1''=(q_1-q)F_1'F_1 \tag{41}$$

instead of (35) and (36). Generally $q_1 \fallingdotseq q$ in an interval of small distance, so that we have simply $F_1 = \sigma_1 Z$. Also the solution of (40) is given by

$$F_0' = A\exp\left(-\frac{q\sigma_1}{2}Z^2\right) - \frac{\dot{p}_1\sigma_1}{q}\left\{1-\exp\left(-\frac{q\sigma_1}{2}Z^2\right)\right\} \tag{42}$$

or

$$F_0 = (\sigma_0 - \sigma_b + H(1))\, Erf(\beta Z)/Erf(\beta) - H(Z) + \sigma_b \tag{43}$$

where A is an integration constant and $Erf(Z)$ is an error function. Also $H(Z)$ is given by

$$H(Z) = \frac{\dot{p}_1\sigma_1}{q}\left\{Z - \frac{\sqrt{\pi}}{2\beta}Erf(\beta Z)\right\}, \quad \beta = \sqrt{q\sigma_1/2}$$

The result of numerical computation of this model by dividing the range into the same small intrervals as in the previous case is shown in Fig. 6. by use of the same constants, which gives the intermediate pattern of the density between the model of the previous section and that described just above, although current pattern is the same as that of the case $A/K=10$ shown in Fig. 4.

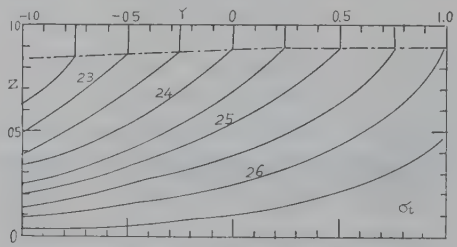

Fig. 6. Density field with linearly varying $\dot{p}$ for $A/K=10^3$.

7. Ciruculation produced by arbitrary distribution of the surface density

The solution which is expanded in power series of Y can be obtained only in a limited case of the boundary condition that the surface density is expressed by linear function of Y. In any other form of the boundary value, the series become infinite and ordinary differential equations for each coefficient F_i of Y^i are non-linear and prohibitively complicated.

On the other hand, when we give up the boundary condition which demands a predescribed surface value of density, we can obtain finite form of the solution of type $F(Y)\ G(Z)$ which is mathematically exact. This type of solution gives

the density distribution which has a similar vertical profile all over the ocean, which is not true in actual case, since generally thermocline in the lower latitudes are more shallow than that of higher latitudes. Moreover, in this type of a solution we cannot specify the surface value of density except at two points of the surface, because for definite function $G(Z)$, $F(Y)$ is defined as a solution of the second order ordinary differential equation.

Neverthless, we can obtain various kinds of distribution of density by changing parameters, which correspond to many actual conditions of the ocean, and comparison of such density field with corresponding current pattern gives some interesting explanation concerning the relationships between circulation and density distribution.

The solution within the boundary layer is the same as in the previous section and we have only to consider the solution of (15). When we introduce a new variable defined by

$$(1+\gamma Y)^2 dY = dX \qquad \text{or} \qquad X = (1+\gamma Y)^3/3\gamma \tag{44}$$

the equation (15) is transformed into

$$\frac{\partial^2 \sigma}{\partial Z^2} = \alpha\kappa\,(3\gamma X)^{\frac{2}{3}}\left(\frac{\partial^2 \sigma}{\partial X^2}\,\frac{\partial \sigma}{\partial Z} - \frac{\partial \sigma}{\partial Z}\,\frac{\partial^2 \sigma}{\partial X \partial Z}\right) \tag{45}$$

This equation has a type of solution $F(X)G(Z)$ and also the general form of the solution is expressed by

$$\sigma = F(X)G(Z) + f(X) + \sigma_b \tag{46}$$

where σ_b is an arbitrary constant and $f(X)$ is a function having a next form

$$f(X) = b + a\int^{x} F dX \tag{47}$$

in which a and b are integral constants.

The main problem of solving (28) is therefore to get $F(X)$ and $G(Z)$ and when we substitute (29) into (28), we have

$$\frac{G''(Z)}{\alpha\kappa G(Z) G'(Z)} = \frac{F''(X)F(X) - \{F'(X)\}^2}{(3\gamma X)^{-\frac{2}{3}} F(X)} = \text{const.} \tag{48}$$

This constant may be taken arbitrary, so that we put it 1 or -1 without losing generality.

The equation concerning $G(Z)$ is integrated immediately, by use of the same method as in previous sections. As the first step, we assume that $f(X) = 0$, in order to simplify the solution. Thus the boundary condition at the bottom for $G(Z)$ is such that $G(0) = 0$, corresponding to the condition that vertical current

vanishes there or $\partial\sigma/\partial Y=0$. Further, we can consider $F(X)>0$ without loss of generality, since when $F(X)<0$, we only have to change of the sign of constant of the equation (48). Then we should put $G'(Z)<0$ corresponding to stable stratification in the ocean. Then we obtain two types of solution for $G(Z)$ to different values of integration constant of (48), such as

$$\left.\begin{aligned} G&=-c\tanh rcZ \quad (\text{for } 1) \quad (\text{C})\\ G&=-c\tan rcZ \quad (\text{for } -1) \quad (\text{D}) \end{aligned}\right\} \tag{49}$$

where c is an integration constant to be determined from the boundary conditions such that

$$c\tanh rc=m \quad (\text{C}) \qquad c\tan rc=m \quad (\text{D}) \qquad \left(r=\frac{\alpha\kappa}{2}\right)$$

These two types of solution give quite different profiles in vertical section of density, so that it is important to include both signs in the constant of (48), whereas its numerical values are adjusted by changing the boundary values of $G(1)=-m$, so that it does not harm generality to put it ±1.

The differential equation for $F(X)$ becomes

$$F''F-(F')^2=\pm(3\gamma X)^{-\frac{2}{3}}F \qquad (\text{for C and D}) \tag{50}$$

is also non-linear type and it can be integrated by some approximate process. First of all we express the function $(3\gamma X)^{-\frac{2}{3}}$ approximately by an exponential function of a type

$$j(X)=\exp(a_0+a_1X+a_2X^2) \tag{51}$$

by taking suitable constants a_0, a_1 and a_2, which is possible as shown in the next section. Then we put

$$F(X)=j(X)\exp\{\phi(X)\} \tag{52}$$

and we have

$$F''F-(F')^2=(\phi''+2a_2)F^2.$$

Therefore the equation (50) is transformed into

$$F'+2a_2=\pm\exp(-\phi) \quad (\text{for C and D}) \tag{53}$$

By multiplying ϕ' to both sides of this equation, we can integrate, because $\phi'\exp(-\phi)=\dfrac{-d\exp(-\phi)}{dX}$, and we have

$$(\phi')^2=\mp2\exp(-\phi)-4a_2\phi+l \tag{54}$$

where l is an integral constant and minus sign corresponds to the case (C) and plus corresponds to (D). From (54) we get easily

$$\phi'=\pm\{\mp2\exp(-\phi)-4a_2\phi+l\}^{\frac{1}{2}} \tag{55}$$

or

$$\pm\int_{\phi_0}^{\phi}\{\mp 2\exp(-\phi)-4a_2\phi+l\}^{-\frac{1}{2}}d\phi=X-X_0 \qquad (56)$$

where ϕ_0 corresponds to the value of ϕ at X_0, the lower limit of X in the considered domain and the double sign before the integral sign should be taken so as to give the positive value of the left hand side of the equation, whereas the minus sign within the parentheses corresponds to (C) and the plus corresponds to (D).

8. *Preliminary discussion for numerical computation of Section 7.*

The behavior of the function $F(X)$ is rather complicated, because has very intricate form and also it has two integration constants to be determined from the boundary conditions, whereas $G(Z)$ is simple in its integrated form and only one parameter However, the difference of vertical profile of $G(Z)$ in two cases (C) and (D) gives a remarkable contrast in a vertical distribution of density pattern, which, in turn, is closely associated with current system, since $F(X)$ is also different in two cases.

In order to illustrate the contrast between (C) and (D), we show vertical distributions of $G(Z)$ for $2r=\alpha_K=1$ to 10^2 by taking $m=1$ in Fig. 7, which indicates that the profile of (C) gives thermocline deeper than that of (D). As shown later, different function $F(X)$ corresponds to different value of m, so that we cannot compare this vertical profile with the previous models. However, it is interesting to note that the vertical profiles of this model are almost similar to the models treated by the author (Ichiye, 1958). which is derived on the basis of balance between planetary vorticity and divergence. Thus, the present case of (C) give profiles similar to vertical density distribution obtained for a westward increasing density field in the previous model, with homogeneous layer in the upper layer. On the other hand, the profiles corresponding to (D) have homogeneous layer near the bottom, similar to those of a eastwards increasing density field. Moreover, in the present model too, a decreasing value of $2r=A/K$ produces the profiles approaching to linear

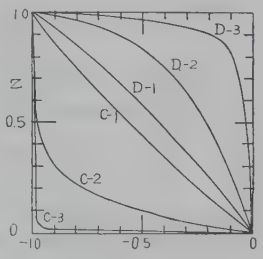

Fig. 7.
Curves of G(Z)
C—Model (C)
D—Model (D)
1—$\alpha_K=1$
2—$\alpha_K=10$
3—$\alpha_K=10^2$

function with the depth, which is considered as a well-mixed state.

For computing $F(X)$, first we have to determine the numerical constants a_0, a_1 and a_2, so that $j(X)$ may give a close approximation to $(3\gamma X)^{-\frac{2}{3}}$, This estimation is done by use of least squares and the result is

$$a_0=1.770, \qquad a_1=-1.937, \qquad a_2=0.572$$

The exact curve of $(3\gamma X)^{-\frac{2}{3}}$ and the approximate curve are shown in Fig. 8, which indicate that the correspond between two curves is good only in a range of X from 0.2 to 1.6 or in a range of Y from -0.9 to 0.6. However, this does not hurt the applicability of the present model, since is we take a larger value of γ, we can cover wider range of X by such approximation. We can integrate the equation (56) by numerical method. or ther approximation process which is to be described in the following sections.

The analytic property of the integral (56) is much changed for different values of parameters ϕ_0 and l. The value of ϕ_0 can be determined from the surface value of density $\sigma(X, 0)$ at the lowest latitude $X=X_0$ and also the parameter m for the function $G(Z)$. When we put $\sigma(X_0, 0)=-\sigma_0+\sigma_b$, then $F(X_0)=\sigma_0/m$ and

$$\phi_0=\log(\sigma_0/m)-\log j(X_0)$$

The integration constant l is determined by another boundary condition. When we put $\eta=\phi-\phi_0$, the equation (56) becomes

$$\pm\int_0^{\eta} e^{\phi_0/2}(\mp 2e^{-\eta}-4a_2\eta e^{\phi_0}+k)^{-\frac{1}{2}}\,d\eta=X-X_0 \tag{57}$$

Further, when we put the value or $\eta=\eta_1$ at $X=X_1$, this is determined only by the ratio of the surface density at $X=X_0$ and $X=X_1$ since

$$\eta_1=\phi_1-\phi_0=\log\sigma_1/\sigma_0-\log j(X_0)/j(X_1)$$

where $\qquad \sigma(X_1, 0)=-\sigma_1+\sigma_b \quad$ and $\quad \phi(X_1)=\phi_1.$

When η is monotonous function of X in the range $X_0\leqslant X\leqslant X_1$ we have take positive or negative sign before the integral of (57) according to positive or negative value of η_1. On the other hand, when η has maximum or minimum in this range, for example, maximum η_m at $X=X_m$, we can express the relation (57) for (C) as

$$\left.\begin{aligned}&(\text{for } X_0<X<X_m)\quad X-X_0=e^{\frac{\phi_0}{2}}\int_0^{\eta}\{2(e^{-\eta_m}e^{-\eta})+4a_2e^{\phi_0}(\eta_m-\eta)\}^{-\frac{1}{2}}\,d\eta\\&(\text{for } X_m<X<X_1)\quad X-X_m=e^{\frac{\phi_0}{2}}\int_{\eta}^{\eta_m}\{2(e^{-\eta_m}-e^{-\eta})+4a_2e^{\phi_0}(\eta_m-\eta)\}^{-\frac{1}{2}}\,d\eta\end{aligned}\right\} \tag{58}$$

and for (D) we only have to change the sign before e^{η}.

9. Various examples of density distribution and circulation pattern

Now we can compute any density destribution and stream function induced by such density pattern by use of (49) (52), (56) and (58). Here we summarize the process to compute these equations so as to give a density distribution which is plausible in the actual ocean. As stated in section 8, we shall determine a value of σ which satisfys the boundary condition that $\sigma=\sigma_b$ at the bottom $Z=0$ and $\sigma=\sigma_b-\sigma_0$ at $X=X_0$ and $\sigma=\sigma_b-\sigma_1$ at $X=X_1$ at the surface (or more precisely at the upper boundary layer).

First we take arbitrarily ϕ_0 (actually the range is limitted in order to obtain a reasonable result) and we determine integration constant k in the equation (57) or η_m in (58) from the boundary condition at $X=X_1$ that $\eta(X_1)=\eta_1=\phi_1-\phi_0$ This process is generally carried out by trial and error method, but actually the range of η_1, η_m is not so large compared with 1 we can express the integral (57) or (57) by elementary functions as described below, so that we can compute these constants rather analytically in most cases. From the relation between η and X thus determined we can compute a function $F(X)$.

For each function $F(X)$ or for each initial constant ϕ_0 one value of m is determined from the relation $m=\sigma_0/F(X_0)$. Then we can compute the function $G(Z)$ from the equation (49) where c is determined from the boundary condition for different values of $r=\alpha\kappa/2$. Therefore for each surface density distribution we can assort various kinds of vertical profiles represented by the function $G(Z)$ according to different values of the ration A/K, say, from the profile with very shallow thermocline for a large value of the ratio, when the function $G(Z)$ belongs to the type (D), to the linear function of Z for a small value of it.

As easily seen, the solution $F(X)$ cannot be uniquely determined only by specifying the surface density at two points, because we can take ϕ_0 arbitrarily and adjust m. Also it is important that we cannot specify the surface density distribution all over the region in the present approach as in the process of section 5 and 6, so that we have to seek various kinds of solution by changing parameters so as to give plausible surface density distribution instead of impose it as a boundary condition.

Singular solution. When $\phi_0 \gg 1$, the integral (57) can be integrated by use of elementary function, since the exponential term in the integrand is negligibly

small, so that for example the equation (56) is written as

$$X-X_0=\frac{1}{2a_2}(l^{\frac{1}{2}}-\overline{l-4a_2\eta}^{\frac{1}{2}})$$

On the other hand, this type of solution corresponds to a singular solution of the original equation (45), since in such condition the equation (53) becomes $\phi''+2a_2=0$. Therefore we have

$$F(X)=F_0e^{\gamma X}$$

where F_0 and γ are constants to be determined from boundary conditions. As we can see at once by substituting this $F(X)$ into (45), $G''(Z)=0$. Therefore the solution for density σ which satisfys the boundary condition described in the last section

(At the surface $Z=1$) $\quad \sigma=\sigma_b-\sigma_0$ at $X=X_0$, $\quad \sigma=\sigma_0-\sigma_1$ at $X=X_1$

(at the bottom $Z=0$) $\quad \sigma=\sigma_b$ (59)

is represented by

$$\sigma=-\sigma_0 Z\exp\gamma(X-X_0)+\sigma_b \tag{60}$$

where $\quad \gamma=[\log(\sigma_1/\sigma_0)]/(X_1-X_0)$

$$X=(1+\gamma Y)^3/\gamma$$

Since this solution does not include the ratio $\alpha\kappa=A/K$, it is considered to represent the condition that the density field and current system adjust themselves so as to annul the effect of vertical mixing.

We take $\sigma_0=5\times10^{-3}$, $\sigma_1=2\times10^{-3}$, $X_0=0.2$, $X_1=1.6$ which corresponds roughtly to the condition treated in section 5 and 6, and numerical results are shown in Fig. 8, where curves of surface density and Ψ, and vertical profiles of density and ψ are drawn against Y. The vertical sections of σ and Ψ are very similar to the model of section 5 and 6 of well mixed state with a small value of A/K, since the surface density is almost uniformly increased with Y and also it is linear function of Z in the present model.

Approximate form to the integral (57) and (58).

When $\eta<1$ and we can put $e^{-\eta}=1-\eta+\frac{\eta^2}{2}$, the integral (57) is written as

$$\text{(C)}\quad \sin^{-1}\left(\frac{\gamma_c}{\sqrt{k_c^2+\gamma_c^2}}\right)-\sin^{-1}\left(\frac{\gamma_c-\gamma_l}{\sqrt{k_c^2+\gamma_c^2}}\right)=(X-X_0)\cdot e^{-\phi_0/2} \tag{61}$$

where $\quad k_c^2=k-2, \qquad \eta_c=1-2a_2e^{\phi_0}$

$$\text{(D)}\quad \sinh^{-1}\left(\frac{\gamma_d}{\sqrt{k_d^2-\gamma_d^2}}\right)-\sinh^{-1}\left(\frac{\gamma_d-\gamma_l}{\sqrt{k_d^2-\gamma_d^2}}\right)=(X-X_0)\cdot e^{-\phi_0/2} \tag{62}$$

where $\quad k_d^2=k+2, \qquad \eta_d=1+2a_2e^{\phi_0}$

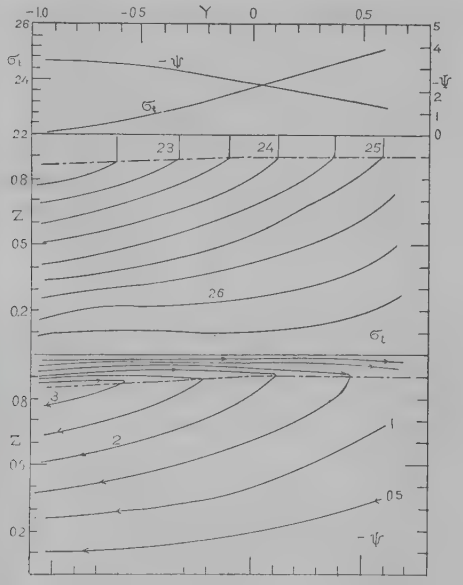

Fig. 8. Surface values (the upper most curves) and vertical sections of density (σ_t) and stream function (in A/φ_0).

Further, when $\eta_1<1$, $\eta_m-\eta_1<1$, we can put

(C) (for $0<\eta<\eta_1$) The same equation as (61) with

$$k_c^2=2(e^{-\eta_m}-1+2a_2e^{\phi_0}\eta_m)$$

(for $\eta_1<\eta<\eta_m$)

where $\sin^{-1}(\xi_c-\eta_m+\eta)/\xi_c \quad \sin^{-1}(\xi_c-\eta_m+\eta_1)/\xi_c=(X-X_m)e^{-\frac{1}{2}(\phi_0+\eta_m)}$ (63)

$\xi_c=2a_2e^{\phi_0+\eta_m}-1$

(D) (for $0<\eta<\eta_1$) The same equation as (62) with

$$k_d^2=2(1-e^{-\eta_m}+2a_2e^{\phi_0}\eta_m)$$

(for $\eta_1>\eta>\eta_m$)

$$\cosh^{-1}(\xi_d+\eta_m-\eta)/\xi_d=(X-X_m)e^{-\frac{1}{2}(\phi_0+\eta_m)} \quad (64)$$

where $\xi_d=1+2a_2e^{\phi_0+\eta_m}$

Examples for different ϕ_0 with the same function $G(Z)$.

Here we discuss the solutions obtained under the same boundary condition (59) with numerical constants equal to those of Fig. 8, whereas we change the con-

stant ϕ_0 from 4 to −1.5. We can determine $F(X)$ for each ϕ_0 and we can combine various kinds of $G(Z)$, but here we assort only one $G(Z)$, in order to show more instructively how is the relationship between mass distribution and circulation which is deduced from the basic relations given in section 2. Here we chose a function $G(Z)$ corresponding to $r'=5$ which is drawn in Fig. 7, where we use r' instead r in order to indicate the parameter in Fig. 7 being for $m=1$. Therefore, the ratio A/K for each value of m with different value of ϕ_0 is computed from

$$A/K \fallingdotseq \alpha\kappa = 2r = 2r'/m$$

whereas m is given by $m=\sigma_0/F(X_0)=\sigma_0/j(X_0)\exp(\phi_0)$. The reason why we chose the value $r'=5$ is that the function $G(Z)$ obtained is intermediate between the extremely shallow or deep thermocline for larger r' and uniformly changing vertical profile for smaller r', which gives more realistic picture of density distribution.

The results are represented in similar way to Fig. 8 and the values of ϕ_0 for each figure and corresponding ratio A/K are shown below. The function $F(X)$ for each ϕ_0 is mostly computed for the case (D), since this type of vertical profile is more realistic in the ocean.

Table

No. of Model	I	II	III	IV	V	VI	VII
No. of Fig.	9	10	11	12	13	14	15
ϕ_0	4	1	0	−.5	−.75	−.954	−1.5
A/K	2.84×10^5	1.44×10^4	5.2×10^3	3.2×10^3	2.5×10^3	2.0×10^3	1.1×10^3

The model I is similar to the previous solution of (60) except its vertical profiles, and it has abnormally high value of A/K in order to maintain vertical profile similar to other cases described in this paragraph, so that it is rather a theoretical purpose to show it here than a purpose for applying the obtained distribution to the actual ocean. On the other hand, the model II, III and so on gives interesting picture, which deviates from the linear surface distribution in section 5 and 6. Generally the surface density or $F(X)$ increases very slowly with Y in lower latitudes or for smaller values of Y and indeed in model VI and VII it decreases in some range thus it has minimum surface density.

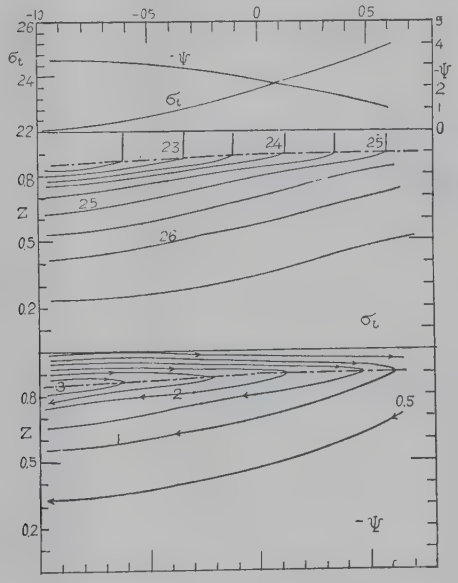

Fig. 9.
Surface values (the upper most curves) and vertical sections of density (in σ_t) and stream function (in A/φ_0) of Model (I).

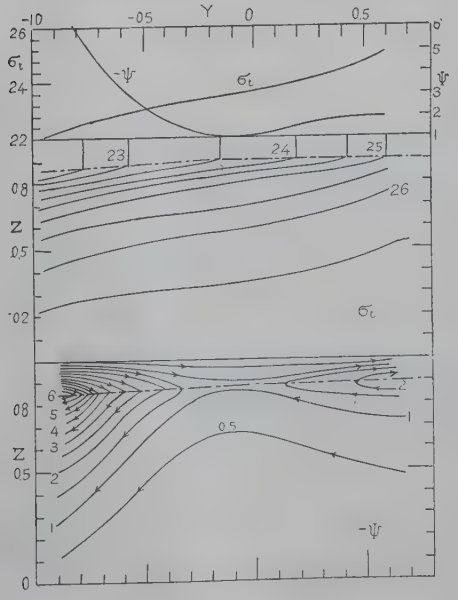

Fig. 10.
Model (II).

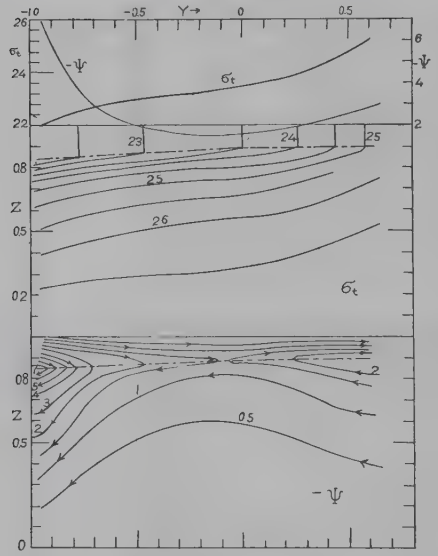

Fig. 11.
Model (III).

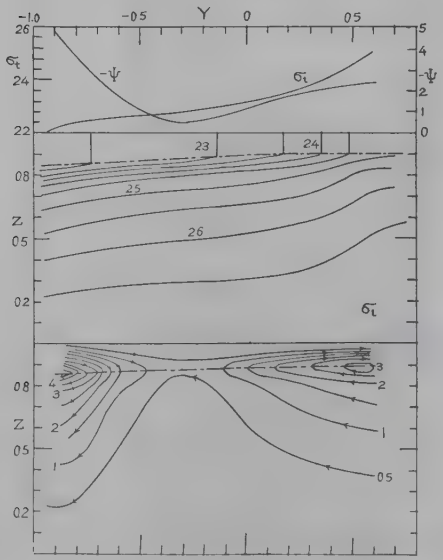

Fig. 12.
Model (IV).

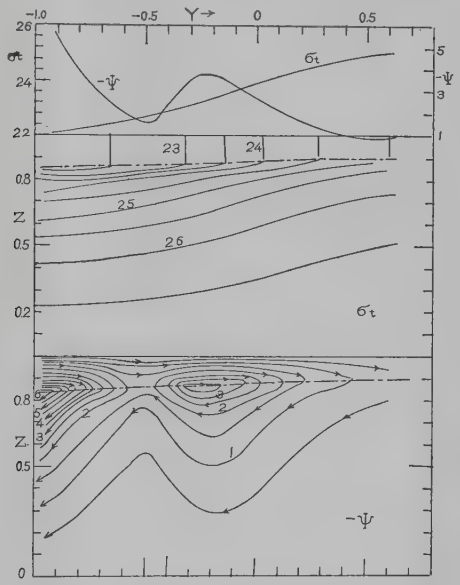

Fig. 13.
Model (V).

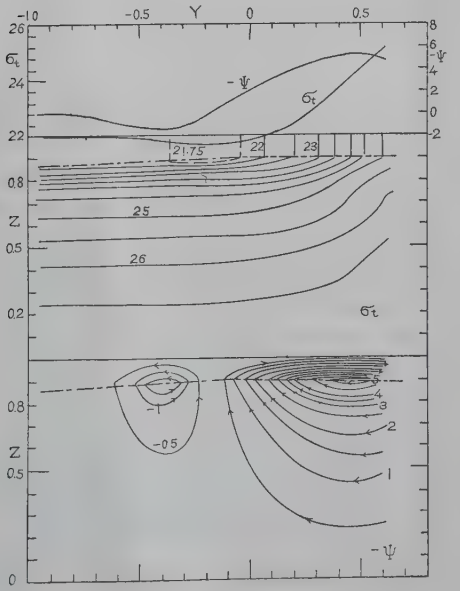

Fig. 14.
Model (VI).

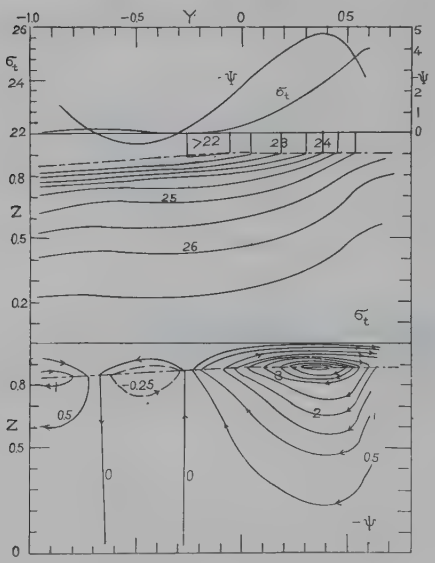

Fig. 15. Model (VII).

On the other hand, in higher latitudes it increases rapidly with Y. (This is described about model (D) of $G(Z)$, and for (C) this statement is not valid as seen later.) Such surface density is reflected in current pattern and there appear two gyres in models II to V, where that in lower latitudes produces sinking motion in the interior region and the in higher latitude causes upwelling, the relative intensity of which charges as changing ϕ_0. In the model VII, there appears three gyre, corresponding to the minimum of surface density, and also the strength of higher latitude gyre is maximum among three, thus producing strong upwelling in the middle latitude. The model VI shows intermediate nature between these two types.

As one model corresponding to the vertical profile of type (C), we get Fig. 16, which is computed for $\phi_0=-.954$ and $A/K=2\times10^2$, with the same constants as the models stated above. The surface density shows a rapid increase for smaller value of Y, contrary to the above models. Therefore, the general vertical current in the interior region is downwards, which contributes to make the thermo-

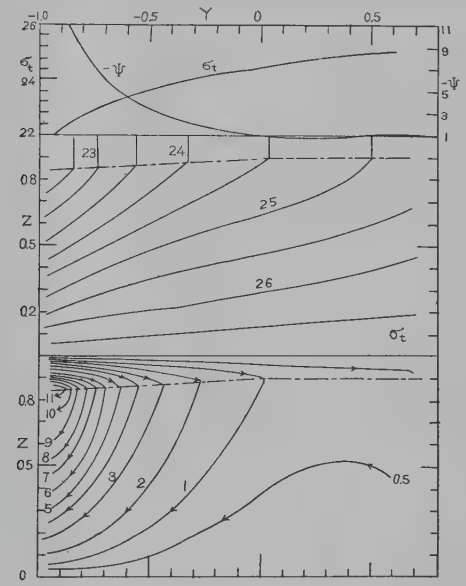

Fig. 16.
Example of a vertical profile of type (C).

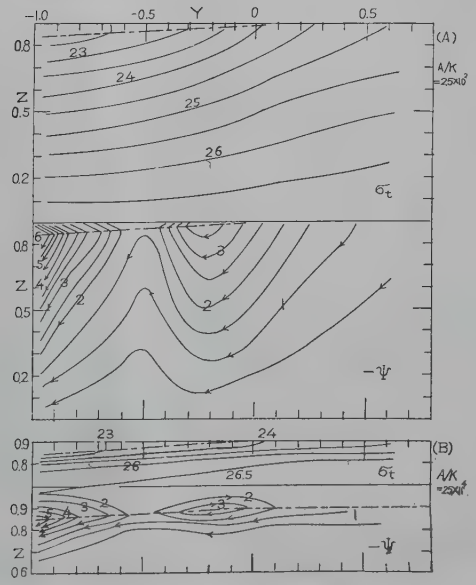

Fig. 17.
Models equivalent to (V) with different ratio A/K.

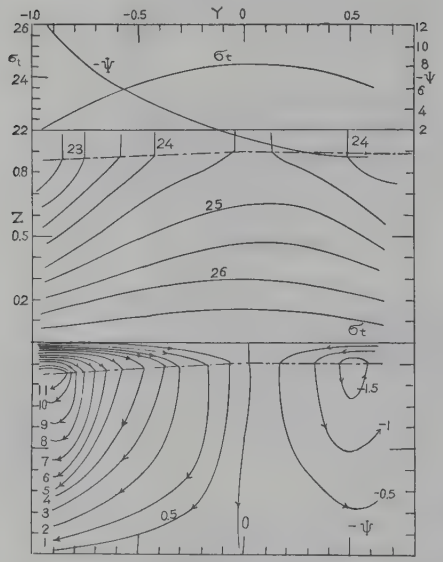

Fig. 18.
Examples of a profile of type (C) with $A/K = 2.5 \times 10^2$.

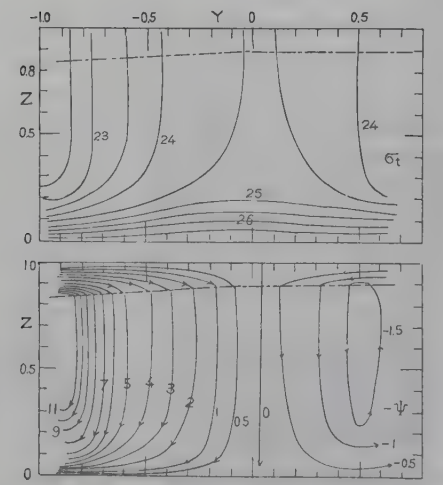

Fig. 19.
Example of a profile of type (C) with $A/K = 2.5 \times 10^3$. (Surface values of σ_t and ψ are equal to those of Fig. 18).

cline deeper than the last cases.

Change of pattern as variable ratio A/K. For the same surface distribution of density or function $F(X)$, vertical profile changes as the ratio A/K has a different value. Examples of such change are illustrated in Fig. 17, where the model V of the last paragraph is taken and patterns of density and current for $A/K=2.5\times10^{2}$ and 25×10^{4} are shown. We can see that increase of A/K to ten times from the original value in the last paragraphy changes the pattern quite remarkably, whereas the decrease to one tenth gives no such conspicuous change.

As another example, we show the model for vertical profile of type (C) in Fig. 18 and 19, with $\phi_0=-.75$ and the ratio A/K is 2.5×10^{2} and 2.5×10^{3}, respectively. This model does not satisfy the condition that $\sigma_1=2\times10^{-3}$, but it gives an example that there exist two gyres, owing to the condition that there is a maximum in the surface density distribution, although these two gyres give both sinking motion below the upper boundary layer. Further, in this (C) type, change of the ratio A/K is reflected in the pattern more sensitively than in the type (D), and thus the increase of A/K to ten times of 2.5×10^{2}, which gives almost uniformly changing vertical profile, change the whole pattern conspicuously, so that in the case of $A/K=2.5\times10^{3}$, the thermocline is almost near tne bottom. Miscellaneous patterns for $\phi_0=-1.5$. Since the model VII gives some interesting features, we shall compute further some examples for $\phi_0=1.5$, but for different values of σ_1. Two of these are shown in Fig. 20, both for the ratio $A/K=1.1\times10^{3}$ as in the model VII. We can see that the decrease of the end value of surface denisty at $X=X_1$ produces more and more intense middle gyre, since the value of σ_1 corresponding to the model VII (Fig. 15) is 1.8×10^{-3} (we specify σ_1 in the model VII as 2×10^{-3}, but we have to determine integral constants by trial and error method, so that some difference exists at the end value.), whereas the pattern of Fig. 20 corresponds to $\sigma_1=0.9\times10^{-3}$ and 2.6×10^{-3}, respectively. This state of condition suggests that the absolute difference in density of the surface water between in polar region and tropical region affects the whole pattern of vertical circulation. A solution containing an additional term (47). This is rather hypothetical model, but it is obtained from mathematically possible solution, by adding a term (47) to a solution heretofore determined. In present model we take a function $F(X)$ similar to the model VI of the previous paragraph, then we add a term $0.3\int_{x_0}^{x}F(x)\,dx$, as stated in the equation (46). The resultant pattern of σ and Ψ are shown in Fig. 21, where we should in-

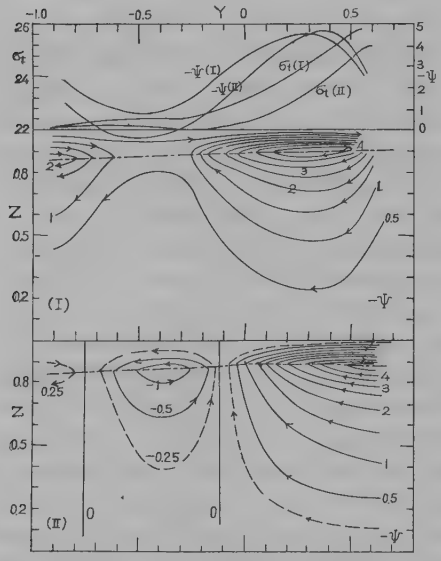

Fig. 20.
Two examples equivalent to Model VII with different density at the polarward limit.

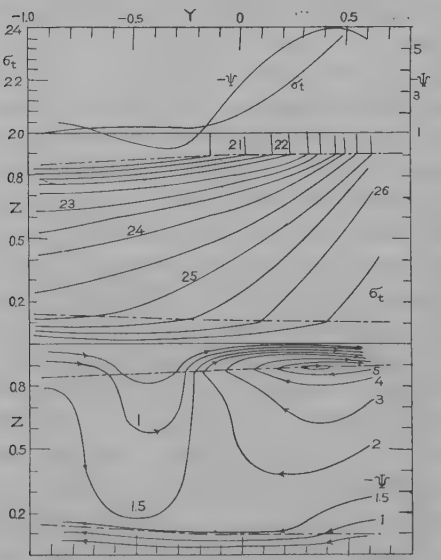

Fig. 21.
Example with a lower boundary layer.

triduce lower boundary layer, so as to make vertical current at the bottom vanish. Comparison of this pattern with that of Fig. 14 suggests us that change in the general current pattern in the interfor region is rather small, although near the lower boundary layer the pattern of the present model is quite different from the previous one. An approximate solution for arbitrarily given surface density.

When we assume that the density distribution is represented by a form as (46) without $f(X)$ term, or by a equation such as

$$\sigma=E(Y)G(Z)+\sigma_0 \tag{64}$$

then we have from the equation (15)

$$G''=2R(Y)GG' \tag{65}$$

where

$$2R(Y)=\frac{\alpha\kappa}{(1+\gamma Y)^2E}\left\{(E''E-E'^2)-\frac{2\gamma}{(1+\gamma Y)}EE'\right\} \tag{66}$$

Therefore, when we divide the interval of Y into small divisions, in which the change of $R(Y)$ is so small that it can be considered constant, we can integrate $G(Z)$ as stated in the section 7 and this function is expressed by formula (49), by replacing r with $R(Y)$. When R is positive, the formula for (C) is applied, and when R is negative, that of (D) is valid. Since $E(Y)$ or $F(X)$ of the previous paragraphs is known when the surface desity distribution is given, so that the resultant vertical profiles are determined for any surface density. In this solution, it depends on a local value of $E(Y)$, $E'(Y)$ and $E''(Y)$ which type of (C) or (D) a vertical profile belongs to.

As an example, we take a linear function for $E(Y)$ such as

$$E(Y)=\sigma_1 Y-\sigma_0$$

and divide the interval $(-1, 1)$ of Y into ten divisions, using the same constant $\sigma_0=3\times10^{-3}$, $\sigma_1=2\times10^{-3}$ and $\alpha\kappa=10^3$ as in the sections 5 and 6. The result of computation is shown in Fig. 22, which is quite similar to the previous example of Fig. 7, which is computed with more tedious process. In this example, we can see that at about $Y=0.2$ the vertical profile changes from type (C) in lower latitudes to type (D) in higher latitudes.

When we assume that $R(Y)$ is constant in the whole region of Y, we can obtain the solutions which has been discussed in the previous paragraphs (written as $F(X)$). Generally, we can conclude, from the results obtained by numerical calculation, that for a vertical profile of (C) the surface density when plotted against Y, has a curve convex downwards, and for type (D) it is

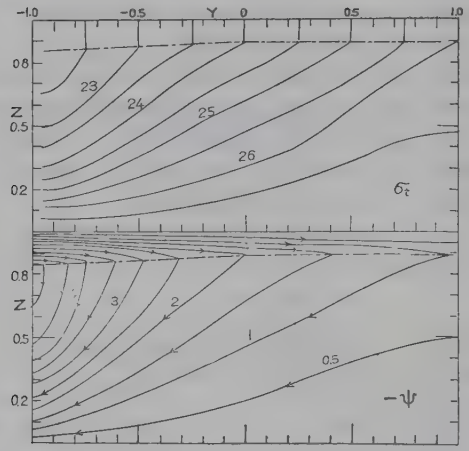

Fig. 22. Model of linearly increasing surface density computed by approximation (65) for $A/K=10^3$.

represented by a curve concave downwards. Such density distribution produces various kinds of current pattern, which are not so simple that we cannot say that (C) is accompanied with sinking and (D) is caused by upwelling, as described in the previous paragraphs.

10. Comparison with observed data.

The models described above are expressed with non-dimensional parameters, which is very convenient particularly to show density distribution. However, for the purpose of estimation of velocity from a chart of stream function ψ, we should give some remarks The values of Ψ in these charts are expressed by an unite of $A/2\rho_0$, when we take numerical constants such as $f_0=10^{-4}$, $a=2\times10^8$, $g=10^3$. Therefore, when we take $A=4$(cm^2/sec), a vertical velocity w and horizontal velocity v expressed by $w=-\frac{A}{2a}\frac{\partial}{\partial Y}\Psi$, $v=\frac{A}{2h}\frac{\partial}{\partial Z}\Psi$, respectively, has a numerical value of $w=-10^{-8}\,\partial\psi/\partial Y$ and $v=10^{-5}\,\partial\psi/\partial Z$, for $h=2\times10^5$. Therefore, one unit difference of Ψ at a distance of $Y=0.1$ corresponds to $w=10^{-7}$(cm/sec), and that of Ψ at a distance of $Z=0.1$ gives $v=10^{-4}$(cm/sec).

In this theoretical model we neglect the zonal pressure difference and we

have assumed that meridional components of flow is not geostrophic but is driven through frictional force produced by geostrophic zonal flow which, in turn, is caused by meridional pressure difference due to density gradient in this direction. Therefore eddy viscosity is rather essential to the meridional circulation in this model, so that this model seems to be valid only in the upper layer of the ocean, say, of about 1000 m thickness, because eddy viscosity is presumably ineffectice below this level in the actual ocean. In a deeper layer, current is actually geostrophic in most cases even in meridional component, toerefore, the model of STOMMEL (1957b), STOMMEL and VERONIS (1957) or that described in another paper by the author (1958).

Indeed, we show the vertical section of σ_t along the middle section of the Atlantic from the Meteor Report (DEFANT, 1936, WÜST, 1936) where the upper

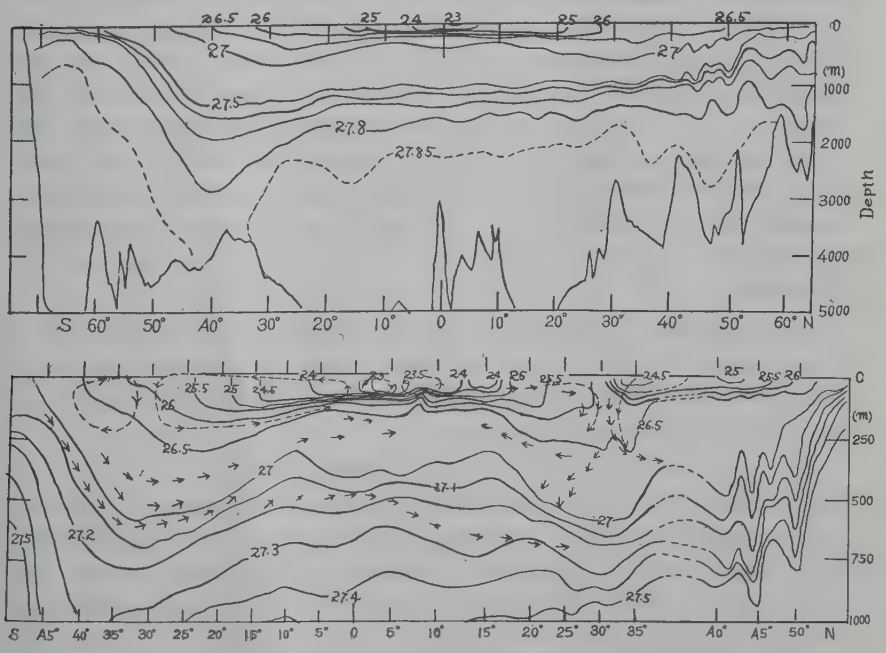

Fig. 23. Vertical section of σ_t along the central part of the Atlantic (after Wüst (1936) for upper chart and Defant (1936) for lower chart)

chart gives the distribution of σ_t to the bottom, and the lower one to 1000 m depth. A glance of the upper chart suggest us that vertical gradient of density below about 1000 m is quite small, so that we need a large value of the ratio A/K for explaining the observed profile from the present theory (of course the profile is type (D) defined in section 9) if we include the ocean to the bottom. A brief estimation gives the ratio A/K of about 10^4 to 10^5 corresponding to the actual profiles of, which gives the value of A 13 to 130 (cm^2/sec) even for a molecular diffusivity of K, since molecular K is about 1.3×10^{-3} when we assume that change of density is mainly due to that of water temperature. Such discrepancy with observed facts seems to be due to the assumption that meridional circulation is caused by frictional force even to the great depth.

Anyhow, hereafter we restrict our discussions within upper 1000 m layer. The first glimpes of the lower chart suggests us that in the polar region, especially in the southern hemisphere, the observed density distribution and meridional circulation seems to correspond to the theoretical model of uniformly increasing surface density described in section 5 and 6, but in middle and lower latitude correspondence between the observed and theoretical distribution fils rather poor. This is due to the fact that the density distribution in the upper layer is not only governed by convective circulation but also of wind current which produces rather intense vertical current below the upper boundary layer or EKMAN layer, as stated below. However, some resemblance is recognized between model VI or VII and middle latitude of the northern Atlantic in circulation pattern.

Representation of density in power series. First we expressobserved σ_t in power series of Y, where we take the whole distance of theregion $2a=40$ deg. latitude (from 10 degrees to 50 degrees), from 200 m to 1000 m depth. As a series we take up to cubic powers of such as

$$\sigma_t=F_0(Z)+F_1(Z)Y+F_2(Z)Y^2+F_3(Z)Y^3$$

and practically $F_i(Z)$ is computed by the estimation of momentum $\int_{-1}^{1}\sigma_t Y^i dY$ from observed values of σ_t. The results are plotted in Fig. 24, which indicate that the term $F_3(Z)$ is very small compared with other terms. Further the positive value of $F_2(Z)$ suggests that circulation induced by density distribution is generally upwelling all over the region as stated in section 4. Comparison of vertical profiles of $F_0(Z)$, $F_1(Z)$ $F_2(Z)$ obtained empirically with theoretical ones of Fig. 1 suggests us that the ratio A/K is about 10^3 if we assumed that the meridional circulation is produced only by convection. Stream function computed

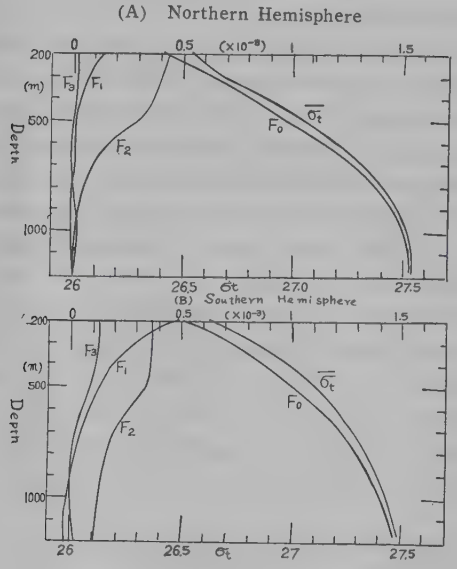

Fig. 24.
Vertical profiles of $\bar{\sigma}_t$ (mean value of σ_t at each depth) and F_t. (Upper scale should be used for F_1, F_2 and F_3, lower scale be used for F_0 and $\bar{\sigma}_t$).

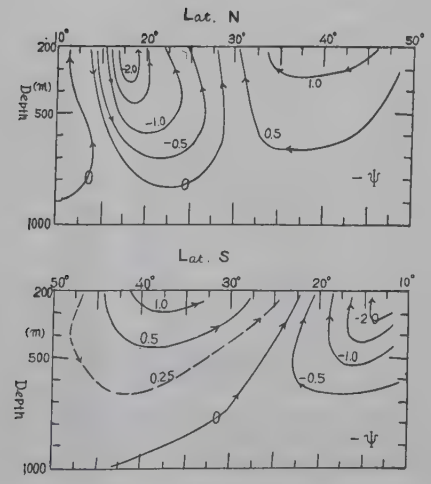

Fig. 25.
Stream function (A/φ_0) computed from observed density field in the Atlantic.

from observed density distribution.

We can compute directly stream function in the considered region from observed density distribution by use of the formula (14). The results are shown in Fig. 25, where some smoothing of original data is applied. These pictures do not represent a real circulation pattern, since the wind stress term in the equation for Ψ is more predominent actually, as stated below. However, it gives some ideas about convective circulation, if it is assumed to be a main factor in the ocean, which produces generally sinking motion in polar region and upwelling in subtropical region.

The effect of wind-driven current on density distribution.

So far as we are concerned with theoretical model, we have neglected wind-stres term in the equation (10). However, rough estimation of this term in the ocean indicates that this term is far more important than density gradient term so long as the value of eddy viscosity is not abnormally large. Since the wind stress term increases with Y, the resultant vertical motion is downwards all over

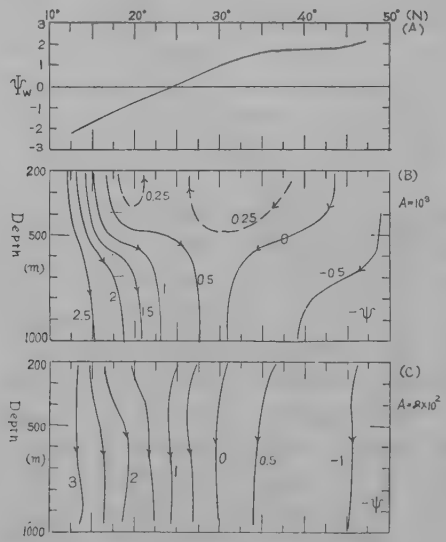

Fig. 26. Stream function induced by wind stress (A) and by combined effect of density field (B and C) in the North Atlantic.

the region and also this motion is constant with the depth below the EKMAN layer, although there is no horizontal motion induced by wind stress there. In Fig. 26 we plot the computed value of stream function due to the wind stress $\Psi_w=\delta_T/(1+\gamma Y)$ by use of the data of MUNK (1950) over the north Atlantic, and also the resultant value of Ψ due to both convection and wind-driven circulation. We can see at once that the latter effect is predominent already for a value of A less than 2×10^2, and only for an abnormally large value of A more than 10^3 the former effect is recognizable.

On the other hand, when we assumed that wind-driven circulation is predominant, we can compute density distribution very simply from the equation

$$\frac{\partial^2\sigma}{\partial Z^2}=W(Y)\frac{\partial\sigma}{\partial Z} \tag{67}$$

where $W(Y)$ is a known function of Y such as

$$W(Y)=-\delta\text{æ}\frac{\partial}{\partial Y}\left(\frac{\tau}{1+\gamma Y}\right) \tag{68}$$

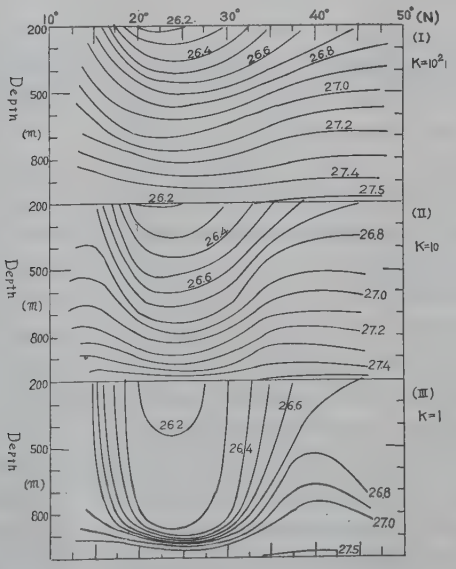

Fig. 27. Density field produced by wind-driven vertical current in the North Atlantic.

and thus the density is given by

$$\sigma=\sigma_b-(\sigma_b-\sigma_s)\,(1-e^{\alpha z})/(1-e^{\alpha})\qquad(69)$$

where σ_b, σ_s are bottom and surface value of b.

We compute the density distribution from this equation by use of observed values of Ψ shown in Fig. 27 and σ_s, σ_b for $K=1,10$ and 100. The result suggests us that we should take an extraordinary large value of K in order to get a picture similar to the observed density distribution. This means that a much larger contribution of vertical diffusion is necessary to counteract the strong downwards current induced by wind stress if we neglect the convective motion. However, it is not the main purpose of present research to discuss in details about the interaction of wind-driven current and convection current, and also it seems that we should build more complicated theory in order to get complete picture of circulation in such intermediate layer, which is another problem different from the present one.

11. Summary and concluding remarks

Assuming zonal ocean, or neglecting zonal difference of all physical quantities, we derived two equations which give the relationships between density structure and current system, where zonal current is produced by geostrophic relation due to meridional gradient of density and meridional circulation is induced by frictional force. When we give the surface density, which is linearly increased polarwards changed, we can get approximate solution of this equation system approximately by several processes, which gives a circulation pattern that in the upper boundary layer or EKMAN layer there is a flow almost horizontal and polarwards and below this layer there is an equatorwards flow accompanying sinking motion. The depth of thermocline decreases as increasing ratio of A/K especially in the polar region, but in lower latitudes it is rather more shallow than in the polar region, contrary to the observed density distribution.

We can get only an approximate solution under the boundary condition that surface density is a linear function of latitude, but we can get exact solution under various kinds of surface density distribution Therefore we can build many circulation pattern induced by each of such surface condition, which have two or three gyres in some cases quite similar to the actual circulation in the meridional section of the ocean. Further, such circulation pattern belongs to two different types according to vertical profiles, one of which has deeper ther-

mocline than the other type. Also the surface density which belongs to a type of deeper thermocline increases rapidly in higher latitudes, whereas that of the other type increases rapidly in lower latitudes. Both types of vertical profiles approaches to the linear distribution with depth when the ratio A/K decreases, which is considered as a well-mixed state of surface and bottom water.

These theoretical models of convective circulation do not agree with observed density distribution and circulation so well, because in the actual ocean vertical current induced by wind driven circulation below EKMAN layer is more predominant. However, this type of circulation induced by convection seems to counteract the effect of wind-driven sinking motion, particularly in middle and lower latitudes, thus we need not so large effect of vertical mixing in order to main tain the observed density structure against such sinking motion.

This work is rather incomplete in regards to applicability to the real condition. However, it gives many examples of convective current from exact solutions of non-linear equation, so that they might be used for interpretation of actual data in many cases.

Acknowledgement

The author wishes his hearty thanks to Mr. Henry STOMMEL for his encouragement and many advices.

References

DEFANT, A., 1936: Schitung und Zirkulation des Atlantischen Ozeans. Die Troposphäre. Wiss. Erg. Deutsch. Atlant. Exp. "Meteor" 1925–27, 6-1.

EKMAN, V. W., 1905: On the influence of the earth's rotation on ocean current. Arkiv för Mat. Astron. och Fysik, 2 (11).

FOFONOFF, N. P., 1954: A theoretical study of zonally uniform ocean flow. Tech. Report 4 for Office of Naval Res. Brown Univ.

ICHIYE, T., 1958: A theory of vertical structure of density. (To be published in Journ. Oceano. Soc. Japan and WHOI Contr. No. 953).

LINEYKIN, P. C., 1955: On the determination of the thickness of the baroclinic layer in the sea. Docklady SSSR Akad. Nauk, 101.

MUNK, W. H., 1950: On the wind-driven circulation. Journ. of Meteor. 7 (2).

STOMMEL, H., 1957a: A survey of ocean current theory. Deep Sea Res. 4 (3).

STOMMEL, H., 1957b: Reflections on the mechanism of the main thermocline. (Unpublished manuscript).

STOMMEL, H. and G. VERONIS, 1957: Steady convective motion in a horizontal layer of fluid heated uniformly from above and cooled non-uniformly from below. Tellus 9 (3).

VERONIS, G., 1957: Thermal circulation. Oceanus 5 (3).

WÜST, G., 1936: Schichtung und Zirkulation des Atlantischen Ozeans. Das Bodenwasser und die Stratosphäre. Wiss. Erg. Deutsch. Atlanti. Exp. "Meteor" 1925-27 6 (1).

The Oceanographical Magazine
Vol. 10. No. 1 June 1958

The Distribution of Dissolved Oxygen in the North-western Part of the North Pacific Ocean in the Aspect of Physical Oceanography

Part I. General Features of the Oxygen Distribution (I)

By

Akira Okubo

Oceanographical Section

Japan Meteorological Agency, Tokyo

Abstract: As a preliminary report on studies on dissolved oxygen in the north-western part of the North Pacific from a standpoint of physical oceanography, the author describes the general features of the spatial distribution of oxygen in waters above upper abyssal depths on the basis of recent data observed in a cooperative survey in summer of 1955 ("NORPAC Expedition").

1. Introduction

Because of its importance in biological processes the distribution of dissolved oxygen in the oceans has been examined very widely. Besides being an index to the biological history of the water, the general character of the distribution of oxygen in deeper waters is helpful in studies of circulations and of mixing processes. Nevertheless, it is as yet theoretically impossible to explain the distribution of dissolved oxygen in the sea by a purely deductive method. This is chiefly because of lack of our knowledges concerning biological and organic chemical processes on which the non-conservative character of oxygen primarily depends.

If the mechanism for exchange of oxygen with the atmosphere through the sea surface were clear, if processes of diffusion and advection were known, and if biological and chemical processes were fully understood, a complete discussion of the oxygen distribution in the oceans will become theoretically possible. This is a distant goal, therefore, in the present situation, instead of the purely deduc-

tive way, the author has to confine himself to either discuss actual distributions of oxygen in somewhat quantitative manner or interprete them not only on the basis of a certain estimation about the biological effects but also in close relation to currents, water masses and distributions of conservative elements such as water temperature, chlorinity and density.

From this standpoint the author intends to discuss the distribution of oxygen in the north-western part of the North Pacific Ocean—by the name "the north-western part" are defined, for the sake of convenience, the areas to the north of of lat. 20°N and to the west of long. 180°E—where any systematic study in the field of physical oceanography has been scarcely developed as to the oxygen distribution except in the adjacent seas of Japan.

As for a few descriptive studies, Ito (1932) examined the oxygen distribution in the south-western portion of the North Pacific (0°～33.5°N, 126.5°～162.5°E) both horizontally and vertically on the basis of the *Mansyu* data, Miyake (1939) studied the oxygen content over the Kuroshio water region, together with the concentrations of other several chemical elements, and recently Kawamoto (1955, 1956) has described a general character of the oxygen distribution in the North Pacific in connection with the stratification of water by use of the $\sigma_t - O_2$ diagram.

On the other hand, recently Ichiye (1954, 1956) has published several papers concerning the distribution of oxygen in the adjacent sea of Japan, in which he contributed to the explanation of oxygen distribution in somewhat quantitatively, besides introducing the oxygen content into the branch of physical oceanography.

To begin with we shall present a preliminary report on the general features of the oxygen distribution in the north-western part of the North Pacific Ocean based on the recent international cooperative survey, so-called "NORPAC Expedition", observed in summer of 1955 (Fig. 1).

2. *The general feature of the horizontal distribution of dissolved oxygen in waters above upper abyssal depths.*

i) At the 100-meter level (Fig. 2)

All over the region in question being expected considerable annual variations of dissolved oxygen in surface layers, especially within waters above 100 m, the distribution at this level represents the general feature only in the season of summer.

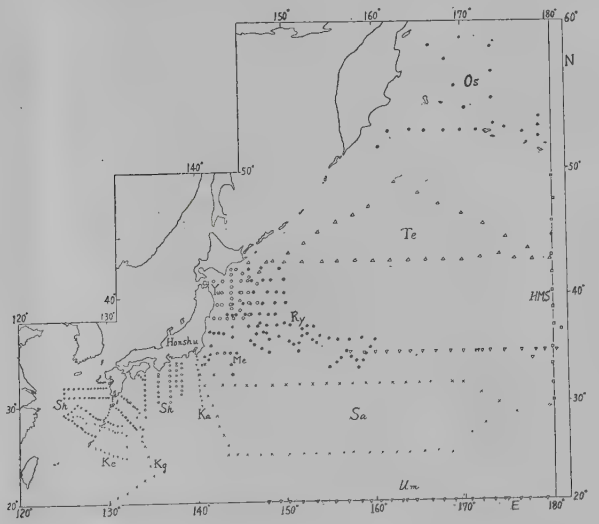

Fig. 1. Map of stations. *Abbreviation;* Os(●)=*Oshioro*, Te(△)=*Tenyo*, Yu(○)=*Yushio*, Ry(◉)=*Ryofu*, Me(⊖)=*Meiyo*, Sa(×)=*Satsuma*, Sh(●, ○)= *Shumpu*, Ka(+)=*Kaiyo*, Ke(+)=*Keiten*, Kg(×)=*Kagoshima*, Um(▽)=*Umitaka*, HMS(□)=Hugh M.Smith.

In the area to the north of the zone of the oceanic polar front where the Central Subarctic (Pacific) Water mass is widely found, one encounters rich oxygen waters dissolving more than 7 ml/L and from there the oxygen content continues to increase still further toward the Bering Sea.

A part of the western Subarctic Water flowed along the Kurile Islands and south as the cold Oyashio, meets the lower oxygen water carried northeast by the warm Kuroshio in the sea east of Honshu, Japan, where are present numerous eddies containing various oxygen values. Along the boundary between the Kuroshio Extension and the Oyashio to the east away from this contact area, an intense mixing of the water masses takes place and gradually forms the water of which oxygen content is more or less uniform ranging from 4 to 5 ml/L.

In the (Western North Pacific) Central Water region widely distribute the waters containing low-oxygen between 4.5 to 5.5 ml/L.

A tongue of less oxygen than 5 ml/L is seen to stretch from the east to the

(a)

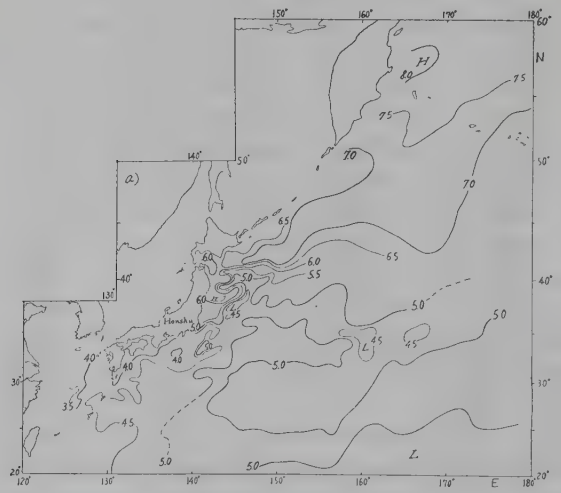

(b)

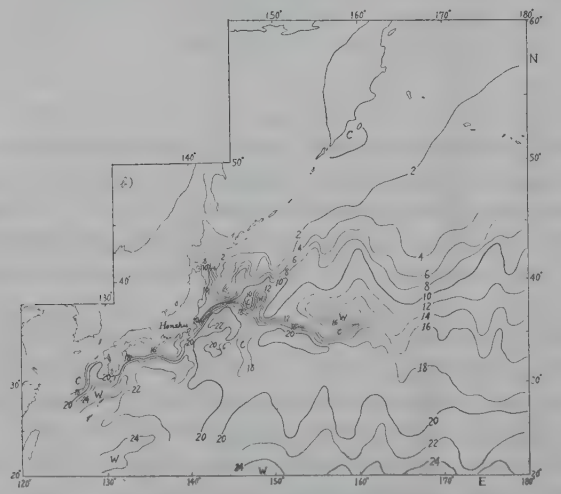

Fig. 2. Horizontal distribution at the 100 meter level.
a) oxygen (ml/L) b) water temperature (°C)

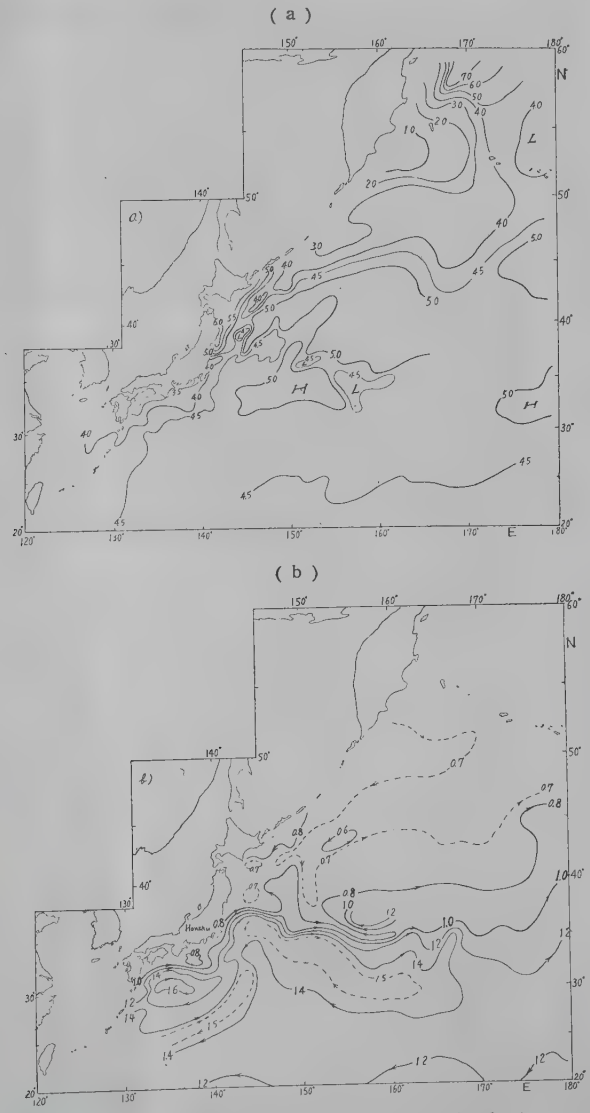

Fig. 3. Horizontal distribution at the 200-meter depth a) oxygen (ml/L) b) dynamic topography over 1000 db level

west of long 140°E, the appearance of which might be unexpected from the distribution of water temperature or chlorinity.

ii) At the 200-meter level (Fig. 3)

Within the Subarctic Water except the Oyashio the oxygen content, below rich-oxygen layers extending from the surface to a depth of about 100 m, decreases rapidly with depth to the value under 4.5 ml/L at a depth of 200 m. While, in the region where the Central Water is found, the oxygen content is nearly uniform from the surface to a depth of 200 m or more, ranging from 4.5 to 5 ml/L. Owing to such conditions the horizontal distribution of oxygen at this level becomes rather simple, as it should be expected.

A belt of the lowest oxygen water contained the value from 3.5 to 4 ml/L exists closely corresponding to the zone of the Kuroshio Current, but the oxygen content increases gradually to 4～4.5 ml/L in the sea far east of Honshu, Japan owing to the admixture of the Subarctic Water containing the high oxygen concentration nearly along an isopycnic surface, untill it reaches the value ranging from 4.5 to 5 ml/L by which is characterized the Central Water.

(a)

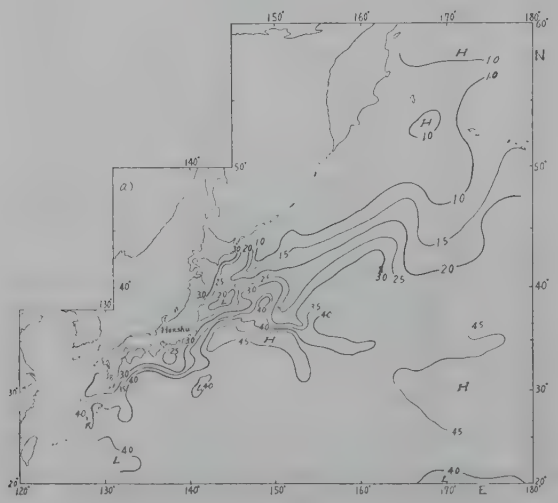

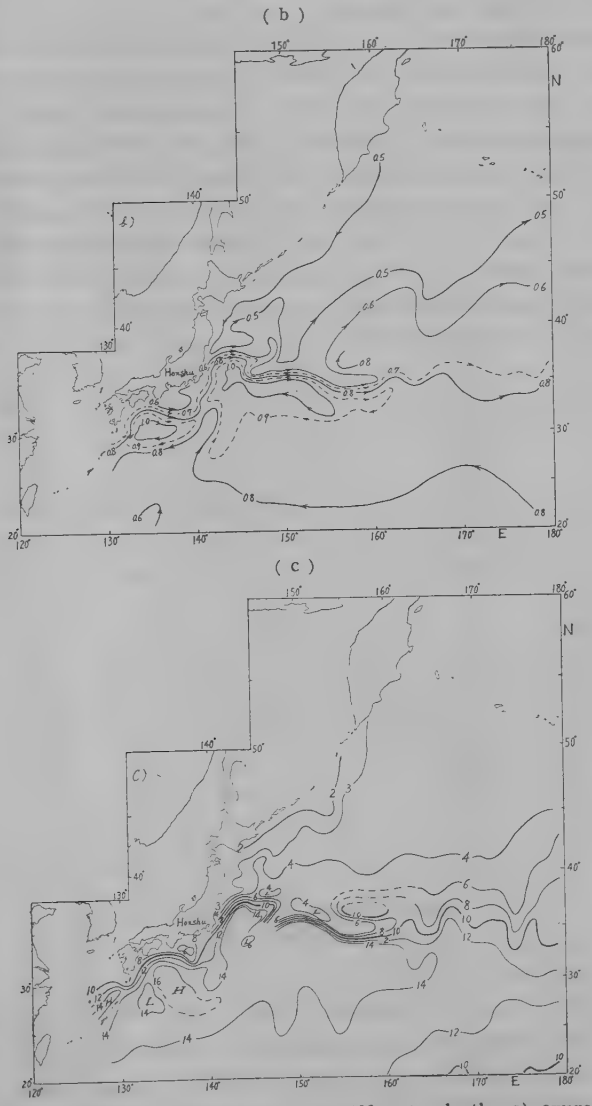

Fig. 4. Horizontal distridution at the 400-meter depth. a) oxygen (ml/L) b) dynamic topography over 1000 db level c) water temperature (°C)

iii) At the 400-meter level (Fig. 4)

The oxygen distribution at this level differs fundamentally from those at surface layers. Namely, within the Subarctic Water, reflecting the property of depleted oxygen that is characteristic in the subsurface layers, the low values less than 2 ml/L are widely found, especially is observed below 1 ml/L in the western part. In addition, this character of low concentration exerts an influence on the water in the sea northeast of Japan. On the other band, the water with oxygen value ranging from 4 to 4.5 ml/L which is only slightly lower than that at the 200-meter level, widely distributes in the Central Water region with the exception of the presence of a low oxygen belt with the value between 3 and 3.5 ml/L closely along the Kuroshio Current.

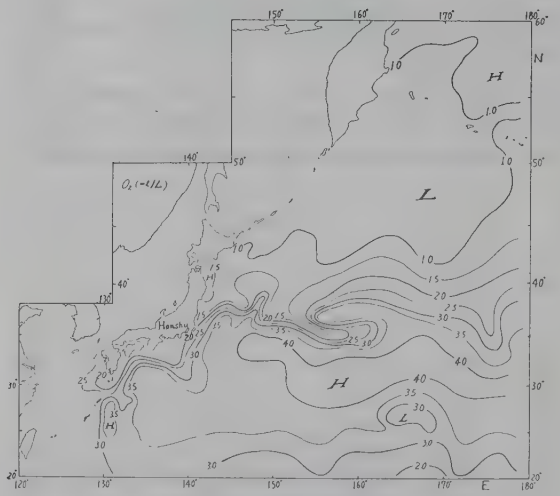

Fig. 5. Horizontal distribution of dissolved oxygen at the 600-meter level

iv) At the 600-meter level (Fig. 5)

The Subarctic region is occupied by the water below 1 ml/L, while in the region where the Central Water developes, waters containing oxygen from 3.5 to 4.5 ml/L are found, especially along about lat. 32°N the water having an oxygen content above 4 ml/L extends in an east-west direction. The sea area off the south coast of Honshu, Japan is characterized by a relatively low oxygen ranging from

1.5 to 2.0 ml/L, which may be attributed to the dynamic condition taking place on the left hand side of the Kuroshio Current so that a denser and less aerated water containing the relatively depleted oxygen may appear at this level. The most striking feature at this depth is the close resemblance of the oxygen distribution to the pattern of flow and, accordingly, to distributions of water temperature and chlorinity. Consequently, the horizontal gradient of oxygen in the domain of the Kuroshio System is considerably large.

v) At the 1000-meter level (Fig. 6)

At this level no remarkable difference of the oxygen content exists between two main water masses, as is illustrated in the figure. Thus, the Subarctic Water has an oxygen content less than 1 ml/L, especially about 0.75 ml/L in the western part. Similarly the water contained an oxygen below 1 ml/L is widely found in the eastern part of the Central Water. On the other hand, waters of slightly higher oxygen than 1.5 ml/L are encountered both to the west of the South Honshu Ridge and in the sea area east of Japan along nearly lat. 35°N.

iv) At the minimum-chlorinity layer (Fig. 7)

As mentioned above, the Subarctic Water carried by the Oyashio contacts with the Kuroshio in the sea north-east of Honshu, Japan, and sinks beneath the lighter

(a)

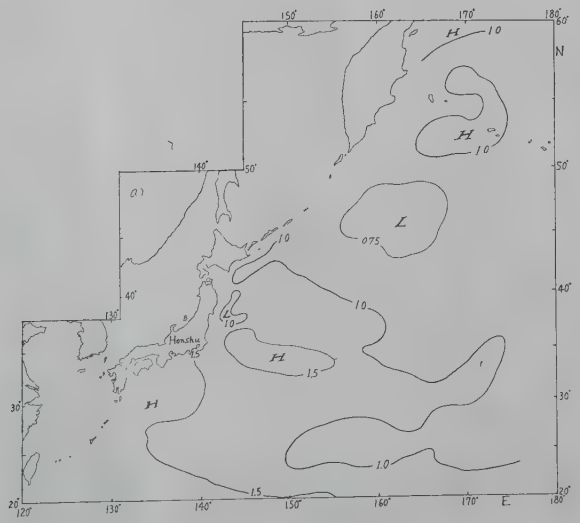

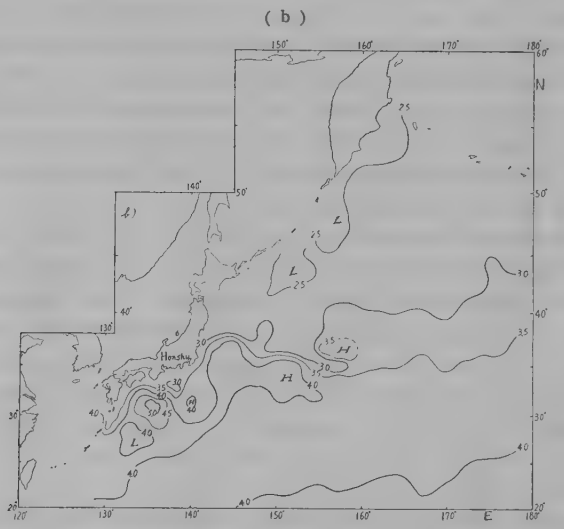

Fig. 6. Horizontal distribution at the 1000-meter level a) oxygen (ml/L) b) water temperature (°C)

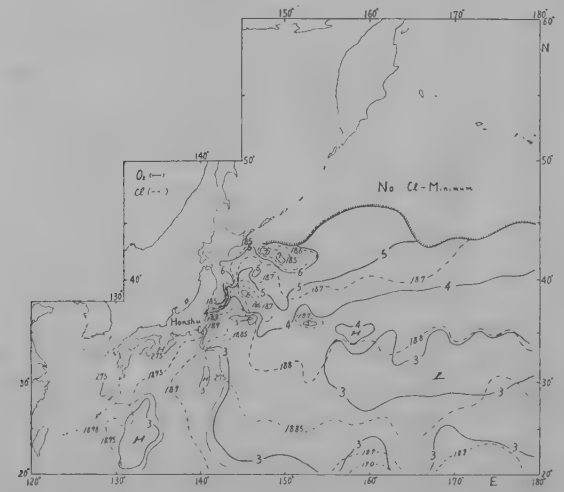

Fig. 7. Distribution of oxygen (ml/L) and chlorinity (‰) at the minimum-chlorinity layer.

Kuroshio water as the North Pacific Intermediate Water. From the area of sinking it is at first transported with the Kuroshio Current or Extension toward the east, then spreads over the greater part of the North Pacific Ocean.

A core of the Intermediate Water can be traced over long distances by means of a chlorinity minimum. (As to whether the layer of minimum-Cl corresponds to a "true core" of the Intermediate Water or not, the author will discuss in future.)

In Fig. 7 we show the distributions of oxygen and chlorinity at the layer of minimum-chlorinity. The main feature of the chlorinity distribution is in good agreement with that has been prepared by Sverdrup *et al* in the somewhat schematic picture (Fig. 202 in "the Ocean").

The distribution of oxygen at the layer of minimum-chlorinity seems to present us some interesting suggestions as to the spreading of the Intermediate Water. Although isolines of oxygen do coincide very well with isohalines in the vicinity of the origin of the Intermediate Water, a difference in the distribution between oxygen and chlorinity gradually appears as we proceed farther from there. Thus, isohalines 18.70 ‰ and 18.80 ‰, approximately coinciding with isooxys 5 ml/L and 4 ml/L, respectively in the sea east of Honshu, Japan, gradually shift to those of 4 ml/L and of 3.5 ml/L, respectively in the sea area farther to the east of Japan. A somewhat large area to the east of lat. 155°E, characterized by the water of which chlorinity is between 18.80 ‰ and 18.85 ‰, has a low oxygen content below 3 ml/L. The isohaline 18.90 ‰ extends not only to the south of 22°N but also toward the west passing over the South Honshu Ridge to which the isooxy 3 ml/L runs nearly parallel.

As the water containing oxygen above 3 ml/L proceeds further toward the west after crossing the Ridge, its oxygen content at first decreases below 3 ml/L, whereas increases again to the value above 3 ml/L to the west of 135°E, in contrast with the fact that its chlorinity continues to increase toward the west.

Another striking feature is shown in the relationship between a depth of minimum chlorinity and that of maximum oxygen within the Intermediate Water. Although the depth of a chlorinity minimum does agree very well with that of an oxygen maximum within waters in the vicinity of the origin of the Intermediate Water, the latter has a tendency to rise gradually above the former as a distance from the origin increases, untill it seems to disappear probably due to mixing with overlying waters of rich oxygen. This suggests us that an effect of vertical

mixing on the formation of the Intermediate Water cannot be always neglected (Okubo, 1957 a) though the concept of lateral mixing primarily along an isopycnic surface (quasi-isentropic analysis) has been applied to the diffusion of the Intermediate Water, considering from the fact that the layer of the chlorinity minimum approximately coincides with a surface $\sigma_t=26.8$.

Fig. 8. Distribution of oxygen (ml/L) at the minimum-oxygen layer

vii) At the oxygen minimum layer (Fig. 8)

Here we shall briefly describe the distribution of oxygen at this layer as an introduction to a more precise discussion in regards to the occurrence of the minimum oxygen concentration at mid-depths.

Within the Subarctic Water the oxygen minimum layer lies generally at a depth between 600 m and 800 m, where a poor-oxygen water below 0.75 ml/L is widely distributed, especially a water containing as much depleted oxygen as 0.5 ml/L is found in the western part. In the Central Water region the minimum value, encountered at a depth between 1000 m and 1500 m, is about 1 ml/L with the only exception of the presence of a depleted oxygen below 0.75 ml/L to the east of lat. 160°E, and, slightly increasing toward the west, becomes about 1.25 ml/L over the South Honshua Ridge, where an abrupt change in the oxygen content

takes place. All over the region on the west side of the Ridge minimum oxygen values are more than 1.5 ml/L, increasing more or less regularly further toward the Ryukyu Islands, where one encounters the highest content above 1.75 ml/L.

This contrast of the minimum oxygen contents between waters on the east and the west sides of the South Honshu Ridge, seems to suggest us that the communication between waters at greater depths than about 1000 m must be more or less restricted, as the biological conditions in both waters, on which the consumption of oxygen within waters depends, are probably similar. In the polar frontal zone the water containing an oxygen over 1 ml/L distributes from the coast of Honshu to long. 160°E.

3. *The general feature of the vertical distribution*

To demonstrate the major feature of the vertical distribution of oxygen, we shall construct five vertical sections, one in a longitudinal and four in a latitudinal directions, along which a great deal of data are available. In the preceding section we have described the general feature of oxygen distribution in relation to the distribution of two main water masses, namely the Subarctic Water and the Central Water.

Here we intend to examine the oxygen distribution in relation to the stratification of water, paying a special attention to the existence of oxygen maxima and minima in the vertical column.

i) Along long. 135°E (Fig. 9)

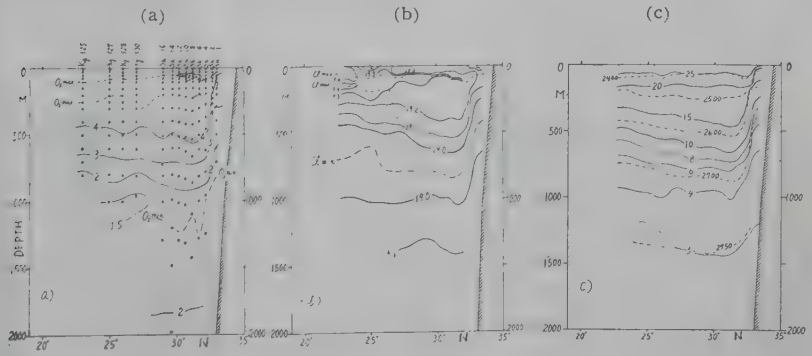

Fig. 9. Distribution in a vertical section along long. 135°E. a) oxygen (ml/L) b) chlorinity (‰) c) water temperature (°C) and density *in situ*.

As this section transverses the western portion of the Central Water mass in a south-north direction, the oxygen distribution is in general monotonous with the only exception that the isooxys bend abruptly upwards to the north of the Kuroshio Current flowing northeastward at about 32.5°N, which may be interpreted on the basis of the dynamic process.

In surface layers are present two maxima of oxygen; the upper one lying at a depth shallower than 100 m seems to be generated as a result of the seasonal variation (Okubo, 1958), while the secondary (lower) maximum with the content between 4.4 and 5.2 ml/L is found at a depth between 200 and 300 m, the occurrence of which remains unknown to be studied in future. It is noticeable event that these maximum layers desend abruptly about 100 m to the very south of the Kuroshio Current, in spite of the fact that isooxys at the deeper layers rise as mentioned above.

The well-defined layer of minimum oxygen at a subsurface level lies closely on an isopycnal 27.3, containing an oxygen between 1.5 and 1.6 ml/L.

ii) Along long. 145°E (Fig. 10)

A sharp transition from the Central Water (the Kuroshio Water) to the Subarctic Water (the Oyashio Water) is best illustrated in this section. At about 38°N and 39°N are situated oceanic polar fronts named the Kuroshio front and the Oyashio front, respectively, where the upward and downward bends of isooxys are remarkable. Low oxygen waters of the Kuroshio develop to the south of the Kuroshio front, while to the north of lat. 39°N is seen another transition to the typical Subarctic Water mass characterized by a rich-oxygen in surface layers and by a poor-oxygen at mid-depths.

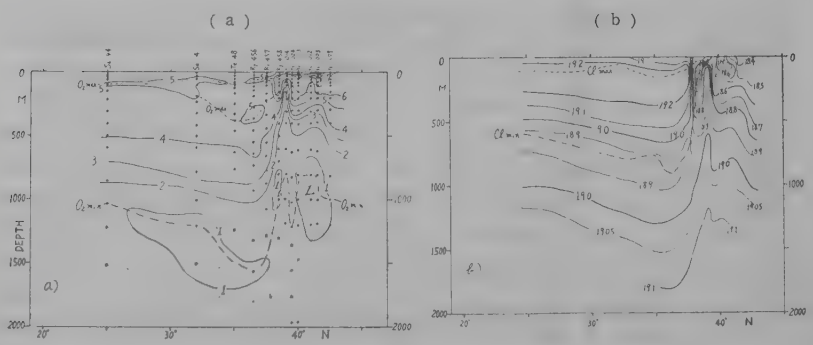

(c)

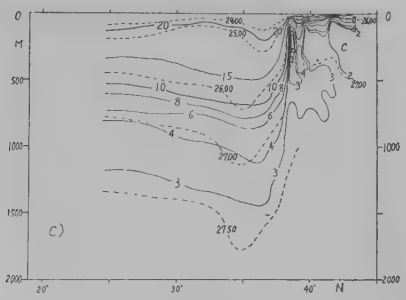

Fig. 10. Distribution in a vertical section along long. 145°E. a) oxygen (ml/L) b) chlorinity (‰) c) water temperature (°C) and density *in situ*.

The secondary maximum, existing at the same depth between 100 and 150 m as the chlorinity minimum (the "core" of the Intermediate Water) and containing about 7 ml/L within the water of the polar frontal zone, disappears to the north of the Oyashio front, while it is found at a depth between 200 and 400 m within the Central Water, where the oxygen content decreases to the value of more or less 5 ml/L. The minimum oxygen layer at the subsurface lying between the 27.3 and 27.5 σ_t surfaces, has a value ranging from 0.8 to 1.0 ml/L within the Oyashio water as well as the Central Water.

(a) (b)

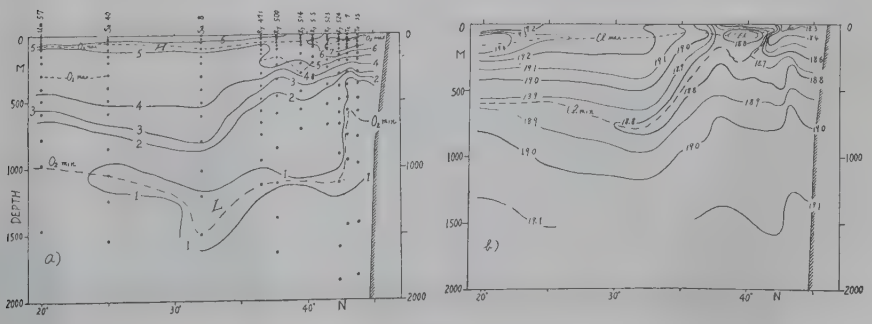

(c)

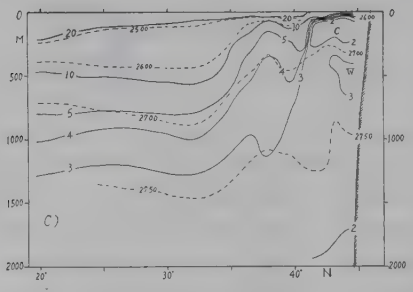

Fig. 11. Distribution in a vertical section along long. 150°E. a) oxygen (ml/L) b) chlorinity (‰) c) water temperature (°C) and density *in situ*

iii) Along long. 150°E (Fig. 11)

With the exception of the presence of a very large body of water developed in a thickness between 600 and 800 m at mid-depths of the Central Subarctic Water within which the oxygen content shows a relatively depleted value ranging from 0.5 to 0.9 ml/L, the character of the oxygen distribution in this section remains practically unchanged from that of section along 145°E. The Kuroshio and Oyashio fronts are located at lat. 36°N and 41°N respectively, presences of which are reflected in the profile of the oxygen distribution.

The depth at which a vertical gradient of oxygen amounts to maximum is found in the vicinity of the Cl-minimum layer in the Central Water region, whereas it is present beneath the rich-oxygen water in the Subarctic Water.

(a)

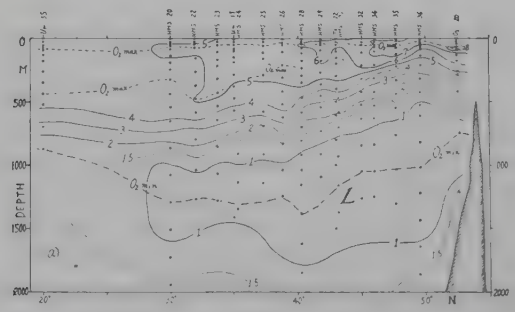

(b)

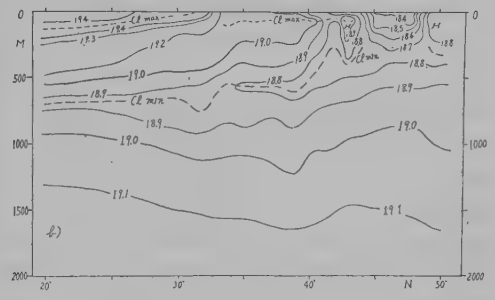

(c)

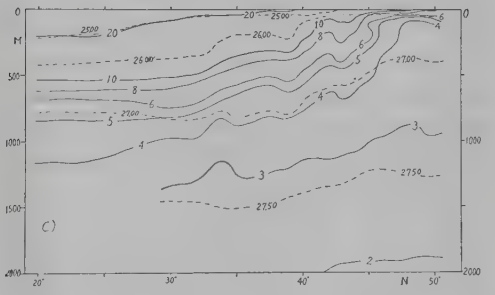

Fig. 12. Distribution in a vertical section along long. 180°E.
a) oxygen (ml/L) b) chlorinity (‰) c) water temperature (°C) and density *in situ*.

iv) Along long. 180°E (Fig. 12)

Being unlike to the north-south sections along longitudes 145° and 150°E, the well-defined polar front is no longer present at long. 180°E, and, accordingly, the oxygen distribution in the vertical section along this longitude become relatively monotonous.

The secondary maximum of oxygen exists only to the south of 40°N, and its depth is found between 200 and 500 m, lying at about 300 m above the core of the Intermediate Water, which is indicated by the line marked Cl-min in the figure.

On an isopycnal about 27.4 is encountered the subsurface oxygen-minimum, which shows a relatively depleted oxygen with values between 0.5 and 0.8 ml/L except within waters in the Central Water region.

To the north of 30°N widely distribute poor-oxygen waters below 1 ml/L in a

thickness from 500 to 1000 m centred at a depth of oxygen-minimum, appearing in the section as a tongue extending towards the south.

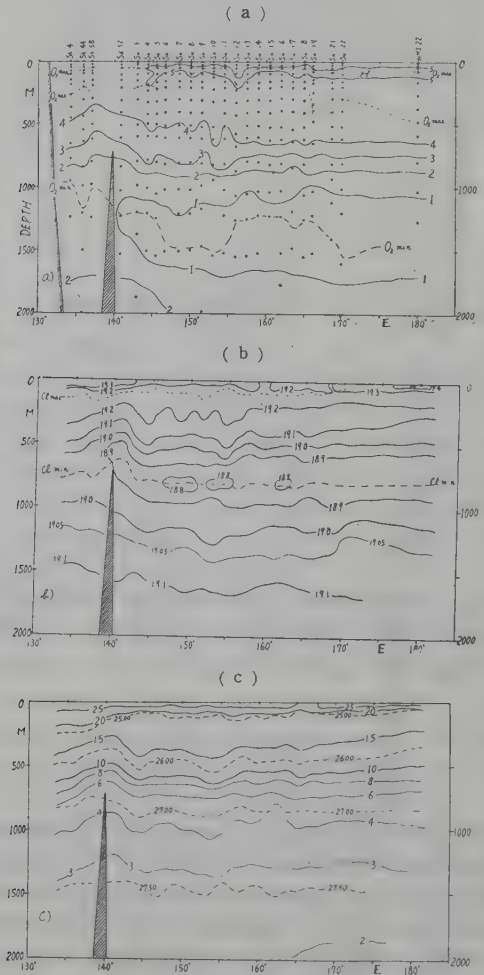

Fig. 13. Distribution in a vertical along lat. 32°N.
a) oxygen (ml/L) b) chlorinity (‰) c) water temperature (°C) and density *in situ*

v) Along lat. 32°N (Fig. 13)

The profile of the oxygen along this latitude is as simple as that along long. 135°E, as might be expected from the fact that this section transverses the Central Water region in an east-west direction.

The secondary maximum of oxygen, though it disappears in some places of the profile, is found at a depth between 200 and 600 m, which seems to have no intimate connection with the Intermediate Water characterized by a chlorinity-minimum. The striking difference of oxygen distribution within deep waters between the west and east sides of the South Honshu Ridge, as often mentioned in the previous section, is most clearly illustrated in this section. Thus, poor-oxygen waters with values ranging from 0.7 to 0.9 ml/L widely develop in a thickness between 400 and 600 m on the east side of the Ridge. On the contrary, even at a depth of the minimum-oxygen on the west side is scarcely encountered the water containing an oxygen below 1.5 ml/L. Considering from the fact that a similar contrast does not seem to exist in the distributions of water temperature and chlorinity, it is suggested that the oxygen distribution must play an important role in studies on a deep-water circulation in the north-western part of the North Pacific Ocean.

4. Concluding remarks for future studies

Concluding the description of the spatial (horizontal as well as vertical) distributions of dissolved oxygen in the north-western part of the North Pacific Ocean, it is summarized that—

1) Within the Subarctic Water the waters of rich-oxygen above 7 ml/L or more extend from the sea surface to a depth of about 100 m below which the oxygen content decreases rapidly with depth, for instance, to a value under 4.5 ml/L at a depth of 200 m, until it reaches a considerably depleted value ranging from 0.5 to 0.9 ml/L at mid-depths, where widely distribute poor-oxygen waters in a thickness from 500 to 1000 m centred at a depth of oxygen-minimum. This great depletion of oxygen is probably due to the oxidation of remains of organisms which fall from the productive surface layers (Miyake and Saruhashi, 1956).

2) In the region where the Central Water covers, the oxygen content is only slowly decreasing from a value about 5.5 ml/L in the surface to 4.5 ml/L at a depth of 200 m or more.

Below this surface layer of nearly homogeneous is often found an oxygen maximum layer at a depth from 200 to 500 m. This intermediate maximum lies at a few hundred meter above the "core" of the Intermediate Water characterized by the well-defined minimum of chlorinity, where a vertical gradient of oxygen is usually largest.

3) In a transition area located at the oceanic polar frontal zone are shown most complicated and, accordingly, interesting distributions on which another studies from a more microscopic standpoint are in progress (Okubo, 1957 a, b).

4) The so-called oxygen-minimum layer in the subsurface lies on an isopycnal between the 27.3 and 27.5 σ_t, containing an oxygen below 0.75 ml/L within the Subarctic Water and about 1 ml/L in the Central Water region except on the west side of the South Honshu Ridge where we encounter the values above 1.5 ml/L.

5) This striking difference of oxygen concentration within deep waters between the west and east sides of the Ridge, will play an important role in the study on a deep-water circulation such as the subject on the communication between waters at greater depths than about 1000 m.

Acknowledgement—The author wishes to express his hearty thanks to Dr. J. Masuzawa for his advice and suggestion.

References

ICHIYE, T. (1954): On the distribution of oxygen and their seasonal variations in the adjacent sea of Japan, (1) and (2). *Oceanogr. Mag.*, **6** (2).

ICHIYE, T. (1956): On the distribution of oxygen and their seasonal variations in the adjacent sea of Japan, (4). *Oceanogr. Mag.*, **8** (1).

ITO, K. (1932): Oxygen-gas content of sea-water in the South-western portion of the North Pacific. *Records Oceanogr. Works Japan* **4** (1)

KAWAMOTO, T. (1955, 1956): On the distribution of the dissolved oxygen in the Pacific Ocean. (in Japanese) Part 1, *Umi To Sora* (*Sea and Sky*), **32**, 23-37; Part 2, *Ibid.*, **32**, 92-98; Part 3, *Ibid.*, **33**, 28-33.

MIYAKE, Y. (1939): *Bull. Chem. Soc. Japan*, **14**, 465.

MIYAKE, Y. and K. SARUHASHI (1956): On the vertical distribution of dissolved oxygen in the ocean. *Deep-sea Res.*, **3**, 242-247.

OKUBO, A. (1957a): Estimation of biological effects in the distribution of dissolved oxygen by use of isopycnic analysis (The distribution of dissolved oxygen in the sea east of Honshu, Japan I). *Oceanogr. Mag.*, **9** (1).

OKUBO, A. (1957b): A note on the super- and undersaturation of dissolved oxygen in surface waters (The distribution of dissolved oxygen in the sea east of Honshu, Japan II) (in Japanese). *Jour. Oceanogr. Soc. Japan*, **13** (4).

OKUBO, A. (1958): Discussions on the annual variation of dissolved oxygen in the ocean. *Jour. Oceanogr. Soc. Japan*, **14** (to be published).

昭和33年 9 月10日印刷
昭和33年 9 月15日発行

編集兼
発行人　気　象　庁
東京都千代田区大手町一ノ七

印刷人　花　崎　実
東京都中央区新富町二ノ十九

印刷所　大東印刷工芸株式会社
東京都中央区新富町二ノ十九